

UNIVERSITÄT
BAYREUTH

Controlled Preparation of Nanoparticles and Polymer Core-Shell Structures for Use in Organogels and Nanocomposites

DISSERTATION

zur Erlangung des akademischen Grades eines Doktors
der Naturwissenschaften (Dr. rer. nat.) an der
Bayreuther Graduiertenschule für Mathematik und
Naturwissenschaften der Universität Bayreuth

vorgelegt von

Daniela Pirner

geboren in Sulzbach-Rosenberg

Bayreuth, 2016

Die vorliegende Arbeit wurde in der Zeit von April 2012 bis Juli 2016 in Bayreuth am Lehrstuhl Physikalische Chemie I unter Betreuung von Herrn Prof. Dr. Stephan Förster angefertigt.

Vollständiger Abdruck der von der Bayreuther Graduiertenschule für Mathematik und Naturwissenschaften (BayNAT) der Universität Bayreuth genehmigten Dissertation zur Erlangung des akademischen Grades eines Doktors der Naturwissenschaften (Dr. rer. nat.).

Dissertation eingereicht am: 29.07.2016

Zulassung durch das Leitungsgremium: 08.09.2016

Wissenschaftliches Kolloquium: 10.02.2017

Amtierender Direktor: Prof. Dr. Stephan Kümmel

Prüfungsausschuss:

Prof. Dr. Stephan Förster (Erstgutachter)

Prof. Dr. Georg Papastavrou (Zweitgutachter)

Prof. Dr. Birgit Weber (Vorsitz)

Prof. Dr. Peter Strohrriegl

Table of Contents

Abbreviations	1
1 Introduction	3
2 Overview of the Thesis	9
3 Theory	27
3.1 Anionic Polymerization	29
3.2 End-functionalization of Polymers	34
3.2.1 Coordinating Groups	35
3.2.2 Hydrogen Bonding Groups	38
3.3 Self-assembly of Block Copolymers	42
3.4 Organogels	49
3.5 Polymer Nanocomposites	50
3.5.1 Inorganic Nanoparticles	50
3.5.2 Polymer Ligands for Nanoparticle Stabilization	53
4 Reinforcement of Nanostructured Organogels by Hydrogen Bonds	67
5 Polymer Ligand Exchange to Control Stabilization and Compatibilization of Nanocrystals	99
6 A General Route to Optically Transparent Highly Filled Polymer Nanocomposites	127

7	Rheological Study of Polymer Nanocomposites: Influence of Nanoparticles on Polymer Chain Dynamics	147
	Summary	177
	Zusammenfassung	179
	List of Publications	181
	Danksagung	183

Abbreviations

¹H-NMR	proton nuclear magnetic resonance
ATRP	atom transfer radical polymerization
bcc	body-centered cubic
CDI	1,1'-carbonyldiimidazole
CMC	critic micelle concentration
CMT	critic micelle temperature
Cryo-SEM	cryogenic scanning electron microscopy
DBP	di- <i>n</i> -butyl phthalate
DEP	diethyl phthalate
DETA	diethylenetriamine
DLS	dynamic light scattering
DMF	dimethylformamide
DMP	dimethyl phthalate
DMSO	dimethyl sulfoxide
DNA	deoxyribonucleic acid
fcc	face-centered cubic
GPC	gel permeation chromatography
HOMO	highest occupied molecular orbital
HRTEM	high-resolution transmission electron microscopy
HSAB	hard-soft acid-base concept
LCST	lower critical solution temperature
LED	light-emitting diode
LUMO	lowest unoccupied molecular orbital
NIR	near-infrared
NMP	nitroxide mediated radical polymerization
NP	nanoparticle
ODT	order-disorder transition
OOT	order-order transition
PDI	polydispersity index

PE	polyethylene
PEHA	pentaethylenhexamine
PEO-PBO	poly(ethylene oxide)- <i>block</i> -poly(butylene oxide)
PEO-PPO-PEO	poly(ethylene oxide)- <i>block</i> -poly(propylene oxide)- <i>block</i> -poly(ethylene oxide)
P3HT	poly-3-hexylthiophene
PI	polyisoprene
PI-PS	poly(isoprene- <i>block</i> -styrene)
PMMA	poly(methyl methacrylate)
PS	polystyrene
P2VP	poly(2-vinylpyridine)
RAFT	reversible addition-fragmentation chain-transfer polymerization
RI	refractive index
SAXS	small-angle X-ray scattering
SDS	sodium dodecyl sulfate
TBAH	tetrabutylammonium hydroxide
TEM	transmission electron microscopy
TGA	thermogravimetric analysis
THF	tetrahydrofuran
TOP	trioctyl phosphine
TOPO	trioctylphosphine oxide
UPy	2-ureido-4[<i>IH</i>]-pyrimidinone
UV	ultraviolet
WLF	Williams-Landel-Ferry model

1



Introduction

Nanostructured materials are designed in a hierarchical manner and complexity that often mimics systems observed in nature.¹ The property-determining heterogeneity on the nanoscale dimension (1-100 nm) leads to materials with new adjustable mechanical, optical, or magnetic properties.¹

Since nanostructured materials are often seen as “materials-by-design”, the focus of research is to understand the relationship between the structures, compositions, the matrices, and the interfaces of the materials to control their properties.¹ The construction of such materials demands well-defined building blocks in the nanometer size regime.¹ Most promising building blocks are macromolecules and/or inorganic nanoparticles with defined size, shape, and chemical functionality.^{1,2} They can be used individually or in hybrid systems where materials with synergetic properties can be achieved.³

The preparation of these nanosized structures can be realized by top-down or bottom-up approaches.¹ Top-down approaches are based on the break-up of macroscopic materials through chemical, mechanical or optical processes. They open up the possibility for straight forward automations, but are rather energy- and cost-intensive.¹ Bottom-up approaches are based on hierarchical assembly strategies (self-assembly or self-organization) starting from small molecules toward nanostructured materials and represent a low-cost alternative for the construction of nanosized building blocks.^{1,2}

Especially block copolymers are ideal candidates for bottom-up fabrication of nanomaterials having tunable chemical and physical properties. Block copolymers can be synthesized in well-defined compositions and functionalities *via* controlled polymerization techniques and are able to self-assemble in solution or in bulk into well-defined, monodisperse building blocks on the nanometer scale.³ Spontaneous self-assembly processes in selective solvents for one block result in micelle formations in dilute systems or lyotropic liquid crystal phases at higher concentrations.³ These self-assembled shapes provide sufficient strength to stabilize the desired structure through amphiphilic interactions.³ For instance, lyotropic liquid crystal phases exhibit highly symmetric architectures, such as body-centered cubic (*bcc*) packing disperse spheres, face-centered cubic (*fcc*) packing spheres or hexagonal structures, but are fragile due to dynamic exchange processes.³ Consequently, their application is often based on their function, but not on their structure. Introducing a second component can increase the mechanical stability caused by attractive interactions without losing structural features, for example the insertion of additional functionalities into the colloids (*e.g.* hydrogen

bonding moieties). Interesting types of such materials are nanostructured organogels, which are within the focus of this thesis. Polymer gels are constructed of macromolecular networks surrounded by a large amount of fluid, which is an organic solvent in the case of organogels.⁴ Well-defined nanostructured organogels can be generated from pre-assembled block copolymer based micelles which are linked *via* functional moieties present on the surfaces of individual micelles. By utilizing attractive forces between the soft nanoparticles, such as hydrophobic interactions,^{5,6} metal-ligand interactions,⁷ ionic associations⁸ or hydrogen-bonding^{9,10}, dynamic or transient properties can be induced resulting in organogels with thermosensitive and reversible mechanical properties.¹¹ At the same time the materials preserve a highly ordered manner on nanometer scale.⁴

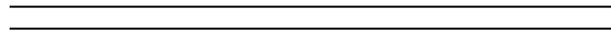
The incorporation of inorganic nanoparticles to organic polymer materials result in hybrid nanocomposites with new material properties for instance improved thermal, mechanical, electrical, and optical properties.¹² Depending on the requirements of the final nanostructured material, the particle size, type and shape can be adjusted.¹² Homogeneous polymer nanocomposites can be achieved under the prerequisite of stable nanoparticles in combination with their compatibilization.¹² Nanoparticles have high surface energies due to their dimensions and tend to aggregate, which is unfavorable for many potential applications.¹² Accordingly, a lot of effort has been made to overcome this problem. The most efficient approaches deal with surface modification of the incorporated nanoparticles producing a compatibility between nanoparticles and polymer matrices.¹³⁻¹⁵ Nanostructured materials, whether of organic or inorganic nature, are constructed of individual, well-defined building blocks interacting with each other and can be precisely tailored to obtain desired material properties. Understanding and investigating their fundamental structure-property relationship, thus, is essential. Consequently, the aim of this thesis is the controlled preparation of nanoparticle and polymer core-shell structures used as building blocks to prepare functional organogels and nanocomposites. Furthermore, structure-property relationships are investigated to get a detailed insight into both systems.

References

1. Huck, Wilhelm T. S, *Nanoscale Assembly: Chemical Techniques* (Springer, New York, 2005).
2. M. Antonietti, "Nanostructured Materials: Self-Organization of Functional Polymers," *Nat. Mater.* **2** (1), 9–10 (2003).
3. S. Förster and T. Plantenberg, "From Self-Organizing Polymers to Nanohybrid and Biomaterials," *Angew. Chem. Int. Ed.* **41** (5), 688–714 (2002).
4. Z. Hu, "Nanostructured Polymer Gels," *Macromol. Symp.* **207** (1), 47–56 (2004).
5. M. Odenwald, H.-F. Eicke, and W. Meier, "Transient Networks by ABA Triblock Copolymers and Microemulsions: A Rheological Study," *Macromolecules* **28** (14), 5069–5074 (1995).
6. H. Bagger-Jørgensen, L. Coppola, K. Thuresson, U. Olsson, and K. Mortensen, "Phase Behavior, Microstructure, and Dynamics in a Nonionic Microemulsion on Addition of Hydrophobically End-Capped Poly(ethylene oxide)," *Langmuir* **13** (16), 4204–4218 (1997).
7. J. B. Beck and S. J. Rowan, "Multistimuli, Multiresponsive Metallo-Supramolecular Polymers," *J. Am. Chem. Soc.* **125** (46), 13922–13923 (2003).
8. A. Eisenberg, B. Hird, and R. B. Moore, "A New Multiplet-Cluster Model for the Morphology of Random Ionomers," *Macromolecules* **23** (18), 4098–4107 (1990).
9. R. P. Sijbesma, F. H. Beijer, L. Brunsveld, Folmer, Brigitte J. B., Hirschberg, J. H. K. Ky, Lange, Ronald E. F. M., Lowe, Jimmy K. L., and E. W. Meijer, "Reversible Polymers Formed from Self-Complementary Monomers Using Quadruple Hydrogen Bonding," *Science* **278** (5343), 1601–1604 (1997).
10. L. Brunsveld, Folmer, B. J. B., E. W. Meijer, and R. P. Sijbesma, "Supramolecular Polymers," *Chem. Rev.* **101** (12), 4071–4098 (2001).

11. B. Folmer, R. P. Sijbesma, R. M. Versteegen, van der Rijt, Joost A. J., and E. Meijer, “Supramolecular Polymer Materials: Chain Extension of Telechelic Polymers Using a Reactive Hydrogen-Bonding Synthone,” *Adv. Mater.* **12** (12), 874–878 (2000).
12. S. Kango, S. Kalia, A. Celli, J. Njuguna, Y. Habibi, and R. Kumar, “Surface Modification of Inorganic Nanoparticles for Development of Organic-Inorganic Nanocomposites-A Review,” *Prog. Polym. Sci.* **38** (8), 1232–1261 (2013).
13. S. Fischer, A. Salcher, A. Kornowski, H. Weller, and S. Förster, “Completely Miscible Nanocomposites,” *Angew. Chem. Int. Ed.* **50** (34), 7811–7814 (2011).
14. H. Skaff and T. Emrick, “Reversible Addition Fragmentation Chain Transfer (RAFT) Polymerization from Unprotected Cadmium Selenide Nanoparticles,” *Angew. Chem. Int. Ed.* **43** (40), 5383–5386 (2004).
15. S. K. Kumar, N. Jouault, B. Benicewicz, and T. Neely, “Nanocomposites with Polymer Grafted Nanoparticles,” *Macromolecules* **46** (9), 3199–3214 (2013).

2



Overview of the Thesis

The aim of this thesis is the development of well-defined polymer-based colloidal building blocks in order to investigate their structure-property relationship in hierarchically build-up nanostructured materials.

The thesis is composed of four articles presented in **Chapter 4** to **7**.

In principal, the presented research deals with controlled preparation of nanoparticles and polymer core-shell structures in order to understand the complex interactions and structure-property relationship in organogels and polymer nanocomposites. Consequently, the different systems studied in this thesis can be divided into organic and hybrid nanostructured materials. Both types of materials are constructed of spherical colloidal building blocks and only differ in the type of nanoparticles.

The organic nanoparticles are generated *via* a “bottom-up” self-assembly process of block copolymers in solution representing soft materials. Prepared hybrid nanostructured materials are fabricated from inorganic nanoparticles, which are stabilized with a polymer shell and incorporated into a polymer matrix. These core-shell nanoparticles represent the rigid material component and they can significantly influence the mechanical and optical properties of the polymer matrix. The overall goal in both spherical core-shell nanoparticle systems with either a soft or hard core was to understand the fundamental interplay of structural characteristic and compositions on the molecular level with the macroscopic properties of the nanostructured material. Based on the gained knowledge tailoring of the nanoscopic structures lead to a directed structure-property relationship, which allows to adjust the desired material properties for potential applications. The used polymers were synthesized *via* living anionic polymerization in order to get narrow distributed, well-defined subunits. For detailed analysis of the structure-property relationship small-angle X-Ray scattering (SAXS) and dynamic-mechanical measurements were applied.

In **Chapter 4** organogels based on block copolymer micelles were investigated. The micelles were modified with a supramolecular hydrogen bonding group in order to increase the attractive forces between the nanoparticles resulting in stimuli-responsive organogels. These organogels are systematically investigated not only with respect to their structural changes but also their mechanical properties. Since the composites form thermoreversible gels, these nanostructured materials are ideal candidates for microimprinting applications.

In **Chapter 5** hybrid nanoparticles with an organic shell and inorganic core were synthesized. A library of different nanoparticles was coated with a variety of well-defined

polymer chains with different molecular weights. This purpose was achieved utilizing a ligand exchange method based on a grafting to approach of the modified polymer chains onto the inorganic nanocrystal surface. The developed ligand exchange method lead to a relatively high grafting density of the polymer chains on inorganic nanoparticle surfaces. In this way, a high miscibility of the inorganic nanoparticles in compatible polymer matrices was realized, presented in **Chapter 6** and **7**. The obtained homogeneous nanocomposites were characterized by significantly improved mechanical and optical material properties compared to a common polymer, as discussed in **Chapter 6**. The physical characteristics of the nanocomposites could be tailored by the type of nanoparticle and polymer. These nanocomposite materials can be used as optical transparent thin films with increasing mechanical properties and scratch resistant surfaces. In **Chapter 7** a detailed study of polymer chain dynamics in nanocomposites was performed on a model system of core-shell nanoparticles to enhance the fundamental understanding of structure-property relation in such systems. More specifically the influence of added nanoparticles on the mechanical properties of the matrix polymer was investigated in a systematic fashion. To complete the picture the molecular weight of the attached polymer chains was varied. The studies reveal that densely grafted nanoparticles were well-dispersed within the polymer matrix and no aggregation of the nanoparticles was induced. In contrary, similar experiments of controlled assembled nanocrystals toward anisotropic nanochains lead to a strong reinforcement of the material and network formation represented by a solid-like behavior in the dynamic mechanical measurements. In the following section the main aspects of the individual chapters are summarized and put into a larger context.

Chapter 4

Reinforcement of nanostructured organogels by hydrogen bonds

In **Chapter 4**, a systematic study of the structure and viscoelastic properties of block copolymer based micelles, which bear covalently linked hydrogen bonding groups at their periphery, is presented. This allows tailoring of the attractive interaction forces between soft colloids in high concentrated solutions and triggering of the macroscopic mechanical properties of these organogels up to high-modulus gels. Furthermore, these

thermoresponsive gels can be easily imprinted toward well-defined micron-sized shapes in a subsequent step.

The narrow distributed poly(isoprene-*b*-styrene) (PI-PS) block copolymer with a PI volume fraction of 0.51 was synthesized *via* anionic polymerization. The living anion was end-capped with ethylene oxide and subsequently protonated, which introduced a hydroxyl group at the periphery of the block copolymer. This allows a further post-polymerization modification introducing an ureidopyrimidinone (UPy) function. The UPy groups have the ability to dimerize and form self-complementary quadruple hydrogen bonds (**Figure 2.1a**). In organic solvents the attractive bonds between the UPy groups are reversible and relatively strong, but non-covalent. Using diethyl phthalate (DEP) as a PS selective solvent the block copolymers, PI-PS-OH and PI-PS-UPy, self-assemble into spherical micelles above the critical micelle concentration (CMC). Monodisperse spherical micelles were obtained as proven by dynamic light scattering (DLS) measurements and cryo-scanning electron microscopy (cryo-SEM) (**Figure 2.1b**). By varying the degree of UPy functionality, the dynamic attractive interactions between the soft colloids were identified, indicated by additional peaks at higher hydrodynamic diameters in DLS measurements.

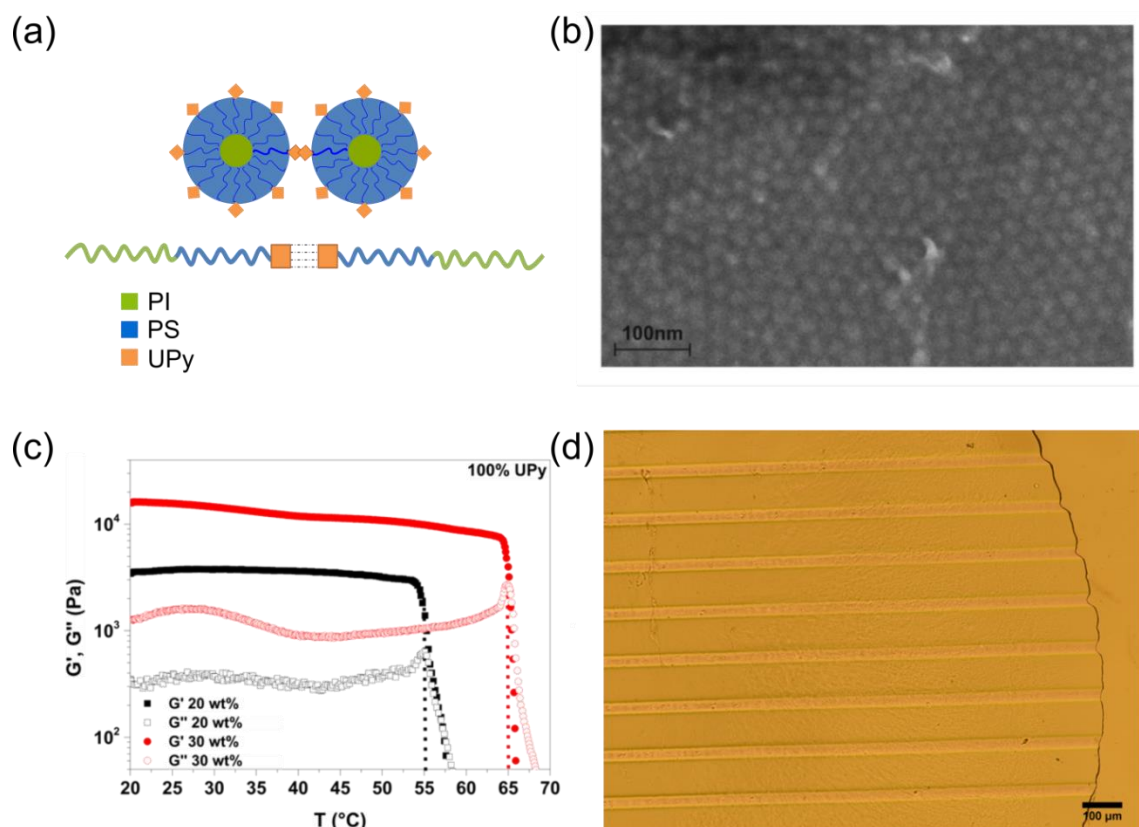


Figure 2.1: (a) Schematic representation of micellar interaction in organogels: Poly(isoprene-*b*-styrene) block copolymers with functional UPy groups at the periphery of the block copolymer micelles. UPy dimerization provides hydrogen bonded micelles. (b) Cryo-SEM image of a typical organogel (30 wt% in diethyl phthalate, DEP) with 100% PI-PS-UPy. (c) Temperature-dependent dynamic-mechanical measurements of two different organogels (20 wt% and 30 wt% in DEP) both containing 100% PI-PS-UPy. (d) Optical micrograph of a nanostructured organogel (30 wt% in DEP, 100% PI-PS-UPy) which was imprinted into micro-sized channels. D. Pirner, M. Dulle, M. E. J. Mauer and S. Förster, *RSC Adv.*, 2016, **6**, 42730. Adapted by permission of The Royal Society of Chemistry.

For detailed investigation the sample concentration was set to 20 wt% or 30 wt% of block copolymers (PI-PS, PI-PS-UPy or mixtures of both) in DEP providing gel-like materials. The influence of the hydrogen bonding group on the material characteristics could be observed by a visual transition of the samples from a fluid to a solid organogel with increasing UPy content. This remarkable phenomenon is based on the association/dissociation of the UPy groups and was intensively investigated *via* dynamic-mechanical measurements and SAXS. Dynamic-mechanical measurements give information about the macroscopic viscoelastic properties, whereas SAXS measurements provide structural parameters of the nanostructured gels. Consequently, by combining the two methods a detailed knowledge of the system and the structure-property relationship under shear and temperature was observed. Therefore, organogels with a continuous increase in UPy content were prepared mixing different weight fractions of PI-PS-OH (inactive chains) with PI-PS-UPy (active chains) within the range of 0-100 wt% of PI-PS-UPy. At room temperature all gels form highly ordered liquid crystalline phases. An

increase of the UPy content does not affect the structure of the micelles nor the ordered assembly, but leads to an increase of the storage modulus and to a solidification of the material. By performing temperature dependent measurements a melting temperature of the gels was observed which increases with higher UPy content and could be correlated to the UPy dimer lifetime (**Figure 2.1c**). Two mechanical models were developed where the molecular-/nano-scale information was combined with the macroscopic viscoelastic properties.

At temperatures between 55 °C and 65 °C the organogels melt into low-viscous solutions and undergo an order-disorder transition. Since the melting transition is reversible micro-sized shapes were prepared by micro-imprinting without using any additional crosslinking agent (**Figure 2.1d**).

The detailed knowledge and investigation of hydrogen-bonded reinforcement of ordered micellar assemblies resulted in the hierarchical build-up of thermoreversible organogels with a very well-defined nanoscale structure. Here, the influence of interaction forces between individual soft spherical micelles on the mechanical properties of close-packed assemblies was studied. This high-modulus, transparent, non-volatile organogels might be of high interest for *e.g.* micro-imprinting applications. In the next chapters these studies are further extended toward structure-property relationships on nanocomposites made from components with significantly different physical properties. The first step is to firmly control the stability of inorganic nanocrystals and prepare homogeneous nanocomposites, as discussed in the next chapter.

Chapter 5

Polymer ligand exchange to control stabilization and compatibilization of nanocrystals

In **Chapter 5**, a new approach toward polymer stabilized nanoparticles *via* a ligand exchange method was developed. This approach resulted in very high grafting densities above 1 nm⁻². These high grafting densities stabilize inorganic nanoparticles in solution and in bulk based on repulsive steric interactions. The attachment of polymer chains can be performed utilizing end-functionalized well-defined polymers, as well as, with commercial copolymers containing functional comonomers. The applicability of the ligand exchange method was successfully proven for many different types of

nanoparticles which were stabilized by different kinds of polymer chains. Furthermore, the variation of the molecular weight of the grafted polymer chains allowed controlling the interparticle distance. In addition, the ligand exchange method can be modified in order to obtain tailored assemblies of polymer-coated nanoparticles leading toward percolation networks with interesting feature properties.

The ligand exchange approach is based on thermodynamic considerations of the exchange of coordinative surface binding groups to the inorganic surface. The low-molecular weight ligands, which stabilize the nanocrystals directly from the synthesis were exchanged with polymer chains bearing suitable coordinative groups (end-functionalized or in the polymer backbone) resulting in polymer-stabilized core-shell nanoparticles or controlled nanoparticle assemblies (**Figure 2.2a**). In the first step of the ligand exchange procedure the nanocrystals, stabilized with a low-molecular weight ligand, are exposed to the polymer ligand chains which should be attached to the nanocrystals in the end. During the exchange procedure there is an equilibrium between four components: (I) the originally low-molecular weight bounded nanocrystals, (II) the polymer ligands, and (III) the original low-molecular weight ligand, (IV) the desired polymer-coated nanocrystals. The goal is to adjust the equilibrium to gain a high yield of polymer-coated nanoparticles. Therefore, three influencing parameters have to be considered based on the law of mass action: a large binding constant, large excess of the polymer ligand, and the removal of the originally bounded low-molecular weight ligand. The ideal binding constant could be found by referring to the hard/soft acid/base (HSAB) concept. However, the investigations revealed that the use of a moderate binding strength is more favorable, since a certain reversibility of surface coordination allows a chain relocalization and an attachment of a dense polymer brush on the inorganic surface.

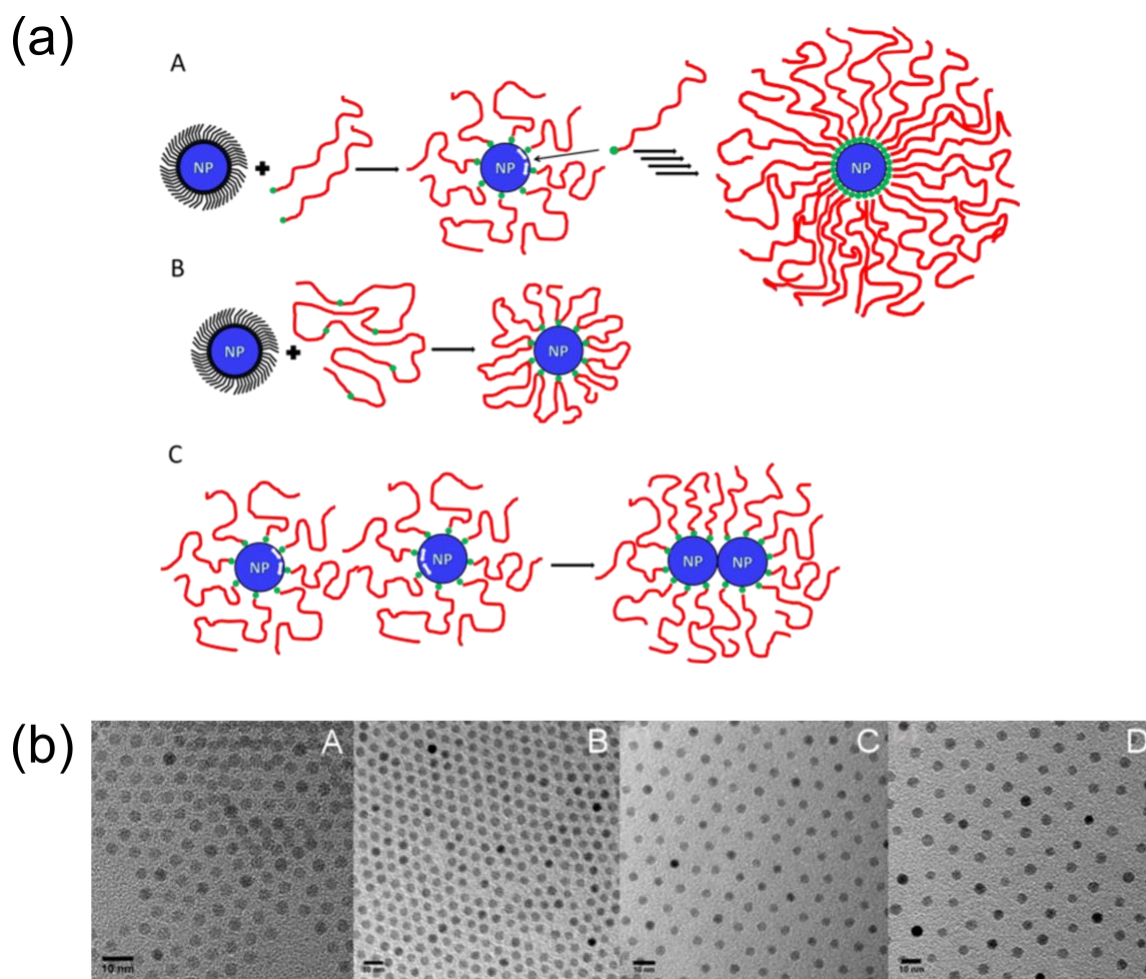


Figure 2.2: (a) Overview of different techniques to stabilize nanocrystals *via* ligand exchange: **A** Ligand exchange of low-molecular weight ligands with end-functionalized polymer ligands *via* a quantitative precipitation and subsequent selective precipitation resulting in densely coated nanoparticles. **B** Ligand exchange with a copolymer, bearing the coordinating groups in the backbone resulting in a flower-like attachment of the polymer layer. **C** Route toward controlled nanoparticle assemblies by lowering the stability of the polymer coated nanoparticles leading to a relocalization of the polymer chains. (b) TEM images of 5 nm Fe_3O_4 nanoparticles coated with **A** oleic acid, **B** 1000 g/mol, **C** 3450 g/mol, and **D** 8450 g/mol polystyrene. Interparticle distance in **B** is smaller than that of oleic acid (scale bar: 10 nm). Reprinted with permission from Ehlert, S.; Mehdizadeh Taheri, S.; Pimer, D. *et al ACS Nano*, 2014, 8 (6), pp 6114–6122. © 2014 American Chemical Society.

To prove the generality of this approach various polymers including polystyrene, polyisoprene, poly(methyl methacrylate) with different coordinating groups (carboxylic acid (-COOH), pentaethylenehexamine (-PEHA), diethylenetriamine (-DETA)) and many nanocrystals like Ag, CdSe, PbS, Fe_3O_4 , ZnO were studied. Based on the synthetic approach all prepared nanocrystals are originally coated with oleic acid. The subsequent ligand exchange was performed in common organic solvents like tetrahydrofuran (THF). Due to the thermodynamic considerations the exchange is divided into two important steps: quantitative precipitation and selective precipitation. In the first step a direct contact between the nanocrystals and the polymer was induced by coprecipitation of both, nanoparticles and polymer ligand. In the second step, the polymer excess and the free oleic acid was removed by selective precipitation of the coated nanoparticles. The

progression of the exchange was monitored by thermo gravimetric analysis (TGA), where high grafting densities compared to conventional grafting to approaches were observed. In addition, DLS measurements illustrate an increase in hydrodynamic diameter compared to the oleic acid stabilized nanoparticles.

Such nanoparticles with dense polymer shells have numerous advantages *e.g.* long-term stability of nanoparticles, compared to lower grafting densities. Usually, the as prepared Ag-nanoparticles start to aggregate after some weeks. After the attachment of a polymer shell *via* the ligand exchange procedure the Ag-nanoparticles showed long-term solution stability.

An additional feature of the developed ligand exchange method is the ability to precisely adjust the interparticle distance in a controlled fashion by variation of the molecular weight of the polymer ligands (**Figure 2.2b**). For instance, polystyrene coated iron oxide nanoparticles were prepared with a remarkable small distance of only 7.2 nm, which corresponds to a very high potential magnetic storage density of 12.4 Tb/inch².

Furthermore, the ligand exchange method allows controlled assembly of nanoparticles toward percolation networks (**Figure 2.2a**), which are interesting for electrical or thermal conductivity applications. In order to build such nanoparticle assemblies the stability of the polymer coated nanocrystals was reduced progressively by reducing the excess of polymer ligand. This could only be realized due to the non-covalent bonding of the polymer ligands resulting in a rearrangement of the polymer chains.

The precise preparation of well-defined polymer stabilized nanoparticles *via* ligand exchange resulted in a huge library of core-shell nanoparticles with different physical properties, as well as, controlled nanoparticle assemblies forming percolation networks. These building blocks are the fundamental subunits for the investigations in the following chapters. In the next chapter, the core-shell nanoparticles are used as fillers in transparent polymer matrices in order to build up highly filled, thin transparent nanocomposite films with new optical and mechanical characteristics.

Chapter 6

A general route to optically transparent highly filled polymer nanocomposites

In this work an efficient approach to incorporate nanoparticles into polymer matrices is presented resulting in transparent polymer films with enhanced mechanical properties and scratch resistance. Based on the previously introduced polymer ligand exchange method, highly miscible, homogeneous nanocomposite materials with high filling ratios of nanoparticles were produced. Usually this is challenging regarding the optical transparency of these systems. This is because at high filling ratios nanoparticles tend to form aggregates inducing turbidity and a loss in optical transmission and efficiency. In addition, incorporating nanoparticles into a polymer matrix allows for tuning the refractive index of the obtained material over a wider range than for pure polymers which are typically in the range of 1.3 to 1.7. Nanoparticles with high refractive index (*e.g.* TiO₂, ZrO₂, ZnS, and Si) as well as low refractive index nanoparticles (*e.g.* Au) can be added to a polymer matrix in order to generate new optical material properties and enter novel areas of application.

In order to prevent agglomeration upon phase transfer the nanoparticles were coated with a dense polymer brush. Commonly, the matrix and the coated polymers on the nanoparticle surface are the same type of polymer to ensure high compatibility. As a result an optical transmittance of up to 90% for nanoparticle weight fractions of up to 45 wt% could be achieved. The investigated systems include noble metal nanoparticles (Au, Ag), semiconductor nanoparticles (ZnO, CdSe, PbS), and magnetic nanoparticles (Fe₂O₃) which were incorporated into transparent polymer matrices such as poly(methyl methacrylate) (PMMA), polystyrene (PS), polyisoprene (PI), and poly(2-vinylpyridine) (P2VP). Theoretical considerations reveal that the intensity of transmitted light of a polymer nanocomposite film is strongly affected by the particle size. With increasing particle volume light scattering strongly increases following a power law. Scattering induces turbidity resulting in an upper feasible particle size limit of 40 nm. Consequently, for the following investigations nanoparticles in a size range of $R < 10$ nm, far below the theoretical limit, were used. Regarding this considerations nanoparticle aggregation will cause a significant increase in turbidity and has to be efficiently suppressed. Thus to ensure nanoparticle stability relatively high grafting densities resulting in a dense brush

are applied. In this high grafting density range complete thermodynamic miscibility of the nanoparticles within the polymer matrix is realized. In **Figure 2.3a** several different transparent nanocomposite films with a film thickness of 100-250 μm are illustrated.

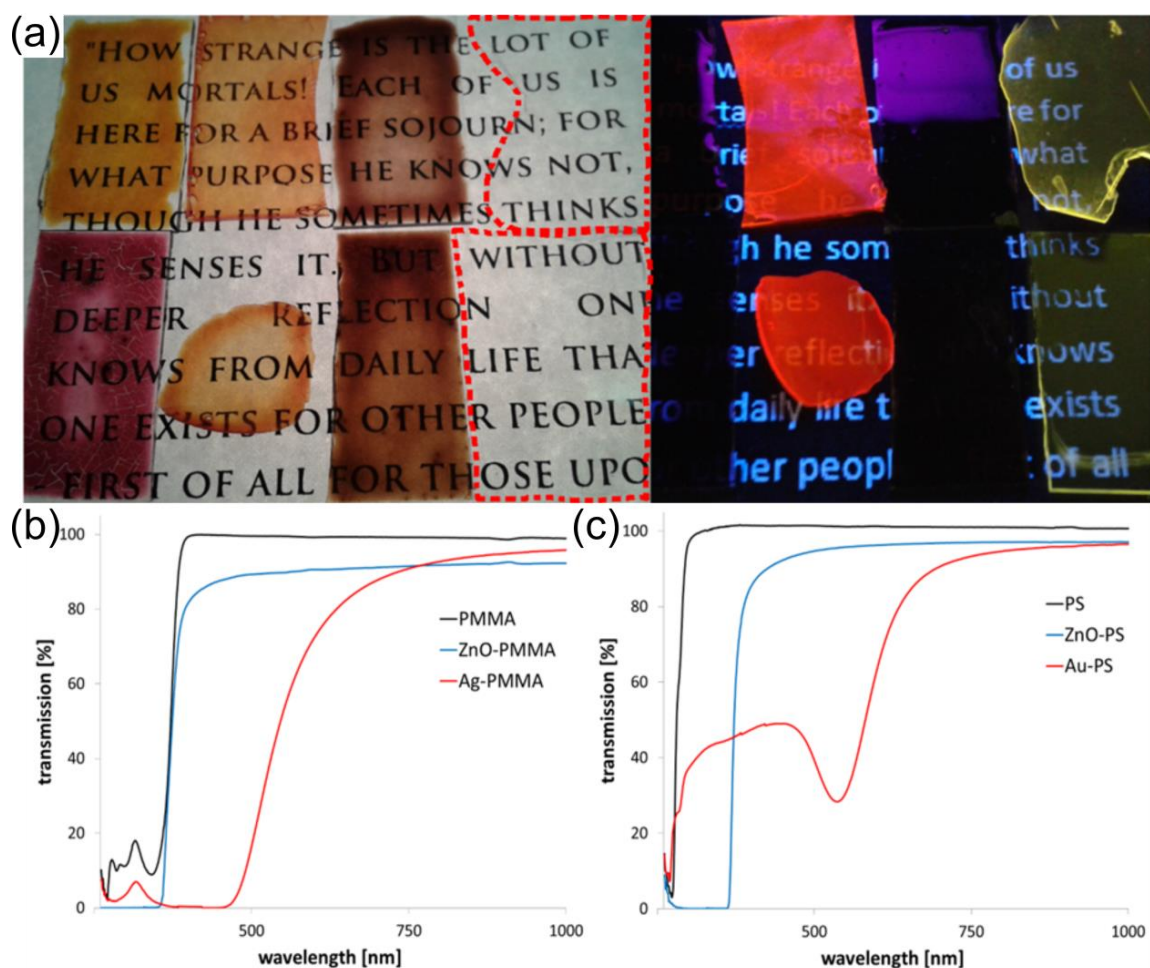


Figure 2.3: (a) Left panel: photographs of transparent nanocomposite films (150 μm) on glass. Upper row: Ag-PMMA (100 μm , 2 wt %), CdSe-PMMA (200 μm , 10 wt %), PbS-PI (10 wt %), and free-standing ZnO-PMMA (250 μm , 10 wt %). Lower row: Au-PS (100 μm , 2 wt %), freestanding CdSe-PS (100 μm , 29 %), Fe_2O_3 -P2VP (5 wt %), and ZnO-PS (150 μm , 45 wt %). The dashed red lines indicate the sample positions of the ZnO-PMMA and ZnO-PS films. Right panel: fluorescence of the same nanocomposites at UV illumination. (b) UV/vis spectra for nanocomposites with (A) PMMA and (B) PS matrices and different nanoparticles (Ag 5 wt %, Au 10 wt %, ZnO 10 wt % in PMMA, and 45 wt % in PS) showing 90-95 % transparency at high loading ratios in the wavelength range above the absorptions edges of ZnO or above the plasmon resonance of Ag and Au. Film thickness is 250 μm for all samples except Ag-PMMA and Au-PS which are 100 μm . Reprinted with permission from Ehlert, S.; Stegelmeier, C.; Pirner, D. *et al Macromolecules*, 2015, 48 (15), pp 5323–5327. © 2015 American Chemical Society.

The represented films were prepared *via* solvent casting on glass slides resulting in optically transparent films of Ag-PMMA, CdSe-PMMA, PbS-PI, Au-PS, Fe_2O_3 -P2VP, ZnO-PS, ZnO-PMMA, and CdSe-PS with a high nanoparticle weight fraction of up to 45 wt%. The nanocomposites constructed of Ag and Au nanoparticles exhibit strong absorption caused by plasmon resonances. Consequently, these nanocomposites were prepared with lower weight fractions of 2 wt% nanoparticles to reach optical transparency in the visible range. Additionally, the nanocomposite films containing CdSe and ZnO

semiconductor particles showed fluorescence upon UV illumination. In **Figure 2.3b** the corresponding UV/vis spectra of the nanocomposites is presented which clearly show transmission of 90-95 % for all systems in combination with characteristic absorption in specific wavelength ranges for the different nanoparticle types. Furthermore, the mechanical properties of PMMA for ZnO/PMMA nanocomposites could be improved, significantly. The elastic modulus increased from 10 GPa to 23 GPa for a weight fraction of 5%, and even to 35 GPa for 10 wt% of nanoparticles. The scratch resistance of these nanocomposites is increased considerably, very important for potential optical applications.

Consequently, a general route toward transparent nanocomposite films using the example of a variety of different systems was demonstrated. The complete miscibility of nanoparticles in the polymer matrix represents the essential point only obtained for complete suppression of any nanoparticle agglomeration. With the incorporation of various different types of nanoparticles (Ag, Au, CdSe, ZnO, Fe₂O₃, and PbS) in a considerable number of polymers (PMMA, PI, PS, and P2VP) the optical and mechanical properties of the generated nanocomposite films can be tuned and tailored for remarkable high filling ratios.

Besides potential applications of thin polymer nanocomposite films, the following chapter deals with the detailed study of the polymer chain dynamics in such nanocomposites. The structure-property relationship of well-stabilized nanocrystals in polymer matrices, as well as, controlled nanoparticle assemblies is discussed.

Chapter 7

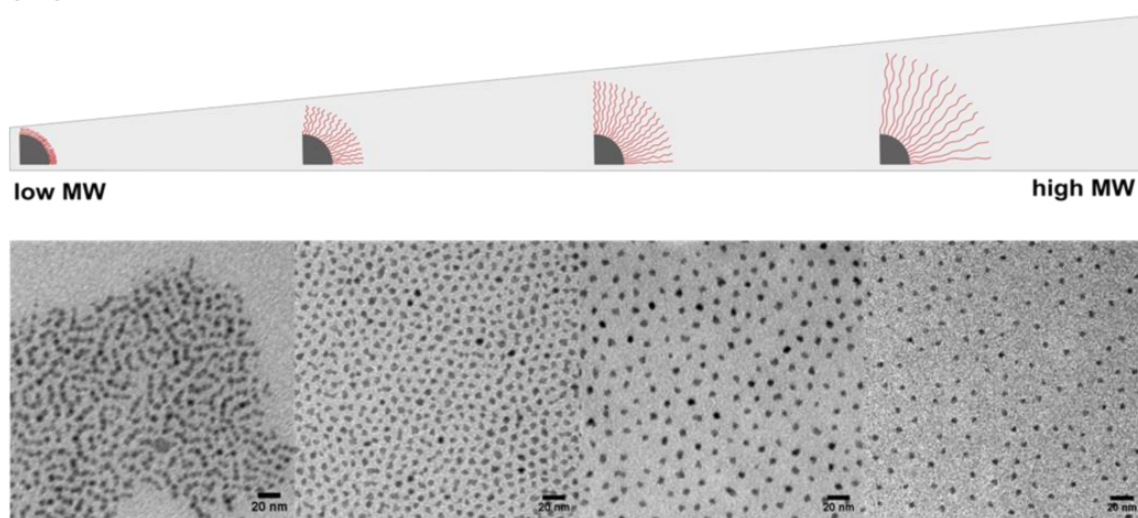
Rheological study of polymer nanocomposites: Influence of nanoparticles on polymer chain dynamics

In this work the polymer chain dynamics of polymer nanocomposites were investigated using PbS-polyisoprene nanocomposites as a model system. The incorporated nanocrystals were coated with polyisoprene chains in order to render them highly miscible in the polyisoprene matrix and to avoid aggregation of the particles. Therefore, the previously introduced ligand exchange approach (**Chapter 5**) was used to generate a relatively high grafting density of polymer chains on the nanoparticle surface.

The aim was to gain detailed insights into the influence of the nanofiller weight fractions on the mechanical properties of the prepared nanocomposites and additionally the

influence of the molecular weight of the attached polymer chains. Thus, the polymer chain length was tuned from low molecular weight of 1.7 kg/mol up to high molecular weight of 58 kg/mol. The structure of the coated nanoparticles and the nanocomposites was characterized applying transmission electron microscopy (TEM) and SAXS. Increasing the molecular weight of the polymer brush layer, an increasing in the layer thickness was observed result in a specific interparticle distance control of the bulk materials (see **Figure 2.4a**).

(a)



(b)

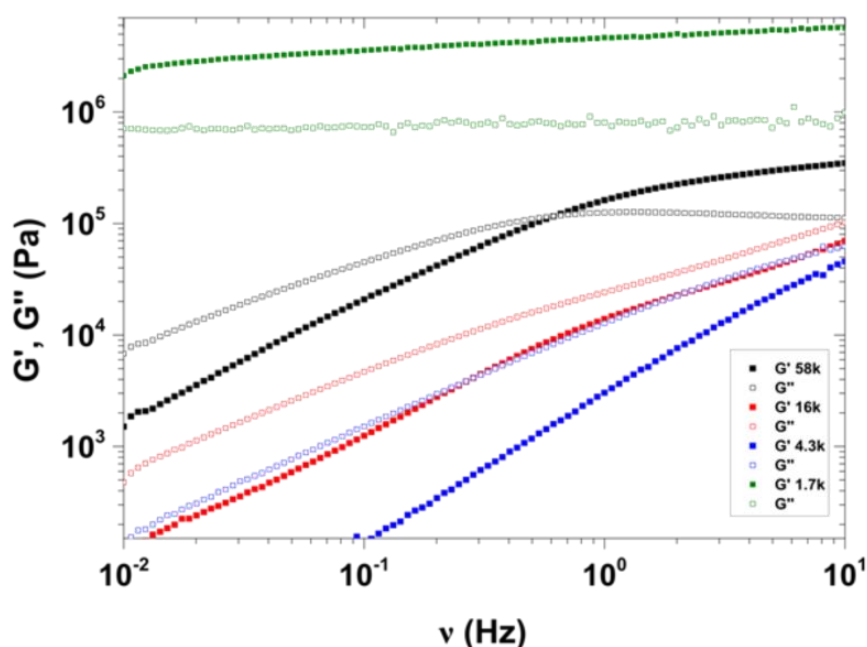


Figure 2.4: (a) Scheme and TEM images of polyisoprene stabilized PbS nanoparticles with different molecular weights of polymer from 1.7k to 58k: With decreasing molecular weight the distance between the particles decreases until a limitation of stabilization occurs at very low molecular weights. (b) Storage modulus G' (closed squares) and loss modulus G'' (open squares) of PbS@PI-X nanoparticles as a function of frequency with varying molecular weights from 1.7 k/mol to 58 k/mol at 10 °C.

In order to study the influence of particle loading, dynamic-mechanical measurements of PbS@PI-58k core-shell nanoparticles in a polyisoprene matrix with a molecular weight of 58 kg/mol were performed. As a result, a characteristic retardation of the polymer chain relaxation with increasing particle loading compared to the neat polyisoprene was observed, which was indicated by an increase of the moduli in the terminal flow.

In **Figure 2.4b** the dynamic-mechanical analysis of four different pure core-shell PbS-polyisoprene nanoparticles with varying molecular weights are shown. Decreasing the molecular weight of the polyisoprene from 58 kg/mol to 4.3 kg/mol does not lead to a solid-like response. Consequently, the densely grafted polyisoprene-PbS nanoparticles are well-stabilized and aggregation effects are absent even in the pure core-shell nanoparticle systems (without additional matrix polymer).

The nanofillers coated with polyisoprene with a molecular weight of 1700 g/mol represent a special type of system. Here, the nanoparticles are not isolated as single spherical particles but rather form controlled nanoparticle assemblies similar to nanochains. These nanoparticle assemblies consist of two to six aggregated nanoparticles, which are nevertheless well-stabilized with polyisoprene as clusters and therefore miscible in the matrix without secondary aggregation. The mechanical analysis of the neat nanochains provides a strong reinforcement effect and a solid-like response (**Figure 2.4b**). The driving force is the formation of interconnected structures due to the anisotropic structure of the nanochains. The nanochains arrange in a network which is only shielded by a thin polymer layer leading to a strong interaction between the particles. The storage and the loss modulus become almost parallel over the accessible frequency range. This could be explained by the direct correlation between the mechanical behavior and the local structure.

Consequently, this chapter focuses on the structure-mechanical property relationship of PbS-PI nanocomposites containing PI coated PbS nanoparticles prepared according to the introduced ligand exchange method in **Chapter 5**. A good dispersibility of the nanofillers in the matrix was obtained. This implies that aggregation effects are absent even for very high filler rates. In addition, controlled nanoparticle assemblies were investigated, which had to be considered as special case due to their anisotropic character. Here, a strong reinforcement of the material was observed based on network formation. The mechanical properties of nanocomposites are strongly dependent on the interactions in the system. The structure of the fillers has a great influence on the mechanical response.

Contribution to joint publications

The publications contained in this thesis were prepared in collaboration with other co-authors listed below. The individual contributions of the involved researchers are described.

* Denotes the corresponding author.

Chapter 4

This work has been published in *RSC Advances* 6, pp. 42730-42738 (2016) under the title:

“Reinforcement of nanostructured organogels by hydrogen bonds”

*By Daniela Pirner, Martin Dulle, Miriam E. J. Mauer, and Stephan Förster**

I performed the syntheses, sample preparation, the characterization and wrote the manuscript. Martin Dulle performed the SAXS measurements and was involved in scientific discussions. Miriam E. J. Mauer performed cryo-SEM. Stephan Förster was involved in scientific discussions, wrote parts of the manuscript and corrected the manuscript.

Chapter 5

This work has been published in *ACS Nano* 8, pp. 6114-6122 (2014) under the title:

“Polymer ligand exchange to control stabilization and compatibilization of nanocrystals”

*By Sascha Ehlert, Sara Mehdizadeh Taheri, Daniela Pirner, Markus Drechsler, Hans-Werner Schmidt, and Stephan Förster**

I synthesized and end-functionalized the polyisoprene, performed the ligand exchange on nanocrystals and was involved in scientific discussions (contribution 30%). Sascha Ehlert performed the syntheses of nanoparticles and the ligand exchange, and wrote the manuscript. Sara Mehdizadeh Taheri synthesized the iron oxide nanoparticles. Markus

Drechsler was involved in scientific discussions. Hans-Werner Schmidt was involved in scientific discussions. Stephan Förster was involved in scientific discussions, wrote parts of the manuscript and corrected the manuscript.

Chapter 6

This work was published in *Macromolecules* 48, pp. 5323-5327 (2015) under the title:

“A general route to optically transparent highly filled polymer nanocomposites”

*By Sascha Ehlert, Corinna Stegelmeier, Daniela Pirner, and Stephan Förster**

I synthesized and end-functionalized the polyisoprene, performed the ligand exchange and was involved in scientific discussions (contribution 30%). Sascha Ehlert performed the syntheses, sample preparation and sample characterization and wrote the manuscript. Corinna Stegelmeier synthesized the P2VP-iron oxide nanocomposite. Stephan Förster was involved in scientific discussion, wrote parts of the manuscript and corrected the manuscript.

Chapter 7

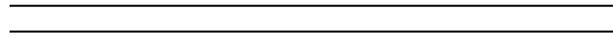
This work will be submitted under the title:

“Rheological study of polymer nanocomposites: Influence of nanoparticles on polymer chain dynamics”

*By Daniela Pirner, Martin Dulle, and Stephan Förster**

I performed the syntheses, sample preparation, in combination with all characterizations and wrote the manuscript. Martin Dulle performed the SAXS measurements and was involved in scientific discussions. Stephan Förster was involved in scientific discussions, wrote parts of the manuscript and corrected the manuscript.

3



Theory

3.1 Anionic Polymerization

The fabrication of well-defined functional colloidal building blocks based on polymers, such as micelles or hybrid materials consisting of inorganic nanoparticle-polymer associations, requires subunits of high quality and low polydispersity. In the case of polymer nanostructures the subunits are individual polymer chains forming complex structures on the next level of hierarchy. The polymer chain architecture itself can be classified into topology (*e.g.* linear, ring-shaped, branched), composition (*e.g.* homopolymer, block copolymer), functionality (*e.g.* end-functionalized, telechelic), molecular weight distribution, and microstructure, respectively.¹ In addition, the type of repeating unit and the overall molecular weight influences the properties of the macromolecules.¹ The synthesis of well-defined polymer chains with narrow molecular weight distribution can be realized by controlled polymerization techniques.²⁻⁴ The basic principle of these techniques is the efficient suppression of termination and transfer reactions during polymerization.³ In addition to controlled radical polymerization methods, *e.g.* atom transfer radical polymerization (ATRP),⁵ reversible addition-fragmentation chain-transfer polymerization (RAFT),⁶ and nitroxide mediated radical polymerization (NMP),⁷ living anionic polymerization is a powerful tool for the precise synthesis of polymers with extremely narrow size distribution. However, this technique comes along with several challenges, especially related to the purity of applied reagents and some limitations with respect to solvents, and monomers. Nevertheless, compared to other synthesis strategies based on radical initiation, anionic polymerization offers many advantages which are not simple to implement with radical polymerization techniques, such as sequential synthesis of block copolymers or quantitative end-functionalization of the polymer chains by controlled termination.³

In general, anionic polymerization is a chain growth polymerization and can be initiated by Brønsted or Lewis bases such as organometallic bases.³ The reactivity of monomers is dependent on the ability of the substituent to stabilize the carbanion (**Figure 3.1**).⁸ Thus, vinyl compounds are the most prominent monomers polymerized *via* “living” anionic polymerization due to their electron attracting substituents or strong delocalization.³

$\text{H}_2\text{C}=\text{CHX}$ with X:

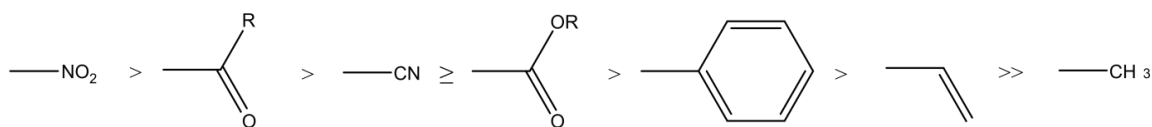
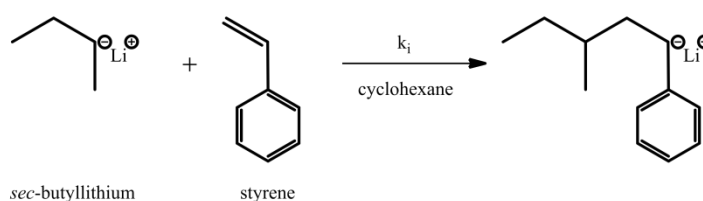


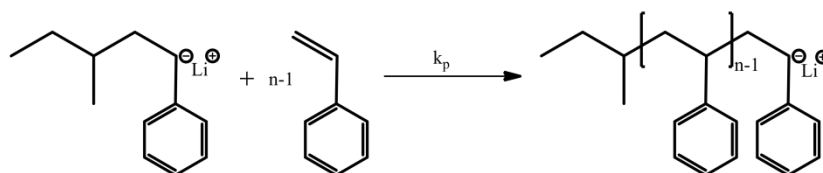
Figure 3.1: Reactivity of different vinyl monomers depending on the stabilizing substituents.⁸

The chain growth polymerization is separated in three steps: initiation, propagation, and termination.³ In **Figure 3.2** a typical anionic polymerization is illustrated using *sec*-butyllithium as initiator and styrene as monomer.³

Initiation:



Propagation:



Termination:

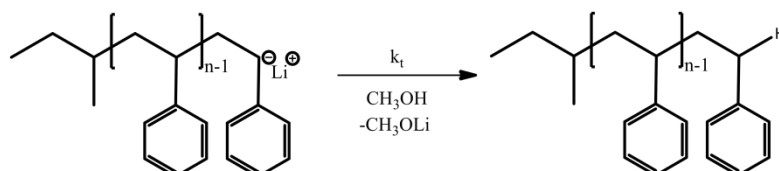


Figure 3.2: Reaction scheme of a typical anionic polymerization in cyclohexane using *sec*-butyllithium as initiator and styrene as monomer. Initiation takes place with a rate constant of initiation k_i , propagation with a rate constant of propagation k_p , and termination with a rate constant of termination k_t , respectively.³

The nucleophilicity of the initiator needs to be equal or higher than the electrophilicity of the monomer to facilitate polymerization.³ Furthermore, the reactivity of the initiator is strongly dependent on the ionic radius of the counterion ($\text{K}^+ > \text{Na}^+ > \text{Li}^+$) and the solvent polarity (THF > toluene).³

In addition, the high nucleophilicity of the initiator leads to special considerations for experimental procedures. To avoid spontaneous termination, it is absolutely necessary to work under inert atmospheric conditions and thoroughly remove oxygen, water, and

protic impurities.³ Moreover, the initiation is required to be much faster than the chain propagation in order to ensure a narrow molecular weight distribution of the product.³ Kinetics of the anionic polymerization of styrene was first investigated in a fundamental work by M. Szwarc^{9,10} in 1956. The rate of polymerization R_p was found to linearly depend on the rate constant of propagation k_p , the monomer concentration $[M]$, and the concentration of active chains $[P^*]$ (**equation 3.1**).³

$$R_p = -\frac{d[M]}{dt} = k_p \cdot [M] \cdot [P^*] \quad (3.1)$$

Since, no termination is present, the concentration of active chains is constant and equal to the initiator concentration.³ This consideration leads to a pseudo first-order relation with an apparent rate constant k_{app} being the slope of the first-order plot and $[M]_0$ as monomer concentration at $t = 0$ (**equation 3.2**).³

$$\ln \frac{[M]_0}{[M]_t} = k_p \cdot [P^*] \cdot t = k_{app} \cdot t \quad (3.2)$$

In addition, no transfer reactions are present during such an ideal polymerization.³ Therefore, the total number of polymer chains $[P]$ is constant with increasing conversion x_p during polymerization (**equation 3.3**).³ Here \bar{P}_n represents the degree of polymerization.

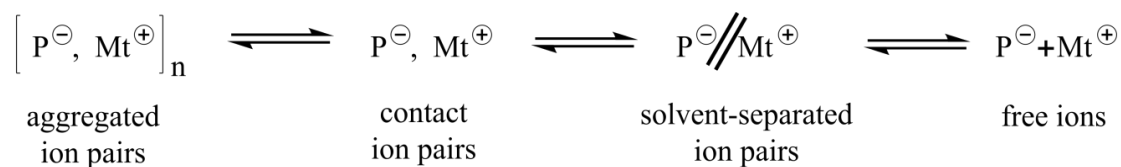
$$\bar{P}_n = \frac{[M_0] - [M_t]}{[P]} = \frac{[M_0]}{[P]} \cdot x_p \quad (3.3)$$

Consequently, anionic polymerization provides linear growth of the polymer chains resulting in a narrow molecular weight distribution characterized by a Poisson distribution.³ The polydispersity index (PDI) is defined by **equation 3.4**.³

$$PDI = \frac{\overline{M}_w}{\overline{M}_n} \approx 1 + \frac{1}{\bar{P}_n} \quad (3.4)$$

The mechanism of polymerization depends on solvent, temperature, concentration, and counterion affecting the state of the present anion R^- and its association with the counterion Mt^+ .³ In **Figure 3.3** possible ion pairs in a polar solvent as a function of concentration are illustrated based on equilibrium conditions for aggregated ion pairs, contact ion pairs, solvent-separated ion-pairs and free anions.³ Each state is defined by a

specific rate constant and by an individual propagation rate constant ($k_{\pm,c}$, $k_{\pm,s}$, and k_-).³ The propagation rate constant of the free anion state k_- is larger than the propagation rate constant of the solvent-separated state $k_{\pm,s}$ and significantly larger than the propagation rate constant of the contact ion pair $k_{\pm,c}$.³



high concentration

low concentration

Figure 3.3: Ion pairs in polar solvent in dependency on concentration. P⁻: active polymer chain; Mt⁺: counterion.³

In non-polar solvents, like cyclohexane, the polymerization mechanism is characterized by a two-state mechanism and equilibrium conditions for aggregated ion pairs and contact ion pairs.³ In this case, monomer addition only takes place in the ion pair state. Therefore, addition of solvating agents like tetrahydrofuran (THF) might be useful to break up aggregated ion pairs.³

Anionic polymerization can be utilized to build-up copolymers consisting of different monomers sequentially and in controlled manner.³ Copolymerization of different types of monomers leads to an extension of polymer architectures and properties. In **Figure 3.4** the different types of common copolymers are illustrated: alternating, statistical (random), graft and block copolymers.¹¹

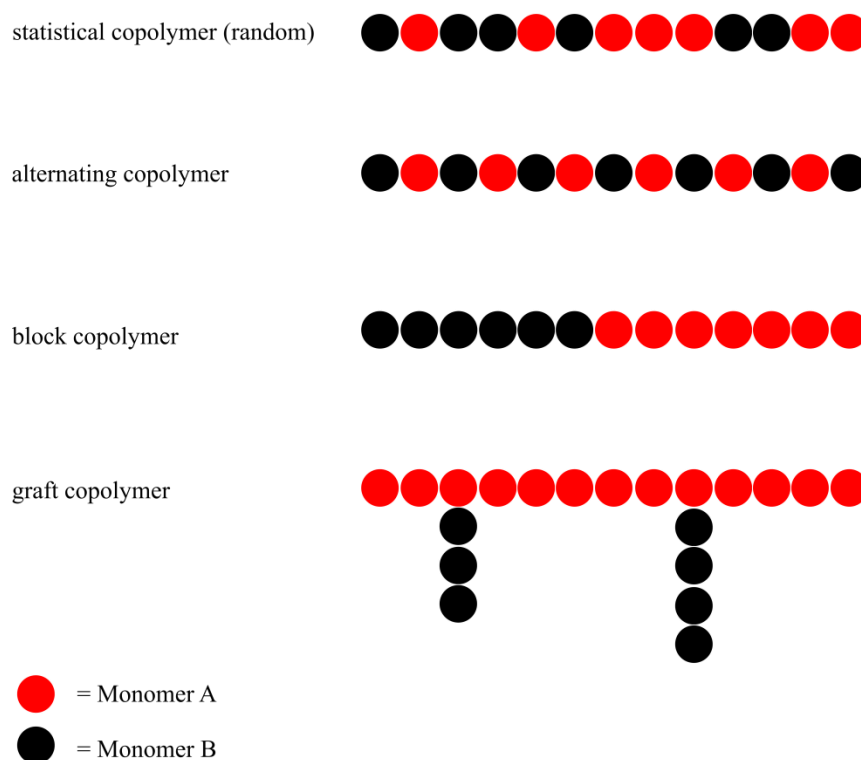


Figure 3.4: Classes of copolymers with two different types of monomers (A (red) and B (black)): statistical (random) copolymer, alternating copolymer, block copolymer, and graft copolymer.

Especially linear AB block copolymers are an interesting class of copolymers due to their amphiphilic character that facilitate the construction of *e.g.* micelles *via* self-assembly methods (see **Chapter 3.3**). On the basis of the absence of termination and transfer reactions, anionic polymerization is very suitable for the controlled synthesis of block copolymers.³ Thus, block copolymers can be achieved by sequential addition of monomers. After complete polymerization of the first monomer A, the second monomer B is added and the propagation proceeds until the monomer molecules are consumed.¹² However, there are some requirements and conditions for a successful sequential synthesis of block copolymers: I) the carbanion of the first polymerized monomer A must be able to initiate the second monomer B.¹² Consequently, the carbanion of the monomer A has to be a stronger nucleophile than monomer B.¹² II) The initiation of monomer B by the anion of monomer A has to be faster than the chain propagation of monomer B in order to ensure a narrow molecular weight distribution of block B and, additionally, the absence of any homopolymer chains from A.¹² III) In order to prevent termination of the living A chains monomer B must not contain any impurities.¹² Otherwise, terminated homopolymer chains from A are produced accompanied by a loss in control of composition of the whole copolymer.¹²

A prominent example for a sequentially synthesized block copolymer is poly(isoprene-*block*-styrene), which can be initiated by *sec*-butyllithium in polar or nonpolar solvents.¹² Polymerization of dienes such as isoprene leads to polymers with different proportions of *cis*-1,4-, *trans*-1,4-, 1,2- or 3,4-isomers (**Figure 3.5**).¹² The composition and microstructure is influenced by the solvent, type of counterion, temperature, and concentration affecting the state of ions in solution.^{3,13} Polymerization in hydrocarbon solvents provides high *cis*-1,4 contents. In contrast, for polar solvents a mixture of 1,4-, 3,4-, and 1,2- microstructures is obtained.¹⁴

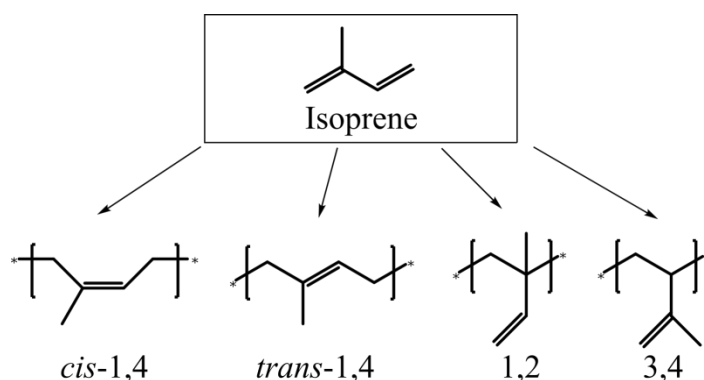


Figure 3.5: Types of microstructures obtained for polyisoprene depending on the polymerization characteristics.^{3,14}

Several kinds of well-defined, narrow distributed polymers (*e.g.* homopolymer or block copolymers) with various properties can be synthesized *via* anionic polymerization.³ Additionally, appropriate functionalization of the polymers, such as living end capping, and post-modifications, provide an even greater number of diversity for various applications discussed in the following chapters.

3.2 End-functionalization of Polymers

The incorporation of special functionalities into linear, narrow distributed polymer chains (*e.g.* homopolymers or diblock copolymers) leads to polymers with tailorable features. Such polymers can serve as building blocks for hierarchical self-assembly of complex structures with unique properties, such as special optical response,^{15–17} thermosensitivity^{17–20} or changes in mechanical properties,^{17,18,21–24} amongst others.

Well-defined and narrow distributed polymers can be synthesized *via* anionic polymerization techniques, described in **Chapter 3.1**. This polymerization method allows

the direct introduction of functionalities by using functional initiators or by termination with suitable electrophiles such as cyclic ethers, and carbonyl or silyl compounds.²⁵ Ethylene oxide is a well-known example of the class of cyclic ethers utilized as termination agent in anionic polymerization. The addition of ethylene oxide to the living carbanion and the subsequent protonation provides a quantitative yield of a hydroxylated end group.²⁶

Subsequently, the end group can be further functionalized *via* polymer analogues reactions as described in the following subchapters resulting in *e.g.* the introduction of coordinating groups at the polymer chain end, which results in polymer chains that can be used to bind on nanoparticle surfaces (**Chapter 5, 6, 7**) or the OH-group can efficiently react with isocyanates to introduce functional derivatives such as hydrogen bonding groups that serves as linker in thermoreversible soft colloidal networks (organogels) (**Chapter 4**).

3.2.1 Coordinating Groups

Polymer-stabilized inorganic nanoparticles are of great interest for various industrial applications, *e.g.* for the preparation of tailored nanocomposites, inducing enhancement in mechanical,²⁷ optical,²⁸ or electrical properties.²⁹ Polymers are able to adhere selectively to inorganic nanoparticles, if they are bearing specific highly absorbing segments that can coordinate or bind to inorganic surfaces. These functionalities can be located at the chain ends or can be a part of the monomer units resulting in the controlled synthesis or/and assembly of organic-inorganic, hybrid colloids.³⁰

Pearson's hard-soft acid-base (HSAB) principle can assist to choose the right functional groups for improving the polymer-metal bonding.³¹ It is based on the Lewis acid-base theory. The acid-base interactions play a key role in the adsorption, and adhesion of polymers to inorganic substrates or nanoparticles. In principle, an acid-base or donor-acceptor interactions can be described as an interaction between an acid (acceptor), having a positive electron affinity, and a base (donor) bearing a lone electron pair that can be shared in a chemical reaction.³² The HSAB theory considers the differences in electronegativity and polarizability of the polymer and metal, whereby they can be divided into soft acids, hard acids, and soft bases, hard bases, but also in border line acids and bases.³² The term "hard" and "soft" is related to difference of the materials' highest

occupied molecular orbital (HOMO) energy and the lowest unoccupied molecular orbital (LUMO) energy.³³

The chemical hardness η was introduced by Pearson as shown in the following **equation 3.5**,³¹

$$\eta = -\frac{1}{2}(E_{HOMO} - E_{LUMO}) \quad (3.5)$$

On the other hand the average energy gap E_g^{Av} is used to determine the value of gap separation between E_{HOMO} and E_{LUMO} (**equation 3.6**).³¹

$$E_g^{Av} = -(E_{HOMO} - E_{LUMO}) \quad (3.6)$$

Combining **equation 3.5** and **equation 3.6** equation **3.7** follows as,³¹

$$\eta = \frac{1}{2}E_g^{Av} \quad (3.7)$$

Consequently, the chemical hardness is directly correlated to the energy band gap.

Therefore, metals are classified as soft substances having a small band gap, whereas polymers are hard being insulator with a large band gap. Regarding this the HSAB theory concludes a simple assumption: all metals are soft, and mostly acids, for example Cd^{2+} , Au^0 , Ag^0 , Fe^{2+} , Pb^{2+} , or Zn^{2+} are borderline acids. Polymers can be bases (*e.g.* polymers with aromatic compounds like polystyrene)³², acids (*e.g.* halogenated polymers like polyvinylchloride)³² or neutral materials (*e.g.* polyethylene) and are hard.³¹ Only substances with similar “hardness” can bind with each other. Consequently, hard acids prefer to bond to hard bases, and soft acids bond to soft bases.³⁰ Therefore hard polymers are only able to bind to soft metals if they are bearing functional groups that change the bonding energy and lead to a softening.³³

Typical functional groups located at the chain end are, *e.g.* carboxyl groups (-COOH), thiols (-SH), or amines (-NH₂). Well-defined polymers synthesized *via* anionic polymerization can be easily functionalized by selective termination of the living chain-end with suitable molecules (**Figure 3.6**).²⁵

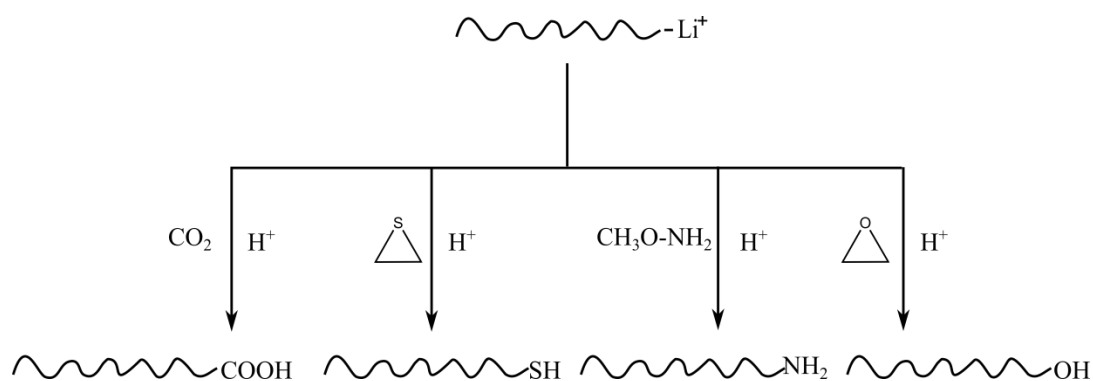


Figure 3.6: Examples for end-functionalization of living polymer chains within anionic polymerization. Synthesis of -COOH, -SH, -NH₂, and -OH end groups based on appropriate chemistry.²⁵

Polymers with carboxylic end groups can be obtained by using carbon dioxide (CO₂) as termination agent.^{25,34–36} Thiol groups can be introduced with ethylene sulfide,³⁷ and amine groups *via* termination with amines *e.g.* methoxyamine.³⁸ Additionally, hydroxylated groups can be generated by adding ethylene oxide to the living chain end. This groups can be further modified to yield *e.g.* amines bearing three (diethylenetriamine, DETA), or six (pentaethylenhexamine, PEHA) amine groups, enhancing the strength of attractive interaction toward nanoparticles compared to single amine groups (**see Chapter 5**). Amine functionalized polymers can be synthesized based on an activation step of the terminal OH-group using an imidazole ester followed by coupling with multi-dentate amines (**Figure 3.7**).³⁹

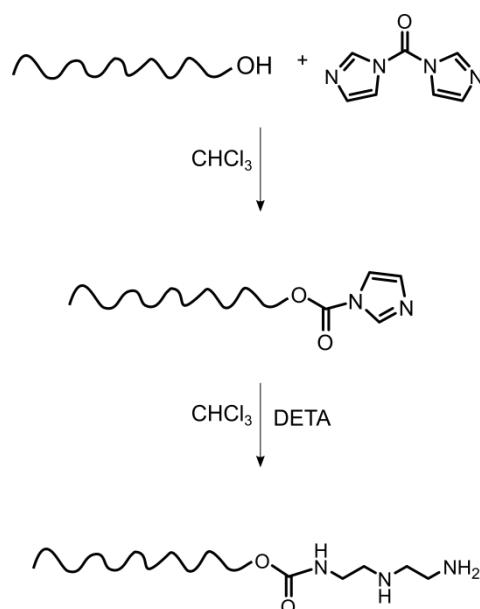


Figure 3.7: Functionalization steps toward multi-dentate amine groups. Activation of the OH-group with 1,1'-carbonyldiimidazole (CDI) and subsequent coupling with diethylenetriamine (DETA).

In order to gain sufficient steric stabilization of nanoparticles a dense polymer brush layer is necessary. Therefore, using functional groups with moderate binding is favorable

compared to high binding strength. The polymer ligand chains can coordinate and decoordinate in a reversible manner to the inorganic surface which allows relocalization of the chains leading to an increase in brush density (see **Chapter 5**).³⁹

3.2.2 Hydrogen Bonding Groups

Inspired by nature the tether of a hydrogen bonding group to a molecule or macromolecule as building block opens up new possibilities for material design and self-assembly processes into organized complex structures.⁴⁰ Most hydrogen bonding molecules are based on modified heterocyclic components to mimic the pattern found in DNA. Besides π - π stacking, electrostatic and hydrophobic interactions, the double helical structure of DNA is formed *via* hydrogen-mediated self-assembly.⁴⁰ Hydrogen bonds play an important role in supramolecular chemistry to build-up functional materials. They are described as an attractive electrostatic interaction of a net dipolar moment between polar molecules or within an individual molecule containing polar groups.⁴⁰ Thus, hydrogen bonds can either act intramolecular or intermolecular. To provide a strong net dipolar moment, hydrogen (H) has to be bound to an electronegative atom such as nitrogen (N), oxygen (O), or fluorine (F).⁴⁰ In principle hydrogen bonding is based on a donor acceptor relationship where hydrogen is the donor and the acceptor is an electronegative opponent. O and N atoms provide the strongest and most robust hydrogen bonds. In supramolecular chemistry, they are most often used in the form of amides or urea derivatives to achieve stable structures. A hydrogen bond can be strong (63-167 kJ/mol), moderate (17-63 kJ/mol) or weak (<17 kJ/mol)⁴¹ and is defined in terms of bond energy which can be expressed by the enthalpy (**equation 3.8**).⁴⁰ Consequently, they cover an intermediate range of bonding strength compared to covalent bonds (200-800 kJ/mol, strong)⁴² and Van der Waals interactions (0.5-5 kJ/mol, weak).

$$\Delta G = \Delta H - T\Delta S = -RT\ln K_a \quad (3.8)$$

The entropy ΔS is always negative due to the loss of freedom during hydrogen bond formation and increases with tightening of the two interacting molecules. In solution the strength of the intermolecular hydrogen bond is reflected by the association constant K_a and is strongly affected by the solvent.⁴⁰ The solvent molecules can form hydrogen bonding by themselves like dimethylformamide (DMF), which is a strong hydrogen

bonding acceptor and can weaken or completely suppress the hydrogen bonding between dissolved molecules. In addition, polar protic solvents like water or methanol behave as both donor and acceptor and compete with the hydrogen bonding molecules. Consequently, the choice of solvent is very important and can influence the binding effects.⁴⁰

Stronger interactions between molecules, compared to single hydrogen bonds, can be realized by increasing the number of hydrogen bonds between the components by using functional groups with an array of hydrogen bonding sites.⁴³ This results not only in an increase of the strength but also in a higher degree of specificity.⁴⁴ For example quadruple hydrogen bonding motifs based on 2-ureido-4[1H]pyrimidinones (UPy) have gained increasing attention in supramolecular self-assembly due to their strong (but reversible) and self-complementary hydrogen bonding which allows the formation of supramolecular polymers.^{40,43,44} In **Figure 3.8a** a scheme of dimers formed by a linear array of four hydrogen bonding sites is presented. The particular arrangement of neighboring donor (D) and acceptor (A) sites is an additional factor which significantly affects the strength of complexation.

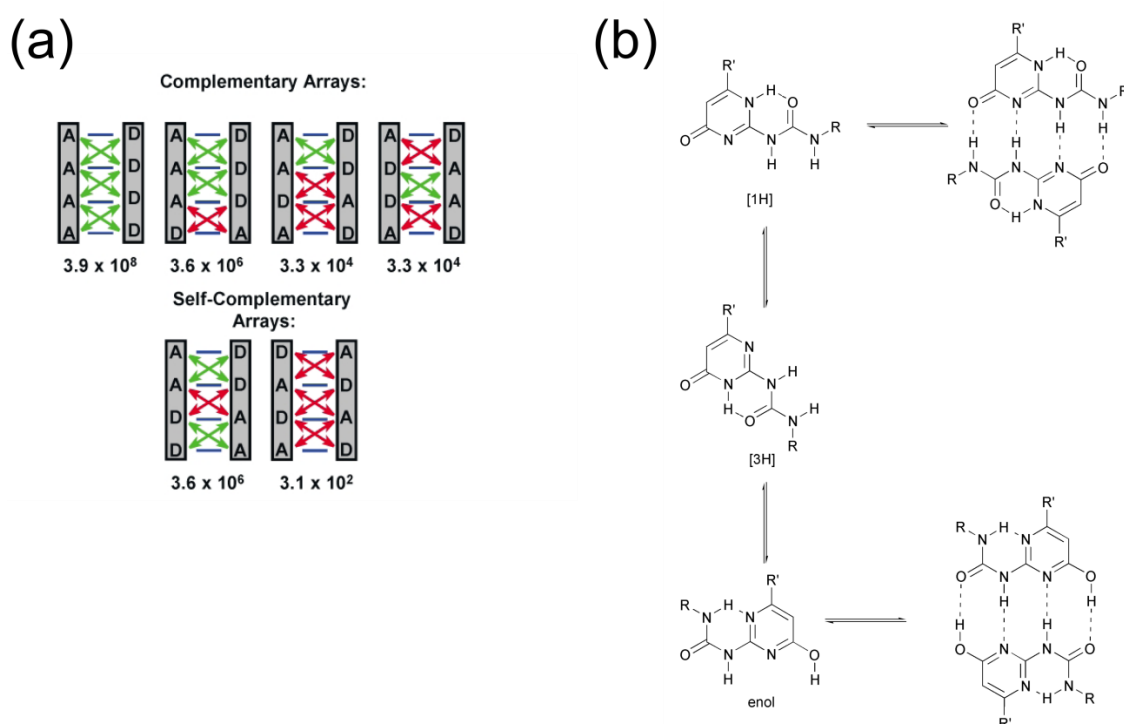


Figure 3.8: (a) Scheme of dimers formed by a linear array of four hydrogen bonding sites (green: attractive interactions, red: repulsive interactions), and their predicted stability constants (in M^{-1} in $CDCl_3$). (b) Equilibrium between monomers and dimers of the three tautomeric forms of ureidopyrimidinones (UPy).⁴⁵ Adapted from R. P. Sijbesma and E. W. Meijer, *Chem. Commun.*, 2003, 5 with permission from The Royal Society of Chemistry.

In the case of four hydrogen bonding sites six different types of quadruple hydrogen bonded dimers are possible (**Figure 3.8a**), two of which contain self-complementary arrays.⁴³ Regarding the applications in supramolecular polymers, self-complementary arrays are of special interest, since complementary arrays require a precise control of stoichiometry.

Meijer *et al.* synthesized supramolecular polymers based on ureidopyrimidinone (UPy) dimerization.⁴⁵ Three different tautomeric forms of the UPy unit were found in solution, which are strongly affected by the used solvent. Only the “keto” form (4[1H]-pyrimidinone) and the “enol” form (pyrimidin-4-ol) are able to dimerize (**Figure 3.8b**).⁴³ Consequently, the present tautomeric form is related to the type of dimer formation ((DDAA)₂ or (DADA)₂) and additionally to the binding strengths between the components. The enol tautomer results in a (DADA)₂ dimer with high number of repulsive forces and a lower association constant compared to the keto tautomer, which dimerize in the (DDAA)₂ form (**Figure 3.8a**).⁴³ The unfavorable [3H] tautomeric form, which cannot dimerize, can be found *e.g.* in dimethyl sulfoxide (DMSO), where the solvent strongly competes with the hydrogen bonding. In chloroform a mixture of the keto and the enol tautomers is obtained.⁴³ However, the keto tautomer is more dominant resulting in dimerization constants K_{dim} of approximately $2 \cdot 10^7 \text{ M}^{-1}$ at 298 K.⁴³ In toluene an even higher dimerization constant of 10^8 M^{-1} at 298 K was found.⁴³ The lifetime of the dimers was identified to persist 0.1 s in chloroform at 298 K, while in toluene the lifetime increase to 1.7 s,⁴³ which indicates a higher stability due to the absence of competing molecules as described earlier for polar protic solvents.

In the work of Meijer, they synthesized a huge number of bi-endfunctionalized UPy derivatives from hydroxyl-telechelic polysiloxanes,⁴⁶ poly(ethylene/butylenes),⁴⁷ polyethers, polyesters and polycarbonates⁴⁸ acting as linkers.⁴³ The functionalization involves the urethane formation between the hydroxyl-telechelic polymers and synthon (2(6-isocyanatohexylaminocarbonylamino)-6-methyl-4[1H]pyrimidinone) by using dibutyltindilaurate as a catalyst. The electrophilic isocyanate can react with the nucleophilic end group (OH-group) (**Figure 3.9**).

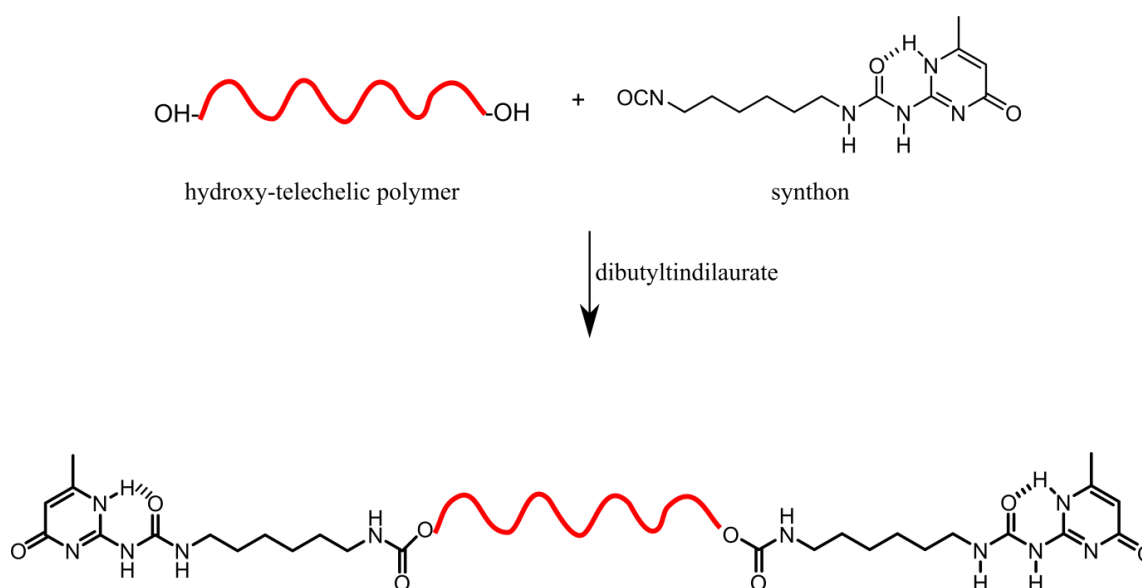


Figure 3.9: Synthesis of ureidopyrimidinone (UPy) functionalized telechelic polymers.⁴⁷

The hydroxyl-telechelic precursor polymers are viscous liquids at room temperature.⁴⁸ Incorporation of UPy-functionalized polymer results in dramatic changes of the mechanical properties due to dimerization of the functional groups and an elastic solid was formed.⁴⁸ As a consequence, the viscosity increased significantly and is in a range of high molecular weight polymers.⁴⁸ Additionally, compared to their non-functionalized partners, their mechanical properties show a strong temperature dependency as expected for physical cross-linked, supramolecular polymers.⁴⁴ At room temperature a polymer-like viscoelastic behavior is observed, whereas at elevated temperatures liquid-like characteristics are received. Consequently, they prepared powerful materials with both low melt viscosity of organic compounds and the mechanical properties of high molecular weight macromolecules.⁴⁸

Instead of producing supramolecular polymers, the dimerization of UPy units can also be used to build up nanostructured, micelle-based organogels. In this special case, the UPy units are localized on the surface of block copolymer micelles and act as linker in the soft colloid network introducing reinforcement of the material (see **Chapter 4**).

3.3 Self-assembly of Block Copolymers

The simplest case of a block copolymer is an AB diblock copolymer composed of two different, covalently linked A and B polymer chains (blocks).⁴⁹ Usually, diblock copolymers designed of two incompatible blocks show an amphiphilic character. In general, amphiphilic molecules are defined by having an affinity for both hydrophilic (water) and hydrophobic (oil) solvents.⁵⁰ By reason of incompatibility and supplemental covalent linking, block copolymers have the ability to spontaneously self-assemble in solution or undergo microphase separation in bulk with characteristic length scales in the range of 100 nm down to molecular dimensions.⁴⁹ Thus, diblock copolymers represent suitable candidates for fabrication of hierarchically ordered structures.

Considering an A-B diblock copolymer, the chemical incompatibility induces long-range repulsions between the two blocks. Simultaneously, the strong chemical bond between the blocks acts as a strong linkage resulting in short range attractive forces and therefore the blocks cannot separate macroscopically. On that account, these two competing forces provide the formation of ordered domains on the mesoscale (**Figure 3.10a**).⁵⁰ As a consequence, block copolymers facilitate the preparation of various microstructured materials such as micelles and vesicles in solution or *fcc*- and *bcc*-packed spheres, hexagonally packed cylinders (HEX), and lamellae (LAM) in thin films and bulk (**Figure 3.10b, c**).⁵¹

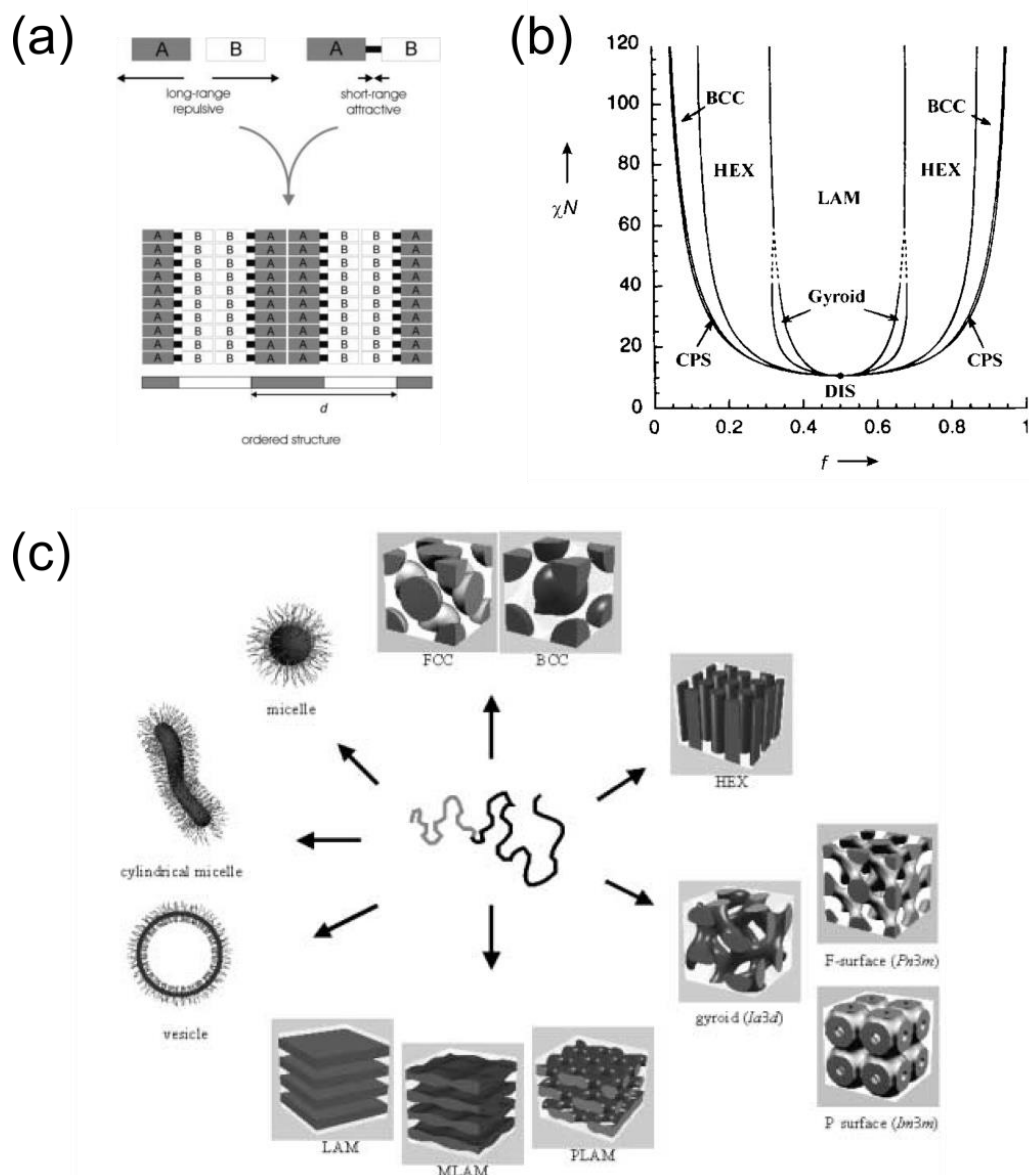


Figure 3.10: (a) Long-range repulsive and short-range attractive forces in AB block copolymers leading to the formation of ordered structures with a periodic length d of the structure. (b) Theoretical phase diagram of AB block copolymers with various ordered superlattices as a function of block length ratio f (CPS: close-packed spheres, DIS: disorder, BCC: *bcc*-packed spheres, HEX: hexagonally packed cylinders, LAM: lamellar).⁵² (c) Self-organized structures of block copolymers: spherical micelles, cylindrical micelles, vesicles, *fcc*- and *bcc*-packed spheres (FCC, BCC), hexagonally packed cylinders (HEX), various minimal surfaces (gyroid, F surface, P surface), simple lamellae (LAM), as well as modulated and perforated lamellae (MLAM, PLAM).^{51,52} Förster, S.; Plantenberg, T. *Angew. Chem. Int. Ed.* 2002, 41, 688-714. © 2002 WILEY-VCH Verlag GmbH, Weinheim, Fed. Rep. of Germany.

Considering the melt behavior of block copolymers a temperature phase diagram can be derived as presented in **Figure 3.10b** based on theoretical assumptions in terms of interaction and molecular weight.^{51,52} The tendency for segregation between the block increases with the block molecular weight and decreases with decreasing temperature.⁵⁰ In the complex phase diagram various ordered domains with different geometries can be found. The type of structure depends on the product of the χ -parameter and the total degree of polymerization χN and the block length ratio f . The total degree of

polymerization N of the block copolymer is obtained by summation of the degrees of polymerization of the individual blocks A and B. Furthermore, the strength of the repulsive interaction is represented by χ , which is the Flory-Huggins or χ -interaction parameter. The magnitude of the Flory-Huggins parameter is determined by the physico-chemical properties of the A-B pair and the temperature. With increasing temperature the Flory-Huggins parameter χ decreases with $\chi \sim 1/T$. As a consequence, the polymer segments become thermodynamically miscible beyond a critical temperature characterized by an order-disorder transition T_{ODT} . The block length ratio f is defined by the degree of polymerization, $f = N_A/N$, and allows to control and predict the kind of ordered structure by varying the block lengths.⁵² The characteristic length scale d of a microdomain depends on the polymer molecular weight, $d \sim M_w^{0.5-0.67}$. Typically, a periodicity ranging from 3 to 150 nm is accessible with well-defined block copolymers.⁵³ Besides the interesting morphologies obtained in bulk, block copolymers can self-assemble in selective solvents toward several ordered structures (*e.g.* spherical micelles, cylinders or vesicles) related to those found in neat block copolymers (**Figure 3.10c**).^{50,51} In contrary to the melt behavior, where the driving force is based on repulsive interaction between the different monomers, the situation changes using selective solvents.⁵⁰ In selective solvents one block is soluble and the other is insoluble which induces micellization. An essential parameter regarding the micelle formation is the critical micelle temperature (CMT) and the critical micelle concentration (CMC), which is well-described for surfactant molecules with polar head groups and a hydrocarbon chain (*e.g.* sodium dodecyl sulfate (SDS)).⁵⁴ In this case the micelle formation is caused on the one hand by the hydrocarbon chains which are hydrophobic and want to minimize the contact to water. On the other hand repulsive forces between the head groups are present on short distances.⁵⁴ Therefore the micellization has some limitations regarding the growth process.⁵⁴ At a certain size the micelles stop to grow even when more surfactant is added.⁵⁴ Above the CMC further addition of surfactants only generate new micelles rather than a growing of existing micelles.⁵⁴ Consequently the self-assembly of molecules is a physicochemical process, where the amphiphilic molecules are associated physically.⁵⁴ Accordingly, micelles can vary their shape or size by changing the environmental conditions such as temperature, concentration, pH, and pressure.⁵⁴ Analogues to surfactant molecules block copolymers self-assemble in solution. In a selective solvent the obtained micelles are in a thermodynamic equilibrium with the unimers.^{50,55} The soluble

polymer chain orients toward the solvent and forms the corona, whereas the insoluble blocks are shielded from the solvent and form the cores of the micelles. Depending on the composition and environmental conditions block copolymers can self-assemble into spherical micelles, vesicles, cylinders or planar bilayers (**Figure 3.10c**).⁵¹

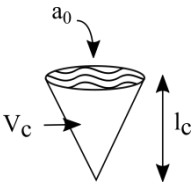
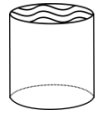
Consequently, self-assembly is based on the relative strength of the interactions, the composition and the architecture of the block copolymer.⁵⁰ Regarding the self-assembly process block copolymers can be classified into ionic and nonionic block copolymers. In ionic block copolymer systems the electrostatic interactions between the free charges are the main influencing parameters.⁵⁰ Apparently in nonionic block copolymer the driving force depends on the solvent. Using aqueous solutions the self-assembly process is usually entropic driven, whereas in organic solvents the enthalpic contributions dominate.⁵⁰ Therefore in organic solvents the negative standard Gibbs energy ΔG^0 results from the standard enthalpy ΔH^0 and the standard entropy ΔS^0 values ($\Delta G^0 = \Delta H^0 - T\Delta S^0$).⁵⁶ The entropy is negative which originates from the loss of combinatorial entropy caused by the less swollen polymer chains in the micelles compared to the polymer unimers in the unassociated state, and additionally, the loss of possible conformations due to the creation of a core/shell interface.⁵⁶ The negative enthalpic values arise from the exothermic process of micellar core formation which is attributed to the balance of polymer/solvent and polymer/polymer interactions.⁵⁶ The core-forming polymer block replaces the polymer/solvent interaction for one with the identical polymer block, whereas the shell-forming block remains interacting with the selective solvent.⁵⁷

Based on the dimensionless packing parameter P for amphiphilic molecules introduced by Israelachvili⁴² micellar structure types can be predicted. P can be calculated using the following **equation 3.9**.⁴²

$$P = \frac{V_c}{l_c \cdot a_0} \quad (3.9)$$

Here V_c is the volume, l_c the length of the core forming block and a_0 the surface area of the corona-forming polymer chains. In **Table 3.1** typical limits of the packing parameter, corresponding packing shapes and resulting structures are listed.⁴²

Table 3.1: Packing parameters, corresponding packing shapes and structures for amphiphilic molecules.⁴²

Packing parameter P	Packing shape	Structure
$< 1/3$	Cone 	Spherical micelles
$1/3 - 1/2$	Truncated cone 	Cylindrical micelles
$1/2 - 1$	Truncated cone 	Flexible bilayers, vesicles
~ 1	Cylinder 	Planar bilayers
> 1	Inverted truncated cone 	Inverted micelles

Consequently, block copolymers can undergo micellization in selective solvents.^{30,50,51,58–60} At low concentrations the micelles are isolated and have no or low spatial correlations.⁵⁰ At higher concentrations the formation of lyotropic and/or thermotropic liquid crystalline phases is induced, which display similarities of both solution and bulk morphologies.⁵⁰ Consequently, *fcc*- and *bcc*-packed spheres, hexagonally packed cylinders, gyroid and simple lamellae are possible morphologies (**Figure 3.10c**).⁵¹ In **Figure 3.11** the phase transition of a block copolymer in a selective solvent to packed spheres is schematically sketched.⁶¹ At very low concentrations the block copolymers exist as unimer. At a certain CMC the amphiphilic polymer unimers self-assemble into spherical micelles. With increasing concentration the spherical micelles start to pack and overlap with each other and form an ordered, gel-like material.⁵⁰

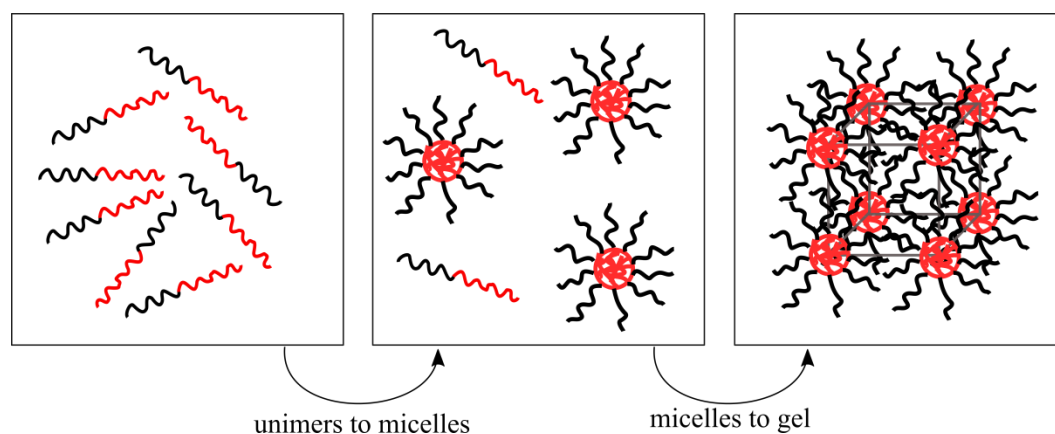


Figure 3.11: Phase transition of block copolymers in a selective solvent with increasing concentration.⁶¹ Adapted with permission from Liu, S.; Li, L. *ACS Appl. Mater. Interfaces*, 2015, 7 (4), pp 2688–2697. © 2015, American Chemical Society.

The phase behavior of packed block copolymer micelles can be greatly affected by the concentration, and temperature. Such self-assembled structures on the mesoscale were first observed and studied in aqueous systems, e.g Pluronic (poly(ethylene oxide)-*b*-poly(propylene oxide)-*b*-poly(ethylene oxide), PEO-PPO-PEO) or poly(ethylene oxide)-*b*-poly(butylene oxide) PEO-PBO micelles in water.^{62–66} In the case of PEO-PBO block copolymers in water PEO forms the corona of the micelles being a hydrophilic, thermoresponsive polymer, whereas PBO forms the hydrophobic core. At low temperatures PEO is well soluble and stretched in water. Consequently, the obtained micelles pack as *bcc* lattice.⁶⁶ Increasing temperature leads to a decrease in solvent quality for the PEO corona, characterized by a lower critical solution temperature (LCST), and a phase transition to *fcc* structure.⁶⁶

Poly(isoprene-*block*-styrene) (PI-PS) block copolymer micelles are an excellent example for polymers forming micelles in organic solvents, *i.e.* dialkyl phthalates representing styrene-selective solvents.^{59,67–71} In this systems temperature dependent effects are mainly attributed to the strong temperature dependency on solvent selectivity with respect to the PI core (instead of the corona). Thus, for elevated temperatures thermoreversible order-disorder or order-order transitions are induced. Small temperature changes can result in large structural changes including lamellae (LAM) to gyroid (G), G to LAM, G to hexagonally packed cylinders (HEX), HEX to G, HEX to *bcc* or *fcc* spheres, and *bcc* or *fcc* spheres to HEX transitions for one system.⁷¹ Additionally, the concentration of micelles within the dialkyl phthalates plays an important role. For low concentrations and diluted systems typical micellar structures *e.g.* vesicles, spherical or cylindrical micelles, can be obtained.^{59,67,71} In contrast, moderate concentrations result in ordered structures,

e.g. *bcc* or *fcc* lattices of packed spherical micelles.^{69–71} For very high concentrations a transition to hexagonally packed cylinders, lamellae or gyroid structures is observed.^{68,71} The transitions and structures at different concentration ranges are always dependent on the block copolymer composition, temperature, and solvent selectivity. In **Figure 3.12** a phase diagram of a PI-PS block copolymer in diethyl phthalate (DEP) is shown.⁷¹ With increasing concentration/ volume fraction of the polymer in DEP transitions to various kinds of structures (micelles → packed spheres (both *fcc* and *bcc*) → hexagonally packed cylinders → gyroid → lamellae + cylinders coexistence → lamellae) are observed. Additionally, an increase in temperature leads to a disordered phase.⁷¹

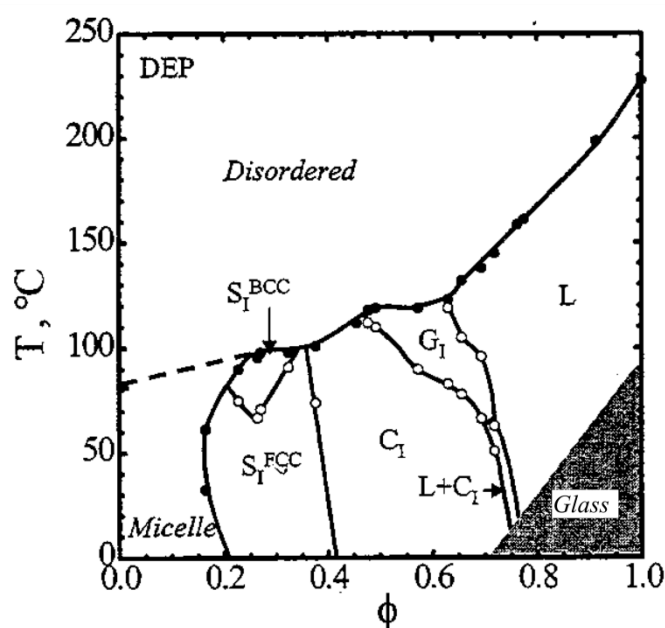


Figure 3.12: Phase diagram of a PI-PS block copolymer ($f_{PS} = 0.5$) in diethyl phthalate (DEP). At different polymer volume fractions ϕ various types of morphologies and transitions are obtained depending on temperature. Micelles, packed spheres (S_1^{BCC} or S_1^{FCC}), hexagonally packed cylinders (C_1), gyroid (G_1), coexistence of lamellae (L) + cylinder, lamellae, disordered phase.⁷¹ Reprinted with permission from Lodge, T. P.; Pudil, B.; Hanley, K. J. *Macromolecules*, 2002, 35 (12), pp 4707–4717. © 2002, American Chemical Society.

Thermoreversible order-order or order-disorder transitions were found for fixed volume fractions, *e.g.* an order-order transition from *fcc* to *bcc*, which is based on the core swelling with increasing temperature allowing the coronal chains to overlap.⁷¹ The mechanical properties of such materials can be strongly affected by reversible intermolecular attractions provided, *e.g.* by hydrogen bonds to form supramolecular networks (see **Chapter 4** and following section).

3.4 Organogels

Polymer gels are defined as a three-dimensional crosslinked network constructed of large macromolecules, which are interpenetrated by a fluid.¹⁸ There are several subclasses of gels and generally they are classified as organogels and hydrogels depending on the liquid phase (organic solution or water).¹⁸ In addition, the crosslinking can be permanent (covalent bond) or non-permanent based on non-covalent bonds such as hydrogen bonding, van der Waals or π -stacking.⁷² Recently, non-permanent crosslinked gels have achieved a lot of attention and are often named “smart” gels due to their ability to respond to physical stimuli (*e.g.* temperature,⁷³ electrical fields,⁷⁴ and magnetic fields⁷⁵) or on chemical stimuli (*e.g.* pH changes⁷⁶).¹⁸ The external stimuli associate with a change in shape, volume, or mechanical properties.⁵⁵ These triggered properties open up various fields including medical and industrial applications.⁷⁷ One can construct such networks in many ways for example by using responsive polymers, supramolecular polymers, but also nanostructured materials such as block copolymer micelles. Supramolecular polymers can be generated from self-assembly of low molecular mass oligomers toward polymers which are linked with an non-covalent, reversible, but highly directional bond.⁷⁸ A prominent example are urea-based supramolecular polymers like the above described UPy-group, but also many others.⁷⁹ In these systems the low molecular compound are comparable to organogelators and build up gels with special features.⁷⁸ For example supramolecular polymers can be used as self-healing materials based on their reversible cross-links.^{80–82} In addition self-assembled block copolymer micelles are able to form non-permeant networks. Many investigated systems are water-based, such as PEO-PPO-PEO ABA-triblock copolymers (Pluronics), where the B-blocks form the core and micelles are linked *via* the A-blocks (see **Chapter 3.3**).⁸³ At high concentrations the micelles associate over a narrow temperature interval and form a rigid network.⁸³ Typically, dynamic-mechanical measurements are used to characterize the mechanical properties, associative phenomena, micelle-gel transitions, and relaxation characteristics. Temperature dependent measurements exhibit a sharp transition from a Newtonian liquid to a solid-like gel, which is a thermoreversible behavior.^{83,84}

Both supramolecular polymer gels and block copolymer micelle networks are characterized by a reversible stimuli-responsive behavior with respect to external triggers such as temperature.^{18,80,82} Upon heating and subsequent cooling, these gels possess a

reversible sol-gel phase transition.^{24,85} In order to construct reproducible and high quality gels, it is necessary to prepare polymer networks with homogeneity on the nanoscale range. In **Chapter 4** a route toward organogels with unique properties is described utilizing hydrogen bonded tethered micelles.

3.5 Polymer Nanocomposites

Polymer nanocomposites are composed of a polymer matrix filled with inorganic nanofillers.⁸⁶ As a result novel, high-performance materials with new functions are obtained that find many applications in various industrial fields.⁸⁶ The incorporation of nanoparticles often leads to unfavorable aggregation of the nanoparticles in the melt, which eliminates the benefits of these materials.⁸⁶ Therefore many synthetic approaches were developed to stabilize nanoparticles sufficiently in order to achieve well-dispersed nanoparticles in the matrix.⁸⁶ The following subchapters describe the synthesis of monodisperse nanoparticles and possible strategies to stabilize them in bulk and in solution.

3.5.1 Inorganic Nanoparticles

Nanoparticles are characterized by their small dimensions (1-100 nm) resulting in a huge surface to volume ratio. In the case of inorganic nanoparticles the increasing number of surface atoms is responsible for significant changes in physical (*e.g.* melting point) and chemical (*e.g.* reactivity) properties compared to bulk material.⁸⁷

A variety of synthetic approaches were developed to synthesize inorganic nanoparticles.⁸⁷⁻⁸⁹ In principle these techniques can be divided in “top-down” and “bottom-up” methods.⁸⁷ However, for many applications monodisperse nanoparticles are necessary. This requirement represents a challenge and is most often not achieved utilizing “top-down” approaches.⁸⁷ Consequently, wet chemical approaches (bottom-up) are the method of choice to prepare large scales of nanoparticles with controlled size, shape, and surface functionality.⁹⁰ In order to control and improve the synthesis, understanding of particle formation is essential. LaMer and Dinegar developed the well-

known theory of “burst nucleation”.⁹¹ Here, many nuclei are generated at the same time during initiation above the critical precursor concentration (short period) and start to grow directly without any additional nucleation, due to a fast drop in precursor concentration.⁹¹ A single nucleation step is essential for the synthesis of monodisperse nanocrystals leading to a separation of nucleation and growth process.⁸⁷ This is obtained in homogeneous nucleation solutions.⁸⁷ The homogeneous nucleation possesses the formation of nuclei without the presence of any seeds (*e.g.* dust) and heterogeneous nucleation is suppressed. For homogeneous nucleation a high energy barrier has to be surpassed before the system spontaneously forms the heterogeneous phase (**Figure 3.13**).^{87,91}

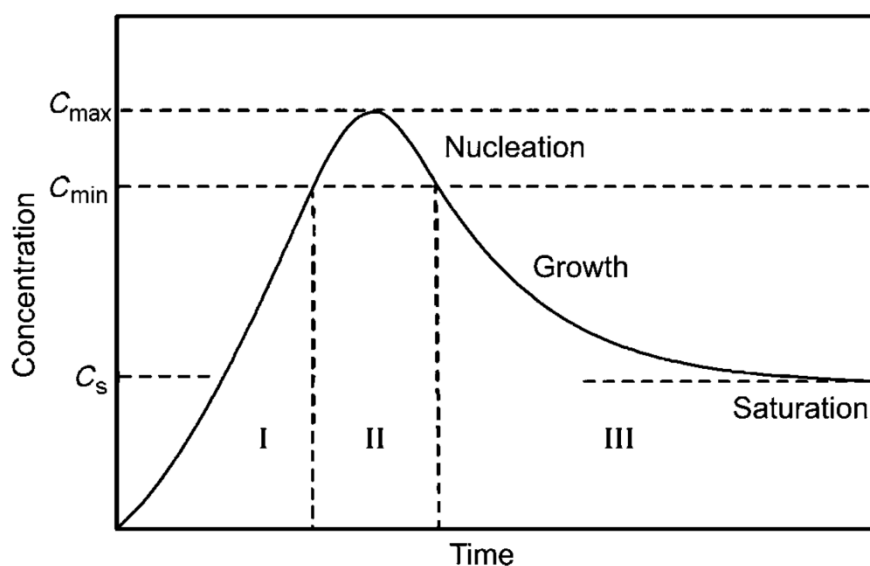


Figure 3.13: Schematic plot of concentration vs. time for the nucleation and growth model of LaMer and Dinegar (“burst nucleation”).⁸⁸ Goesmann, H.; Feldmann, C. *Angew. Chem. Int. Ed.* 2010, 49, 1362-1395. © 2010 WILEY-VCH Verlag GmbH & Co. KGaA, Weinheim.

The LaMer plot can be divided into three parts: I) A fast increase of free “monomer” representing the minimum subunit of bulk crystals. II) Above a critical concentration (C_{\min}) the monomers undergo burst nucleation, which leads to a reduction of free monomers in solution. After the monomer concentration drops below the critical concentration again no additional nucleation occurs. III) Free growth of present nanocrystals without additional secondary nucleation. The particles grow under the control of monomer diffusion as long as the solution is supersaturated.^{87,88}

The energy barrier of the nucleation process can be described by the Gibbs free energy ΔG including the assumption of a spherical particle of radius r , a surface free energy per unit area γ , and ΔG_v as the change in free energy (**equation 3.10**).⁸⁷

$$\Delta G = 4\pi r^2 \gamma + \frac{4}{3}\pi r^3 \Delta G_v \quad (3.10)$$

Plotting ΔG versus r results in a function with a maximum value of ΔG at a characteristic particle radius, since γ is always positive and $\Delta G_v = (-RT \ln S)/V_m$ is negative as long as the solution is supersaturated (V_m is the molar volume of bulk crystals). The radius at the maximum for ΔG is named critical radius r_c (**equation 3.11**).⁸⁷

$$r_c = \frac{-2\gamma}{\Delta G_v} \quad (3.11)$$

The critical radius r_c is the minimum radius of the particles that is stable and, thus, persists in solution. After particle formation, Ostwald ripening is dominant. Small particles are dissolved and large particles grow.⁸⁷ This process is exothermic and leads to the minimization of the free surface energy within the system.⁸⁷ Consequently, this unfavorable process has to be suppressed for the production of monodisperse nanoparticles.⁸⁷ The obtained inorganic nanoparticles can be stabilized either sterically or electrostatically.⁸⁸ Electrostatic stabilization has some limitations especially in organic solvents. Thus, in organic solvents nanoparticles are most often stabilized *via* steric repulsions utilizing hydrophobic ligand molecules (surfactants), *e.g.* short alkyl chains or polymers (**Figure 3.14**).⁸⁸

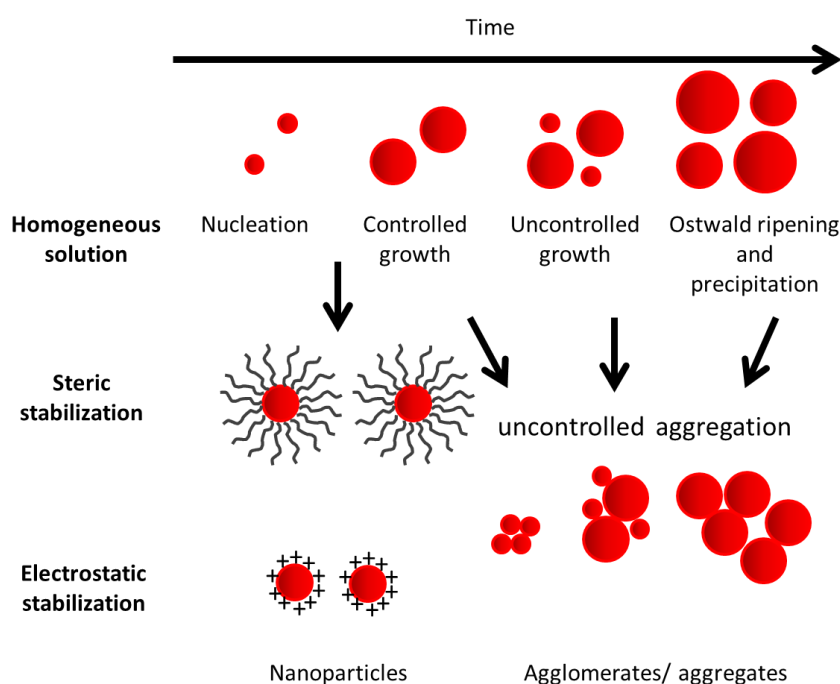


Figure 3.14: Growth and stabilization of nanoparticles.⁸⁸ Goesmann, H.; Feldmann, C. *Angew. Chem. Int. Ed.* 2010, 49, 1362-1395. © 2010 WILEY-VCH Verlag GmbH & Co. KGaA, Weinheim.

Solution-based chemical approaches for the preparation of monodisperse nanoparticles can be realized for example *via* thermal decomposition methods.⁸⁷ At high temperatures a decomposition of precursors is induced in the presence of surfactant molecules to generate monodisperse nanoparticles of different sizes and shapes.⁸⁷ This so called hot-injection method was developed by Bawendi *et al.*⁹² for the synthesis of high-quality CdS, CdSe, and CdTe semiconductor nanocrystals. A rapid injection of an organometallic precursor into a hot surfactant solution leads to a homogenous nucleation.⁹² Uniform surface derivatization and a regular core structure are realized by subsequent slow growth and annealing of the solution.^{87,92} In the hot-injection method particles can be stabilized sterically or electrostatically directly after the nucleation step, which prevents the system from further Ostwald ripening or agglomeration.⁸⁸ Electrostatic stabilization is realized by selective adsorption of ions (*e.g.* H⁺, OH⁻, RCOO⁻) on the particle surface in polar solvents.⁸⁸ Sterical stabilization is carried out by the adsorption of long chain, organic molecules (*e.g.* oleylamin, oleic acid, trioctylphosphine) in non-polar solvents. The growth process is usually carried out at slightly lower temperatures by aging.^{87,88}

3.5.2 Polymer Ligands for Nanoparticle Stabilization

Instead of using low molecular weight ligands for steric stabilization of nanoparticles, polymer ligands can be used enabling new applications, *e.g.* in polymer nanocomposites.^{21,22,93-95} Polymer nanocomposites consist of a polymer matrix filled with inorganic nanoparticles⁹⁶ and are used for various applications, *e.g.* as coatings for surfaces to enhance their mechanical and chemical stability⁹⁷ or as transparent films (see **Chapter 6**). Adding just a few volume fractions of nanoparticles often results in significant property changes of the polymer material due to synergistic effects between matrix and filler.⁹⁸ Additionally, specific properties and functions can be integrated into the system following this approach.^{96,98,99} Consequently, nanocomposites are a simple and low cost system to tailor and adjust desired mechanical, optical or electrical material properties by combining two individual components rather than develop new polymer materials.⁹⁸ The advantage of adding nanofillers results from their small size and the increase in surface area.⁹⁸ Especially, electrical and optical material properties of nanocomposites are caused by new physical effects such as quantum confinement effects due to nanoscale dimensions.⁹⁸ However, a limiting factor is the tendency of nanoparticles to undergo aggregation within in the polymer matrix due to incompatibility.

This is accompanied by drawbacks as a result of unfavorable, irregular distributed material properties.¹⁰⁰ Large effort has been applied to avoid this phenomenon. One of the most promising approaches is to coat the incorporated nanoparticles with a polymer layer (usually the same as the matrix) to make them compatible with the matrix.^{22,93,101} In principle, there exist two main approaches for nanoparticle surface coating: grafting from^{96,102} and grafting to.^{96,103} The grafting from method is based on the polymerization of monomers initiated directly at the nanoparticle surface. In this approach the nanoparticle surface bears covalently linked initiator groups and the polymer chains can grow directly from the nanoparticle surface *via e.g.* controlled radical polymerization techniques.¹⁰² Consequently, the grafting from approach provides relatively high grafting densities.¹⁰² In contrast, the grafting to method allows the precise pre-synthesis and characterization of well-defined polymer chains bearing a functional end-group (see **Chapter 3.2.2**), which can be linked to the nanoparticle surface. This approach usually results in low grafting densities due to sterically hindrance of the polymer chains compared to grafting-from methods.¹⁰² Instead of a permanent, covalent bond between polymer chain-ends and the inorganic surfaces (*e.g.* gold-thiol¹⁰⁴), the use of polymer chains bearing functional groups that can coordinate reversibly to the inorganic surface is an alternative grafting to route to stabilize nanoparticles in solution or in polymer matrix and to achieve much higher grafting densities (see **Chapter 5**).

References

1. K. Hatada, T. Kitayama, and O. Vogl, *Macromolecular Design of Polymeric Materials* (M. Dekker, New York, 1997).
2. G. G. Odian, *Principles of Polymerization*, Fourth edition (Wiley, Hoboken, N.J., 2004).
3. Müller, Axel H. E. and K. Matyjaszewski, *Controlled and Living Polymerizations: Methods and Materials* (Wiley-VCH, Weinheim, 2009).
4. D. Baskaran and A. H. Müller, “Anionic Vinyl Polymerization—50 Years after Michael Szwarc,” *Prog. Polym. Sci.* **32** (2), 173–219 (2007).
5. K. Matyjaszewski, “Atom Transfer Radical Polymerization (ATRP): Current Status and Future Perspectives,” *Macromolecules* **45** (10), 4015–4039 (2012).
6. G. Moad, E. Rizzardo, and S. H. Thang, “Radical Addition–Fragmentation Chemistry in Polymer Synthesis,” *Polymer* **49** (5), 1079–1131 (2008).
7. C. J. Hawker, A. W. Bosman, and E. Harth, “New Polymer Synthesis by Nitroxide Mediated Living Radical Polymerizations,” *Chem. Rev.* **101** (12), 3661–3688 (2001).
8. B. Tieke, *Makromolekulare Chemie: Eine Einführung*, 2., vollst. überarb. und erw. Aufl. (Wiley-VCH, Weinheim, 2005).
9. M. Szwarc, “‘Living’ Polymers,” *Nature* **178** (4543), 1168–1169 (1956).
10. M. Szwarc, M. Levy, and R. Milkovich, “Polymerization Initiated by Electron Transfer to Monomer. A New Method of Formation of Block Polymers 1,” *J. Am. Chem. Soc.* **78** (11), 2656–2657 (1956).
11. A. D. Jenkins, P. Kratochvíl, R. F. T. Stepto, and U. W. Suter, “Glossary of Basic Terms in Polymer Science,” *Pure Appl. Chem.* **68** (12) (1996).

12. N. Hadjichristidis, *Block Copolymers: Synthetic Strategies, Physical Properties, and Applications* (John Wiley & Sons, 2002).
13. H. L. Hsieh and R. P. Quirk, *Anionic Polymerization: Principles and Practical Applications* (Marcel Dekker, New York, 1996).
14. M. M. Al-Jarrah, R. L. Apikian, and E. Ahmed, "Living Polymerization-1. Solvent Effect on the Stereoregularity of Polyisoprene Initiated by n-Buthyllithium," *Polym. Bull.* **12**, 433–436 (1984).
15. J. Kao and T. Xu, "Nanoparticle Assemblies in Supramolecular Nanocomposite Thin Films: Concentration Dependence," *J. Am. Chem. Soc.* **137** (19), 6356–6365 (2015).
16. H. Awada, H. Medlej, S. Blanc, M.-H. Delville, R. C. Hiorns, A. Bousquet, C. Dagron-Lartigau, and L. Billon, "Versatile Functional Poly(3-hexylthiophene) for Hybrid Particles Synthesis by the Grafting Onto Technique: Core@Shell ZnO Nanorods," *J. Polym. Sci. Part A: Polym. Chem.* **52** (1), 30–38 (2014).
17. A. Bertrand, F. Lortie, and J. Bernard, "Routes to Hydrogen Bonding Chain-End Functionalized Polymers," *Macromol. Rapid Commun.* **33** (24), 2062–2091 (2012).
18. Z. Wei, J. H. Yang, J. Zhou, F. Xu, M. Zrínyi, P. H. Dussault, Y. Osada, and Y. M. Chen, "Self-Healing Gels Based on Constitutional Dynamic Chemistry and their Potential Applications," *Chem. Soc. Rev.* **43** (23), 8114–8131 (2014).
19. A. Sanchez-Sanchez and J. A. Pomposo, "Single-Chain Polymer Nanoparticles via Non-Covalent and Dynamic Covalent Bonds," *Part. Part. Syst. Charact.* **31** (1), 11–23 (2014).
20. F. Herbst and W. H. Binder, "Comparing Solution and Melt-State Association of Hydrogen Bonds in Supramolecular Polymers," *Polym. Chem.* **4** (12), 3602–3609 (2013).
21. S. Srivastava, J. L. Schaefer, Z. Yang, Z. Tu, and L. A. Archer, "25th Anniversary Article: Polymer-Particle Composites: Phase Stability and Applications in Electrochemical Energy Storage," *Adv. Mater.* **26** (2), 201–234 (2014).

-
22. M. Bieligmeyer, S. M. Taheri, I. German, C. Boisson, C. Probst, W. Milius, V. Altstädt, J. Breu, H.-W. Schmidt, F. D'Agosto, and S. Förster, "Completely Miscible Polyethylene Nanocomposites," *J. Am. Chem. Soc.* **134** (44), 18157–18160 (2012).
23. J. Peng, R. Dong, B. Ren, X. Chang, and Z. Tong, "Novel Hydrophobically Modified Ethoxylated Urethanes End-Capped by Percec-Type Alkyl Substituted Benzyl Alcohol Dendrons: Synthesis, Characterization, and Rheological Behavior," *Macromolecules* **47** (17), 5971–5981 (2014).
24. Dankers, Patricia Y W, T. M. Hermans, T. W. Baughman, Y. Kamikawa, R. E. Kieltyka, Bastings, Maartje M C, H. M. Janssen, Sommerdijk, Nico A J M, A. Larsen, van Luyn, Marja J A, A. W. Bosman, E. R. Popa, G. Fytas, and E. W. Meijer, "Hierarchical Formation of Supramolecular Transient Networks in Water: A Modular Injectable Delivery System," *Adv. Mater.* **24** (20), 2703–2709 (2012).
25. M. A. Tasdelen, M. U. Kahveci, and Y. Yagci, "Telechelic Polymers by Living and Controlled/Living Polymerization Methods," *Prog. Polym. Sci.* **36** (4), 455–567 (2011).
26. R. P. Quirk and J.-J. Ma, "Characterization of the Functionalization Reaction Product of Poly(styryl)lithium with Ethylene Oxide," *J. Polym. Sci. A Polym. Chem.* **26** (8), 2031–2037 (1988).
27. van Zyl, W. E., M. García, Schrauwen, B. A. G., B. J. Kooi, De Hosson, J. Th. M., and H. Verweij, "Hybrid Polyamide/Silica Nanocomposites: Synthesis and Mechanical Testing," *Macromol. Mater. Eng.* **28** (2), 106–110 (2002).
28. C.-H. Hung and W.-T. Whang, "Effect of Surface Stabilization of Nanoparticles on Luminescent Characteristics in ZnO/Poly(hydroxyethyl methacrylate) Nanohybrid Films," *J. Mater. Chem.* **15** (2), 267–274 (2005).
29. S. Singha and M. Thomas, "Dielectric Properties of Epoxy Nanocomposites," *IEEE Trans. Dielect. Electr. Insul.* **15** (1), 12–23 (2008).
30. S. Förster and M. Antonietti, "Amphiphilic Block Copolymers in Structure-Controlled Nanomaterial Hybrids," *Adv. Mater.* **10** (3), 195–217 (1998).

31. L. H. Lee, *Fundamentals of Adhesion* (Springer US, 1991).
32. I. A. Starostina, O. V. Stoyanov, and R. Y. Deberdeev, *Polymer Surfaces and Interfaces: Acid-Base Interactions and Adhesion in Polymer-Metal Systems* (Apple Academic Press, Toronto, 2014).
33. K. E. Geckeler and H. Nishide, *Advanced Nanomaterials* (Wiley, Weinheim, 2009).
34. J. Kim, S. S. Kim, K. H. Kim, Y. H. Jin, S. M. Hong, S. S. Hwang, B.-G. Cho, D. Y. Shin, and S. S. Im, “Applications of Telechelic Polymers as Compatibilizers and Stabilizers in Polymer Blends and Inorganic/Organic Nanohybrids,” *Polymer* **45** (10), 3527–3533 (2004).
35. L. Hong, F. Zhu, J. Li, T. Ngai, Z. Xie, and C. Wu, “Folding of Long Multiblock Copolymer (PI-*b*-PS-*b*-PI)_n Chains Prepared by the Self-Assembly Assisted Polypolymerization (SAAP) in Cyclohexane,” *Macromolecules* **41** (6), 2219–2227 (2008).
36. D. P. Wyman, V. R. Allen, and T. Altares, “Reaction of Polystyryllithium with Carbon Dioxide,” *J. Polym. Sci. A Gen. Pap.* **2** (10), 4545–4550 (1964).
37. R. P. Quirk, M. Ocampo, M. J. Polce, and C. Wesdemiotis, “Functionalization of Poly(styryl)lithium with Thiiranes: Sulfur Extrusion vs Ring-Opening Mechanisms,” *Macromolecules* **40** (7), 2352–2360 (2007).
38. R. P. Quirk and P. L. Cheng, “Functionalization of Polymeric Organolithium Compounds. Amination of Poly(styryl)lithium,” *Macromolecules* **19** (5), 1291–1294 (1986).
39. M. S. Nikolic, C. Olsson, A. Salcher, A. Kornowski, A. Rank, R. Schubert, A. Frömsdorf, H. Weller, and S. Förster, “Micelle and Vesicle Formation of Amphiphilic Nanoparticles,” *Angew. Chem. Int. Ed.* **48** (15), 2752–2754 (2009).
40. Z.-T. Li and L.-Z. Wu, eds., *Hydrogen Bonded Supramolecular Structures*, Aufl. 2015 (Springer Berlin Heidelberg, Berlin, Heidelberg, 2015).
41. G. A. Jeffrey, *An Introduction to Hydrogen Bonding* (Oxford University Press, New York, 1997).

-
42. J. N. Israelachvili, *Intermolecular and Surface Forces*, 2nd ed. (Academic Press, London, 1992).
43. R. P. Sijbesma and E. W. Meijer, "Quadruple Hydrogen Bonded Systems," *Chem. Commun.* (1), 5–16 (2003).
44. A. W. Bosman, R. P. Sijbesma, and E. Meijer, "Supramolecular Polymers at Work," *Mater. Today* **7** (4), 35–39 (2004).
45. R. P. Sijbesma, F. H. Beijer, L. Brunsveld, Folmer, Brigitte J. B., Hirschberg, J. H. K. Ky, Lange, Ronald E. F. M., Lowe, Jimmy K. L., and E. W. Meijer, "Reversible Polymers Formed from Self-Complementary Monomers Using Quadruple Hydrogen Bonding," *Science* **278** (5343), 1601–1604 (1997).
46. Hirschberg, J. H. K. Ky, F. H. Beijer, H. A. van Aert, Magusin, Pieter C. M. M., R. P. Sijbesma, and E. W. Meijer, "Supramolecular Polymers from Linear Telechelic Siloxanes with Quadruple-Hydrogen-Bonded Units," *Macromolecules* **32** (8), 2696–2705 (1999).
47. H. M. Keizer, R. van Kessel, R. P. Sijbesma, and E. Meijer, "Scale-up of the Synthesis of Ureidopyrimidinone Functionalized Telechelic Poly(ethylenebutylene)," *Polymer* **44** (19), 5505–5511 (2003).
48. B. Folmer, R. P. Sijbesma, R. M. Versteegen, van der Rijt, Joost A. J., and E. Meijer, "Supramolecular Polymer Materials: Chain Extension of Telechelic Polymers Using a Reactive Hydrogen-Bonding Synthone," *Adv. Mater.* **12** (12), 874–878 (2000).
49. I. W. Hamley, *The Physics of Block Copolymers* (Oxford University Press, Oxford, New York, 1998).
50. B. Lindman and P. Alexandridis, *Amphiphilic Block Copolymers. Self-Assembly and Applications*, 1st ed. (Elsevier, Amsterdam, New York, 2000).
51. S. Förster and T. Plantenberg, "From Self-Organizing Polymers to Nanohybrid and Biomaterials," *Angew. Chem. Int. Ed.* **41** (5), 688–714 (2002).
52. M. W. Matsen and F. S. Bates, "Unifying Weak- and Strong-Segregation Block Copolymer Theories," *Macromolecules* **29** (4), 1091–1098 (1996).

53. H. Hu, M. Gopinadhan, and C. O. Osuji, "Directed Self-Assembly of Block Copolymers: A Tutorial Review of Strategies for Enabling Nanotechnology with Soft Matter," *Soft Matter* **10** (22), 3867–3889 (2014).
54. D. F. Evans and H. Wennerström, *The Colloidal Domain: Where Physics, Chemistry and Biology Meet*, 2. ed. (Wiley, New York, 1998).
55. J. Rodríguez-Hernández, F. Chécot, Y. Gnanou, and S. Lecommandoux, "Toward 'Smart' Nano-Objects by Self-Assembly of Block Copolymers in Solution," *Prog. Polym. Sci.* **30** (7), 691–724 (2005).
56. G. Riess, "Micellization of Block Copolymers," *Prog. Polym. Sci.* **28** (7), 1107–1170 (2003).
57. P. Somasundaran, *Encyclopedia of Surface and Colloid Science*, 2nd ed. (Taylor & Francis, New York, 2006).
58. Y. Mai and A. Eisenberg, "Self-Assembly of Block Copolymers," *Chem. Soc. Rev.* **41** (18), 5969–5985 (2012).
59. J. Bang, S. Jain, Z. Li, T. P. Lodge, J. S. Pedersen, E. Kesselman, and Y. Talmon, "Sphere, Cylinder, and Vesicle Nanoaggregates in Poly(styrene-*b*-isoprene) Diblock Copolymer Solutions," *Macromolecules* **39** (3), 1199–1208 (2006).
60. L. Zhang and A. Eisenberg, "Multiple Morphologies of "Crew-Cut" Aggregates of Polystyrene-*b*-poly(acrylic acid) Block Copolymers," *Science* **268** (5218), 1728–1731 (1995).
61. S. Liu and L. Li, "Multiple Phase Transition and Scaling Law for Poly(ethylene oxide)-Poly(propylene oxide)-Poly(ethylene oxide) Triblock Copolymer in Aqueous Solution," *ACS Appl. Mater. Interfaces* **7** (4), 2688–2697 (2015).
62. K. Mortensen, W. Brown, and B. Nordén, "Inverse Melting Transition and Evidence of Three-Dimensional Cubatic Structure in a Block-Copolymer Micellar System," *Phys. Rev. Lett.* **68** (15), 2340–2343 (1992).
63. J. A. Pople, I. W. Hamley, J. P. A. Fairclough, A. J. Ryan, B. U. Komanschek, A. J. Gleeson, G.-E. Yu, and C. Booth, "Ordered Phases in Aqueous Solutions of Diblock

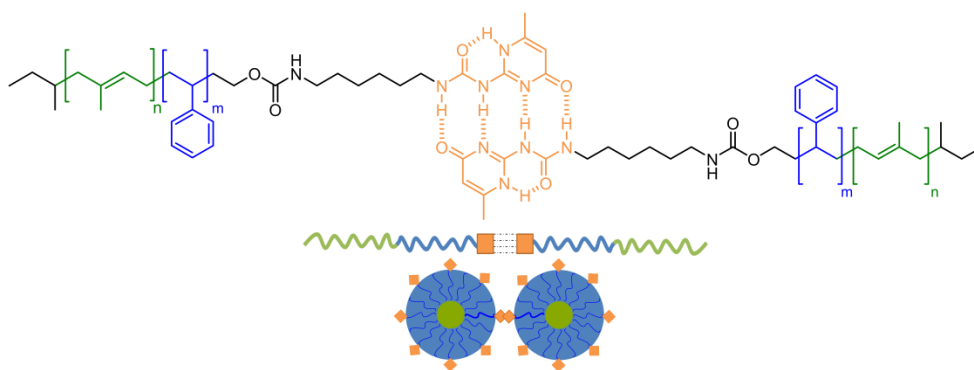
-
- Oxyethylene/Oxybutylene Copolymers Investigated by Simultaneous Small-Angle X-ray Scattering and Rheology,” *Macromolecules* **30** (19), 5721–5728 (1997).
64. N.-J. Deng, Y.-Z. Luo, S. Tanodekaew, N. Bingham, D. Attwood, and C. Booth, “Gelation of Micellar Solutions of Diblock-copoly (oxyethylene/oxybutylene) in Aqueous K₂SO₄. An Investigation of Excluded Volume Effects,” *J. Polym. Sci. B Polym. Phys.* **33** (7), 1085–1096 (1995).
65. G. Wanka, H. Hoffmann, and W. Ulbricht, “Phase Diagrams and Aggregation Behavior of Poly(oxyethylene)-Poly(oxypropylene)-Poly(oxyethylene) Triblock Copolymers in Aqueous Solutions,” *Macromolecules* **27** (15), 4145–4159 (1994).
66. I. W. Hamley, J. A. Pople, C. Booth, Y.-W. Yang, and S. M. King, “A Small-Angle Neutron-Scattering Study of Shear-Induced Ordering in the Cubic Phase of a Block Copolymer Gel,” *Langmuir* **14** (12), 3182–3186 (1998).
67. T. P. Lodge, J. Bang, K. J. Hanley, J. Krocak, S. Dahlquist, B. Sujan, and J. Ott, “Origins of Anomalous Micellization in Diblock Copolymer Solutions,” *Langmuir* **19** (6), 2103–2109 (2003).
68. K. J. Hanley and T. P. Lodge, “Effect of Dilution on a Block Copolymer in the Complex Phase Window,” *J. Polym. Sci. Part B Polym. Phys.* **17** (36), 3101–3113 (1998).
69. J. Bang and T. P. Lodge, “Mechanisms and Epitaxial Relationships between Close-Packed and BCC Lattices in Block Copolymer Solutions,” *J. Phys. Chem. B* **107** (44), 12071–12081 (2003).
70. K. J. Hanley, T. P. Lodge, and C.-I. Huang, “Phase Behavior of a Block Copolymer in Solvents of Varying Selectivity,” *Macromolecules* **33** (16), 5918–5931 (2000).
71. T. P. Lodge, B. Pudil, and K. J. Hanley, “The Full Phase Behavior for Block Copolymers in Solvents of Varying Selectivity,” *Macromolecules* **35** (12), 4707–4717 (2002).

72. M. Suzuki and K. Hanabusa, "Polymer Organogelators that Make Supramolecular Organogels Through Physical Cross-Linking and Self-Assembly," *Chem. Soc. Rev.* **39** (2), 455–463 (2010).
73. N. Kotobuki, K. Murata, and K. Haraguchi, "Proliferation and Harvest of Human Mesenchymal Stem Cells Using New Thermoresponsive Nanocomposite Gels," *J. Biomed. Mater. Res., Part A* **101** (2), 537–546 (2013).
74. H. Qi, E. Mäder, and J. Liu, "Electrically Conductive aerogels Composed of Cellulose and Carbon Nanotubes," *J. Mater. Chem. A* **1** (34), 9714–9720 (2013).
75. F. Xu, C.-A. M. Wu, V. Rengarajan, T. D. Finley, H. O. Keles, Y. Sung, B. Li, U. A. Gurkan, and U. Demirci, "Three-Dimensional Magnetic Assembly of Microscale Hydrogels," *Adv. Mater.* **23** (37), 4254–4260 (2011).
76. A. Matsumoto, K. Yamamoto, R. Yoshida, K. Kataoka, T. Aoyagi, and Y. Miyahara, "A Totally Synthetic Glucose Responsive Gel Operating in Physiological Aqueous Conditions," *Chem. Commun.* **46** (13), 2203–2205 (2010).
77. R. Yoshida, "Self-Oscillating Gels Driven by the Belousov-Zhabotinsky Reaction As Novel Smart Materials," *Adv. Mater.* **22** (31), 3463–3483 (2010).
78. B. Isare, S. Pensec, M. Raynal, and L. Bouteiller, "Bisurea-based Supramolecular Polymers: From Structure to Properties," *C. R. Chimie* **19** (1-2), 148–156 (2016).
79. L. Brunsveld, Folmer, B. J. B., E. W. Meijer, and R. P. Sijbesma, "Supramolecular Polymers," *Chem. Rev.* **101** (12), 4071–4098 (2001).
80. J. Hentschel, A. M. Kushner, J. Ziller, and Z. Guan, "Self-Healing Supramolecular Block Copolymers," *Angew. Chem. Int. Ed.* **51** (42), 10561–10565 (2012).
81. P. Cordier, F. Tournilhac, C. Soulié-Ziakovic, and L. Leibler, "Self-healing and Thermoreversible Rubber from Supramolecular Assembly," *Nature* **451** (7181), 977–980 (2008).
82. Y.-G. Jia and X. X. Zhu, "Self-Healing Supramolecular Hydrogel Made of Polymers Bearing Cholic Acid and β -Cyclodextrin Pendants," *Chem. Mater.* **27** (1), 387–393 (2014).

-
83. W. Brown, K. Schillen, M. Almgren, S. Hvidt, and P. Bahadur, "Micelle and gel formation in a poly(ethylene oxide)/poly(propylene oxide)/poly(ethylene oxide) triblock copolymer in water solution. Dynamic and static light scattering and oscillatory shear measurements," *J. Phys. Chem.* **95** (4), 1850–1858 (1991).
84. G. Wanka, H. Hoffmann, and W. Ulbricht, "The Aggregation Behavior of Poly-(oxyethylene)-poly-(oxypropylene)-poly-(oxyethylene)-block-copolymers in Aqueous Solution," *Colloid Polym. Sci.* **268** (2), 101–117 (1990).
85. T. Suzuki, S. Shinkai, and K. Sada, "Supramolecular Crosslinked Linear Poly(Trimethylene Iminium Trifluorosulfonimide) Polymer Gels Sensitive to Light and Thermal Stimuli," *Adv. Mater.* **18** (8), 1043–1046 (2006).
86. S. Li, M. Meng Lin, M. S. Toprak, D. K. Kim, and M. Muhammed, "Nanocomposites of Polymer and Inorganic Nanoparticles for Optical and Magnetic Applications," *Nano Rev.* **1**, 5214 (2010).
87. J. Park, J. Joo, S. G. Kwon, Y. Jang, and T. Hyeon, "Synthesis of Monodisperse Spherical Nanocrystals," *Angew. Chem. Int. Ed.* **46** (25), 4630–4660 (2007).
88. H. Goesmann and C. Feldmann, "Nanoparticulate Functional Materials," *Angew. Chem. Int. Ed.* **49** (8), 1362–1395 (2010).
89. S. Kango, S. Kalia, A. Celli, J. Njuguna, Y. Habibi, and R. Kumar, "Surface Modification of Inorganic Nanoparticles for Development of Organic-Inorganic Nanocomposites-A Review," *Prog. Polym. Sci.* **38** (8), 1232–1261 (2013).
90. G. Schmid, *Nanoparticles: From Theory to Application* (Wiley-VCH, Weinheim, 2004).
91. V. K. LaMer and R. H. Dinegar, "Theory, Production and Mechanism of Formation of Monodispersed Hydrosols," *J. Am. Chem. Soc.* **72** (11), 4847–4854 (1950).
92. C. B. Murray, D. J. Norris, and M. G. Bawendi, "Synthesis and Characterization of Nearly Monodisperse CdE (E = Sulfur, Selenium, Tellurium) Semiconductor Nanocrystallites," *J. Am. Chem. Soc.* **115** (19), 8706–8715 (1993).

93. S. Fischer, A. Salcher, A. Kornowski, H. Weller, and S. Förster, “Completely Miscible Nanocomposites,” *Angew. Chem. Int. Ed.* **50** (34), 7811–7814 (2011).
94. S. K. Kumar, N. Jouault, B. Benicewicz, and T. Neely, “Nanocomposites with Polymer Grafted Nanoparticles,” *Macromolecules* **46** (9), 3199–3214 (2013).
95. H. Pletsch, L. Peng, F. Mitschang, A. Schaper, M. Hellwig, D. Nette, A. Seubert, A. Greiner, and S. Agarwal, “Ultrasound-Mediated Synthesis of High-Molecular Weight Polystyrene-Grafted Silver Nanoparticles by Facile Ligand Exchange Reactions in Suspension,” *Small* **10** (1), 201–208 (2014).
96. A. C. Balazs, T. Emrick, and T. P. Russell, “Nanoparticle Polymer Composites: Where Two Small Worlds Meet,” *Science* **314** (5802), 1107–1110 (2006).
97. A. Ershad-Langroudi, C. Mai, G. Vigier, and R. Vassoille, “Hydrophobic Hybrid Inorganic-Organic Thin Film Prepared by Sol-Gel Process for Glass Protection and Strengthening Applications,” *J. Appl. Polym. Sci.* **65**, 2387–2393 (1997).
98. K. I. Winey and R. A. Vaia, “Polymer Nanocomposites,” *MRS Bull.* **32** (04), 314–322 (2007).
99. D. Paul and L. Robeson, “Polymer nanotechnology: Nanocomposites,” *Polymer* **49** (15), 3187–3204 (2008).
100. R. A. Vaia and H. D. Wagner, “Framework for Nanocomposites,” *Mater. Today* **7** (11), 32–37 (2004).
101. S. Mehdizadeh Taheri, S. Fischer, and S. Förster, “Routes to Nanoparticle-Polymer Superlattices,” *Polymers* **3** (4), 662–673 (2011).
102. N. Tsubokawa, “Surface Grafting of Polymers onto Nanoparticles in a Solvent-Free Dry-System and Applications of Polymer-grafted Nanoparticles as Novel Functional Hybrid Materials,” *Polym. J.* **39** (10), 983–1000 (2007).
103. P. Mansky, Y. Liu, E. Huang, T. P. Russell, and C. Hawker, “Controlling Polymer-Surface Interactions with Random Copolymer Brushes,” *Science* **275** (5305), 1458–1460 (1997).

104. H. Hakkinen, “The Gold-Sulfur Interface at the Nanoscale,” *Nat. Chem.* **4** (6), 443–455 (2012).



4

Reinforcement of Nanostructured Organogels by Hydrogen Bonds

Daniela Pirner, Martin Dulle, Miriam Mauer, and Stephan Förster

Physical Chemistry I, University of Bayreuth, Germany

Published in: RSC Advances, **2016**, 6 (48), 42730-42738

Reproduced with permission from The Royal Society of Chemistry

Abstract

Organogels based on hydrogen-bond reinforced ordered micellar assemblies, having a very well-defined nanoscale structure and dynamic behaviour, are synthesized and investigated. The organogels consist of block copolymer micelles with covalently linked hydrogen bonding groups at their periphery which mediate attractive interactions between adjacent micelles. The structure and the viscoelastic properties of the organogels were systematically investigated by small-angle X-ray scattering and dynamic-mechanical measurements. We find with increasing number of hydrogen bonding groups an increase of the storage modulus, an increase of the melting temperature, and the development of a yield point. We show that the macroscopic viscoelastic properties of the organogels can be described by two theoretical models allowing a direct relation to the nanoscale organogel structure, the number of hydrogen bonds and the hydrogen bond lifetimes. The high-modulus transparent organogels undergo a reversible melting transition which allows them to be processed into well-defined micron-sized shapes.

Introduction

Organogels are gels consisting of a liquid organic phase.¹ They are mechanically stabilized either by covalently cross-linked polymer networks or by self-assembly of low-molecular weight gelators into networks, which are formed by secondary interactions such as van der Waals forces or hydrogen bonds.² Nanostructured micellar organogels consisting of well-defined nanoscale building blocks offer the possibility to tailor gel mechanical properties *via* the size of the building blocks and their interactions in a very controlled way.

Block copolymers have the ability to self-assemble into well-defined nanostructures in solutions, *e.g.* into spherical or cylindrical micelles depending on the relative block lengths and solvent.^{3–6} At higher concentrations micelles further assemble into ordered lyotropic or thermotropic liquid crystalline phases. For spherical micelles, the most common phases are *fcc* (face-centered-cubic) and *bcc* (body-centered-cubic) phases, but also quasicrystalline phases have been reported.⁷ These phases can undergo order-disorder transitions (ODT) with varying temperature, which could be exploited to

generate organogels that can be reversibly molten and solidified by variation of temperature.

The self-assembly and phase behaviour of amphiphilic block copolymers in aqueous solutions is well known and characterized.^{8–10} However, the interesting field of self-assembly in organic solvents and the related liquid crystalline phase behaviour relevant for the generation of organogels has been less developed. Lodge *et al.*^{11–13} investigated the phase behavior of poly(styrene-*b*-isoprene) (PS-PI) block copolymers in three different styrene-selective, low-volatile dialkyl phthalates (di-*n*-butyl phthalate (DBP), diethyl phthalate (DEP), and dimethyl phthalate (DMP)) with varying block copolymer composition, concentration, and temperature. In dilute solutions micellar structures were identified, which undergo a sequence of lyotropic phase transitions with increasing concentration. When the temperature is increased at fixed copolymer composition and volume fraction, thermoreversible order-disorder transitions (ODT) and order-order transitions (OOTs) were observed.

The size of block copolymer micelles can be well tailored *via* block lengths and selectivity of the organic solvent. In order to form stable gels, they need to form networks, that can be either covalent networks or physical networks with a dynamic or transient nature with junctions that can break and recombine. Such junctions can be formed *via* attractive forces between interacting groups, *e.g.* hydrophobic interactions,^{14,15} metal-ligand interactions,¹⁶ ionic associations¹⁷ or hydrogen-bonding.^{18,19} Micelles, which can form transient micellar networks were first discovered for ABA block copolymers selectively dissolved in an B-selective solvent in order to self-assemble into micelles with an A-core surrounded by the B-blocks.¹⁵ The B-blocks can form bridges between the micelles resulting in a network of interconnected micelles. The network junction dynamics of these systems depends strongly on the A/B/solvent-thermodynamics and both cannot be independently varied.

Transient networks involving junctions formed by hydrogen-bonding would have more potential in this respect. The introduction of hydrogen bonding units in polymers leads to interesting material properties and has opened up the field of supramolecular polymers. The reversible, relatively strong, and non-covalent interactions allow the association of hydrogen bonding monomers into macromolecules, similar to “traditional” polymerization. As an instructive example, Meijer *et al.*²⁰ used self-complementary quadruple hydrogen bonding 2-ureido-4[1*H*]-pyrimidinone (UPy) units for the formation of supramolecular polymers. At high concentrations such polymers can form transient

networks due to the hydrogen bonding moieties. The strength and dynamics of dimerizing hydrogen bonded moieties is well-defined and can be quantified by the association constant, which *e.g.* for UPy is $k = 6 \cdot 10^7 \text{ M}^{-1}$ in chloroform at room temperature.

In the present work we investigate stable, well-defined nanostructured organogels based on block copolymer micelles interacting *via* hydrogen-bonding groups at their periphery. The network structure, the association strength and the kinetic time scale of network junction breaking/recombination, which is determined by the hydrogen bond association/dissociation kinetics, can be independently varied to gain insight into the relation between macroscopic mechanical behaviour relevant for applications, and the micro-/nanoscale structure and dynamics of the organogel.

The micelles are formed from monodisperse poly(isoprene-*b*-styrene) (PI-PS) block copolymers synthesized *via* living anionic polymerisation. A part of the block copolymers were subsequently end-functionalized with an UPy hydrogen bonding group (PI-PS-UPy). In diethyl phthalate (DEP), a selective solvent for the PS-block, PI-PS, PI-PS-UPy and selected mixtures thereof form spherical micelles, which can form transient networks *via* the UPy-units. By varying the content of PI-PS-UPy-block copolymers in the micelles, the association strength can be varied, as can be the melting temperature. This allows for the first time to obtain a direct relation between structure, association and hydrogen-bond dynamics on the viscoelasticity of the organogel by using dynamic-mechanical and small-angle X-ray scattering experiments.

Experimental Section

Polymer synthesis and characterization

Poly(isoprene-*b*-styrene) (PI-PS) was synthesized *via* sequential living anionic polymerization in cyclohexane at 40 °C. *sec*-Butyllithium (1.4 M, cyclohexane) was used as initiator. The monomers isoprene and styrene were dried and purified by distillation from calcium hydride and di-*n*-butylmagnesium solution (1 M, heptane) prior to polymerisation. The solvents cyclohexane and tetrahydrofuran (THF) were purified by distillation from a sodium/potassium alloy and a benzophenone/potassium complex. Ethylene oxide was used to introduce a functional OH-end group in the block copolymer. It was purified by stirring over calcium hydride at -60 °C, followed by distillation and

further treatment with *n*-butyllithium at -60 °C. After complete polymerisation of isoprene (≈ 6 h) a precursor is drawn and characterized. The styrene polymerization proceeded for about 5 h. Before the addition of ethylene oxide to the living block copolymer chains a small amount of THF (10% of the solution) was added. The reaction of capping the living chain ends with ethylene oxide was allowed to stir for at least 3 h. The reaction was terminated by adding a small amount of degassed isopropyl alcohol. The block copolymer was precipitated in isopropyl alcohol and dried under vacuum.

The characterization of the polymers was carried out by gel permeation chromatography (GPC) and $^1\text{H-NMR}$. The GPC consist of four SDplus MZ columns with a porosity range from 10^6 to 100 \AA and the measurements were performed at a flow rate of 1 mL min^{-1} in THF. Signals were detected with a Shodex RI-71 detector and a UV-detector. $^1\text{H-NMR}$ spectroscopy was performed in CDCl_3 , using a 300 MHz Bruker Ultrashield 300-spectrometer. The synthesized $\text{PI}_{210}\text{-PS}_{154}\text{-OH}$ has a molecular weight of 30300 g mol^{-1} and a polydispersity of $M_w/M_n = 1.03$.

The subscripts represent the degree of polymerisation. The volume fraction of polyisoprene in the block copolymer is 0.51 and was calculated by using densities of 0.90 and 1.05 g cm^{-3} for PI and PS, respectively. The PI microstructure was determined by $^1\text{H-NMR}$ and found to be 94% 1,4-addition.

The synthesis of 2(6-isocyanatohexylaminocarbonylamino)-6-methyl-4[1*H*]pyrimidinone was carried out according to Keizer *et al.*²² by coupling hexamethylenediisocyanate to methylisocytosine and characterized by $^1\text{H-NMR}$.

The functionalization of OH-terminated PI-PS was performed by refluxing the polymer together with an 4-fold excess of 2(6-isocyanatohexylaminocarbonylamino)-6-methyl-4[1*H*] pyrimidinone in anhydrous toluene at $110 \text{ }^\circ\text{C}$ for 2 h and adding dibutyltindilaurate as a catalyst.²² The reaction was terminated by cooling down to room temperature. The UPy-functionalized polymer was purified by centrifuging the mixture at 4500 rpm for 30 min and decanting off the solution. The residue was extracted with toluene and centrifuged again and decanted. The received polymer was precipitated and dried under vacuum. The PI-PS-UPy was characterized by $^1\text{H-NMR}$ and GPC. The degree of UPy-functionalization was determined to be 81%.

Micelle formation and characterization

As PS-selective solvent diethyl phthalate (DEP) was used in order to form micelles with a PI core and a PS corona.¹² The samples of PI-PS-OH and PI-PS-UPy micelles, as well as the micelles with different UPy content, were prepared by directly dissolving the solid block copolymer powder (or the different weight fraction of PI-PS-OH and PI-PS-UPy) in DEP. The samples were allowed to shake for 24 h to form micelles. The hydrodynamic radii of the micelles were determined by dynamic light scattering (DLS) and were carried out with a Malvern Instruments Zetasizer Nano Series device in dilute solutions in DEP at room temperature. Each sample was passed through a 0.2 μm filter prior measurement. All concentrations investigated were well above the cmc.¹¹

Rheology

Rheological properties of the concentrated micellar solutions ($\phi = 20$ wt% and 30 wt% in DEP) were studied by using a Malvern Instruments Bohlin Gemini HR Nano rheometer with a 8 or 25 mm stainless steel parallel plate-plate setup and gap width of 750 μm . For the temperature ramp measurement the strain was kept in the linear viscoelastic regime and the frequency was set to be fixed at 1 Hz. The temperature is ranging from 20 to 70 $^{\circ}\text{C}$ with a heating rate of 2 $^{\circ}\text{C min}^{-1}$. Flow curves were obtained at a constant temperature of 20 $^{\circ}\text{C}$.

Small-angle X-ray scattering

All SAXS data reported here were measured using the small-angle X-ray system “Double Ganesha AIR” (SAXSLAB, Denmark). The X-ray source of this laboratory-based system is a rotating anode (copper, MicoMax 007HF, Rigaku Corporation, Japan) providing a micro-focused beam at $\lambda = 0.154$ nm. The data are recorded by a position sensitive detector (PILATUS 300K, Dectris). The samples were measured and sheared in a modified Linkam css 450 shear stage. The original glass windows were exchanged with adhesive tape. This tape is very durable, near transparent for X-rays and has a flat signal in the observed q -range. Shearing was performed in an oscillatory fashion with a gap of 1 mm, a strain of 80% and a frequency of 8 Hz for 5 min before a measurement. The circularly averaged data were normalized to the measurement time.

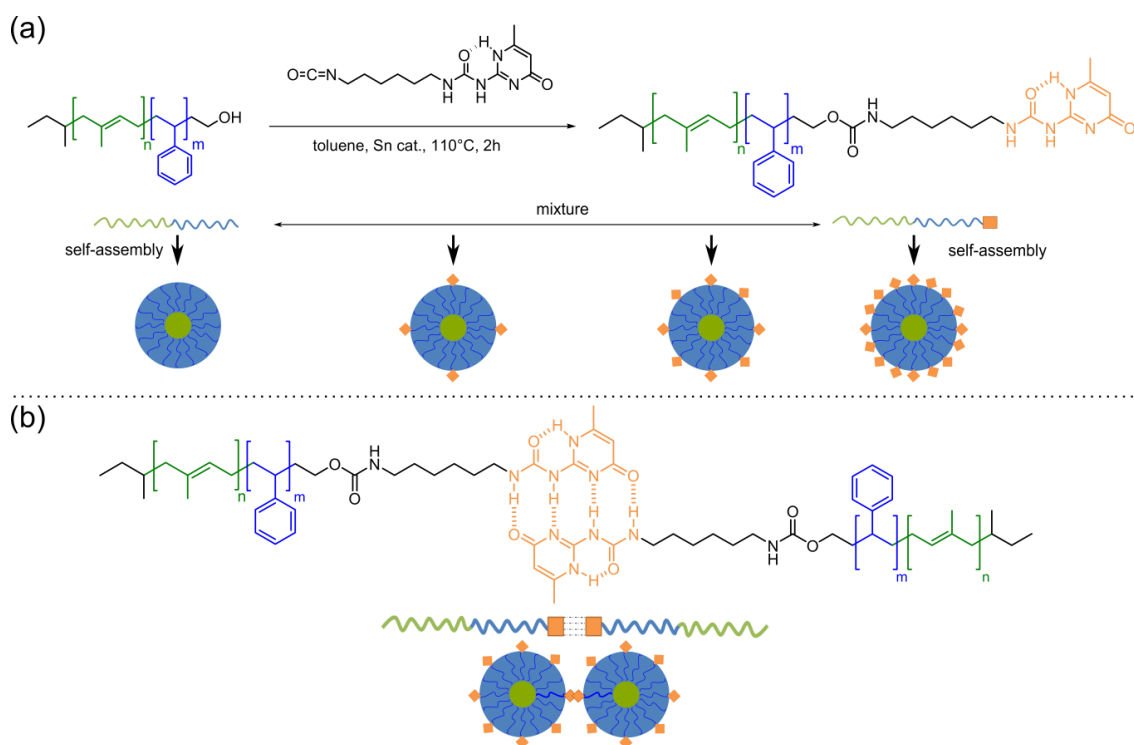
Cryo-SEM

The organogel samples were vitrified using a high-pressure freezing system (Leica EM HPM 100), freeze-fractured and then imaged using a Zeiss Ultra plus FE-SEM at a voltage of 1.0 kV.

Results and discussion

Scheme 4.1a shows the end-functionalization of PI-PS-OH with UPy using diisocyanate as a coupling agent. PI-PS-OH was synthesized by reacting the living PI-PS-anion with ethylene oxide. The diisocyanate is first coupled to methylisocytosine and, after purification, subsequently coupled to the terminal OH-group of the block copolymer.

In DEP, a selective solvent for the PS-block, PI-PS-OH, PI-PSUPy and mixtures thereof form spherical micelles. DEP has a low melting (-40.5 °C) and a high boiling point (295 °C), which made a very broad temperature range accessible. Since evaporation is very low, no influences of concentration changes during dynamic-mechanical and X-ray measurements are observed, even at elevated temperatures. The micelles consisting of a PI-core, a PS-corona and UPy-groups located at the surface of the micelles are shown in **Scheme 4.1b**. The UPy-groups can reversibly form self-complementary quadruple hydrogen bonds that lead to attractive interactions between the micelles.

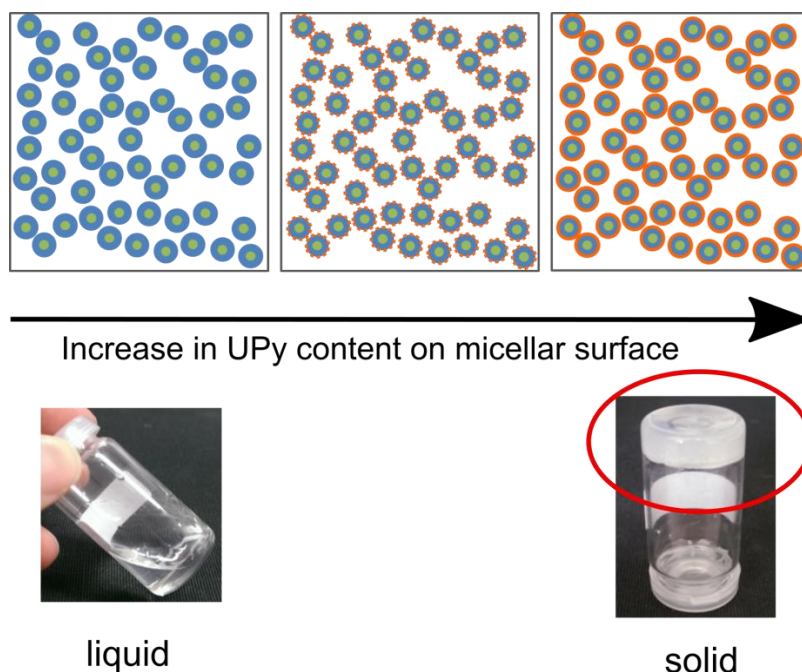


Scheme 4.1: Concept of micelle design: (a) functionalization of PI-PS-OH with a 2-ureido-4[1H]-pyrimidinone (UPy) unit yielding PI-PS-UPy block copolymers. Self-assembly of neat PI-PS-OH, PI-PS-OH + PI-PS-UPy mixtures, and neat PI-PS-UPy block copolymers in a PS-selective solvent (diethyl phthalate) leading to unmodified and surface-modified spherical micelles. (b) Formation of self-complementary 4-fold H bonds between the UPy units on the micellar surface forming a transient micellar network.

Detailed investigations on UPy-dimer formation in different solvents show the existence of three different tautomeric forms. The unfavourable 2-ureido-6[1H]-pyrimidinone is not able to form dimers. The 2-ureido-4[1H]-pyrimidinone and 2-ureido-4-pyrimidinol tautomer develops stable dimers and is dominant in organic solvents. The dimerization constant in chloroform and toluene were found to be $K = 6 \cdot 10^7 M^{-1}$ and $K = 6 \cdot 10^8 M^{-1}$, respectively.¹⁹ The mean dimer lifetimes were determined to be 0.17 s in chloroform and 1.7 s in toluene.²¹

The block copolymer concentrations in DEP were set to 20 and 30 wt%, where the solutions form well-defined lyotropic liquid crystalline phases. Below 20 wt%, the samples form low-viscous liquids, whereas at concentrations higher than 30 wt% the samples form hard solids, which are very difficult to homogenize and equilibrate for rheological studies. PI-PS-OH and PI-PS-UPy were mixed in ratios of $x = 0, 20, 40, 60, 80,$ and 100 wt% PI-PS-UPy. For quantitative calculations we need to keep in mind that the PI-PS-UPy obtained after synthesis has an actual degree of UPy-functionalization of 81% (see Experimental section), such that the above ratios correspond to actual UPy-

content of $f = 0, 16, 32, 49, 65$ and 81 wt%. We observe that the organogels become solid-like with increasing UPy-content as shown in **Scheme 4.2**.



Scheme 4.2: Transient micellar network formation in concentrated solutions in DEP (30 wt%). Increasing the UPy content on the micellar surface results in a transition from a liquid (0% UPy) to a solid (100% UPy) as illustrated in the sample photograph.

Inverting the vials, a clear difference between PI-PS-OH and PI-PS-UPy organogels is observed, where the PI-PS-OH organogels are viscous but still flowing, whereas the pure PI-PS-UPy organogels are homogeneous solids.

The micellar hydrodynamic size and micellar association were characterized by dynamic light scattering in dilute solutions. **Figure 4.1** shows the measured micellar size distributions (intensity average) of the pure PI-PS-OH ($x = 0$ wt%) and selected mixtures with $x = 60$ wt% and 100 wt%. The PI-PS-OH micelles exhibit a narrow size distribution with a hydrodynamic diameter of 39 nm. The UPy modification of the micellar surface leads to formation of aggregates due to attractive intermicellar interactions, leading to an additional peak in the size distribution at larger hydrodynamic diameters. In addition, the intensity of the micellar peak at 39 nm decreases with increasing number of UPy groups on the micellar surface indicating a higher fraction of aggregated micelles.

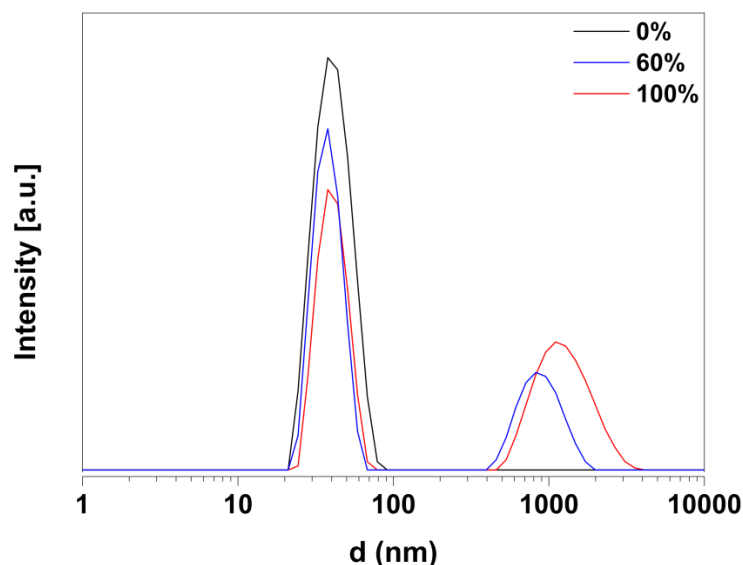


Figure 4.1: Micellar size distribution measured by DLS of PI-PS-OH (0% UPy) and PI-PS-UPy (60% and 100% UPy) micelles at room temperature ($c = 0.01$ wt% in DEP). Hydrodynamic diameter of the micelles is 39 nm. Additional peaks occur at 840 or 1150 nm for PI-PS-UPy 60% or 100% micellar aggregates, respectively.

To characterize the micellar structure in the organogel, we performed cryo-SEM on the 30 wt% PI-PS-UPy samples. The samples were vitrified by high-pressure freezing.

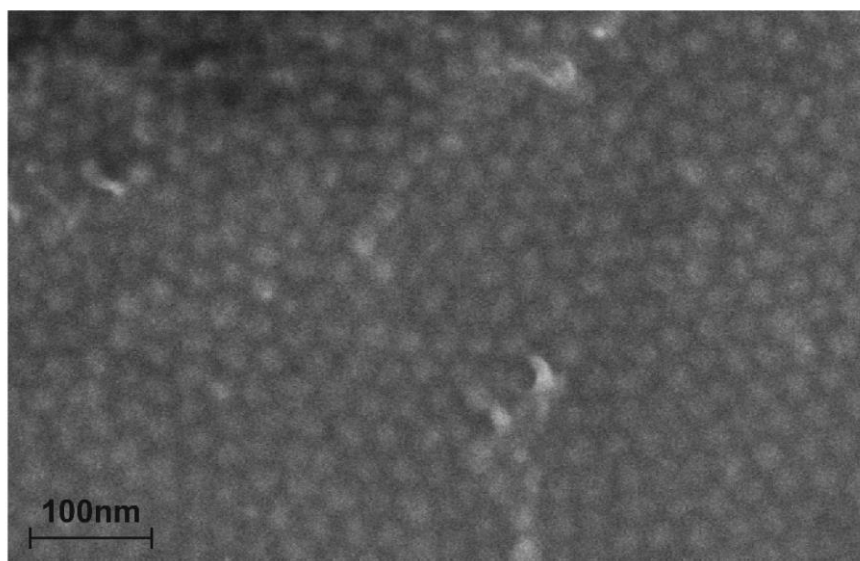


Figure 4.2: Cryo-SEM image of a 30 wt% PI-PS-UPy organogel showing the micellar network structure. The measured diameter of 36 nm is in very good agreement with the results from the SAXS-experiments in **Figure 4.6**.

Figure 4.2 shows a typical cryo-SEM image. The hexagonal close-packed arrangement and the measured intermicellar distance micellar distance of 36 nm is in very good agreement with an FCC unit cell dimension of $a = 51$ nm as determined by SAXS (see below), which corresponds to a nearest neighbour distance of $a_n = a/\sqrt{2} \approx 36.0$ nm. The

measured distance and the diameter of the micelles agree well with the hydrodynamic diameter of 39 nm as determined by dynamic light scattering.

In order to investigate the influence of increasing UPy-content on the viscoelastic properties of the organogels, dynamic-mechanical experiments were performed.

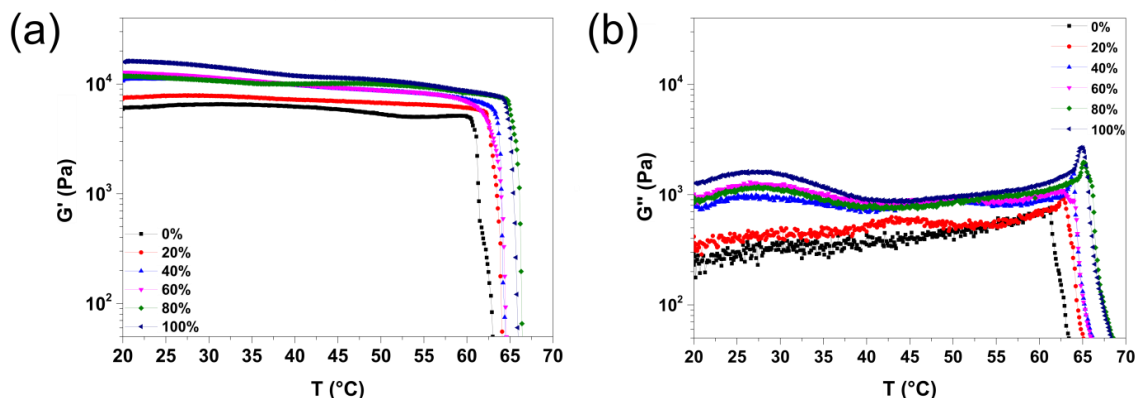


Figure 4.3: Temperature dependence of (a) the dynamic storage modulus G' and (b) the loss modulus G'' at a constant frequency of 1 Hz for micellar samples ranging from 0% up to 100% UPy content at a constant concentration of 30 wt% in DEP. The temperature ramp rate was set to $2\text{ }^{\circ}\text{C min}^{-1}$. The samples are elastic solids until they melt at temperatures between 60 and 65 $^{\circ}\text{C}$.

Figure 4.3 shows the temperature dependent oscillatory shear measurements. The storage moduli G' (**Figure 4.3a**) and the loss moduli G'' (**Figure 4.3b**) of six micellar samples ranging from $x = 0$ -100 wt% at a polymer concentration of $\phi = 30$ wt% in DEP, measured as a function of temperature at a fixed frequency of 1 Hz, are presented. All samples are elastic solid organogels, where the storage modulus G' is larger than the loss modulus G'' , and where G' shows a plateau at room temperature up to a temperature in the range of 60-65 $^{\circ}\text{C}$, above which the samples abruptly become low-viscous liquids. The elastic behaviour of the pure PI-PS-OH micellar organogels at $\phi = 30$ wt% polymer is caused by the high volume fraction of micelles, which form a close-packed structure where the micelles become localized. With increasing UPy-content we observe over the whole temperature range of elastic behaviour (up to 65 $^{\circ}\text{C}$) the storage modulus G' to show a nearly threefold increase with increasing UPy-content, *i.e.* from 6 kPa for $x = 0$ wt% to 16 kPa for $x = 100$ wt%. With increasing UPy-content also the melting temperature increases from 61.3 $^{\circ}\text{C}$ at $x = 0$ wt% to 65.1 $^{\circ}\text{C}$ at $x = 100$ wt%. The solid-to-liquid transition is sharp and reversible. The dynamic-mechanical experiments show that with increasing UPy-content the organogels show a significant increase of their elastic moduli and temperature stability.

In order to study the influence of micelle concentration on the viscoelastic properties, a $\phi = 20$ wt% solution of PI-PS-UPy ($x = 100$ wt%) micelles was compared to $\phi = 30$ wt% PI-PS-UPy (100%) sample (**Figure 4.4**).

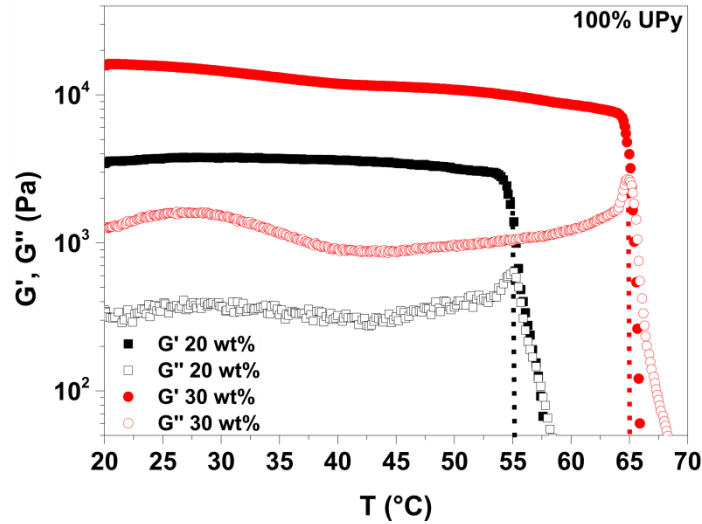


Figure 4.4: Temperature dependence of G' and G'' at 1 Hz for the 100% UPy micelles in DEP at concentrations of 20 wt% and 30 wt%. The melting temperature is shifted from 55 °C to 65 °C. The temperature ramp rate was set to 2 °C min⁻¹.

We observe that the storage modulus of the organogel with only 20 wt% micellar concentration is significantly lower, *i.e.* 3-4 kPa compared to 10-15 kPa of the 30 wt% concentration, and that also the temperature stability is lower, as the melting temperature is only 55 °C compared to 65.1 °C of the 30 wt% solution. This indicates that the melting transition is an disorder-order transition. The less concentrated samples have a lower micellar volume fraction, such that the micellar interactions, their localization in the close-packed structure, and the lattice binding energies are lower, such that lower temperatures are sufficient to melt the structure into a disordered solution. Still, attractive UPy-interaction play a significant role to stabilize the organogel structure, as pure PI-PS-OH micelles at 20 wt% had too small viscosities to be measured with our experimental setup.

The pronounced difference of the mechanical behaviour of the pure PI-PS-OH and the pure PI-PS-UPy samples at the lower concentration of 20 wt% can, however, be demonstrated by measuring the stress as a function of shear rate in a stress-controlled experiment as shown in **Figure 4.5**.

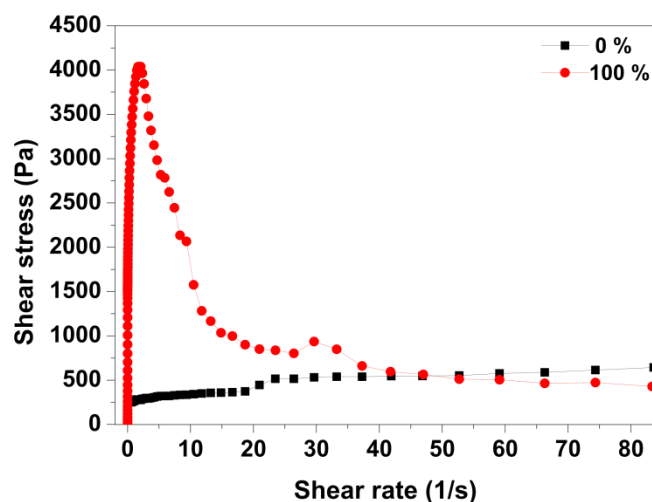


Figure 4.5: Flow curves for 0% and 100% UPy functionalized micelles in DEP (30 wt%). Shear stress is plotted as a function of shear rate showing a yield point of the UPy-functionalized micelles.

At the lowest shear-rates the PI-PS-UPy organogel exhibits a strong increase in shear stress until a maximum of 4040 Pa at a shear rate of $\gamma = 1.7 \text{ s}^{-1}$ is reached. The corresponding characteristic relaxation time of $\tau = 1/\gamma = 0.6 \text{ s}$ is well in agreement with the typical life time of the UPy-dimers in organic solvents, which is between 0.17 s for chloroform and 1.7 s for toluene.²¹ Following the maximum, the shear stress strongly decreases and finally levels off to values of 0.5 kPa at higher shear rates. This shows the existence of a UPy-mediated micellar network structure with a dynamic equilibrium of associating/dissociating UPy-dimers. If shear rates are faster than the inverse dimer lifetime, dimers dissociate due to the applied mechanical force and the network structure breaks down. The rheological behaviour of the unfunctionalized PI-PS-OH micellar organogel is very different. After a slight increase at the lowest shear rates, reaching a value of 320 Pa, the measured stress values reach a plateau with shear stress values being approximately equal to the high shear values measured for the UPy-functionalized micellar organogel, showing that after break-down of the UPy-dimers both micellar networks have equal viscoelastic properties. The unfunctionalized micellar networks are not expected to show a yield stress as their interactions are purely repulsive. The existence of a critical shear rate and yield stress explain the long-time solid-like behaviour observed in **Scheme 4.2**.

To provide insight into structural changes of the micellar organogels as a function of temperature and UPy-content, small-angle X-ray scattering measurements (SAXS) were performed at concentrations of 20 and 30 wt%. For 20 wt% micellar solutions only organogels with an UPy-content of $x \geq 0.4$ are investigated, because at lower contents the

solutions are low-viscous liquids. **Figure 4.6** shows the sets of measured SAXS-curves for the 20 and 30 wt% solutions. We observe typical scattering curves of ordered liquid crystalline micellar phases.

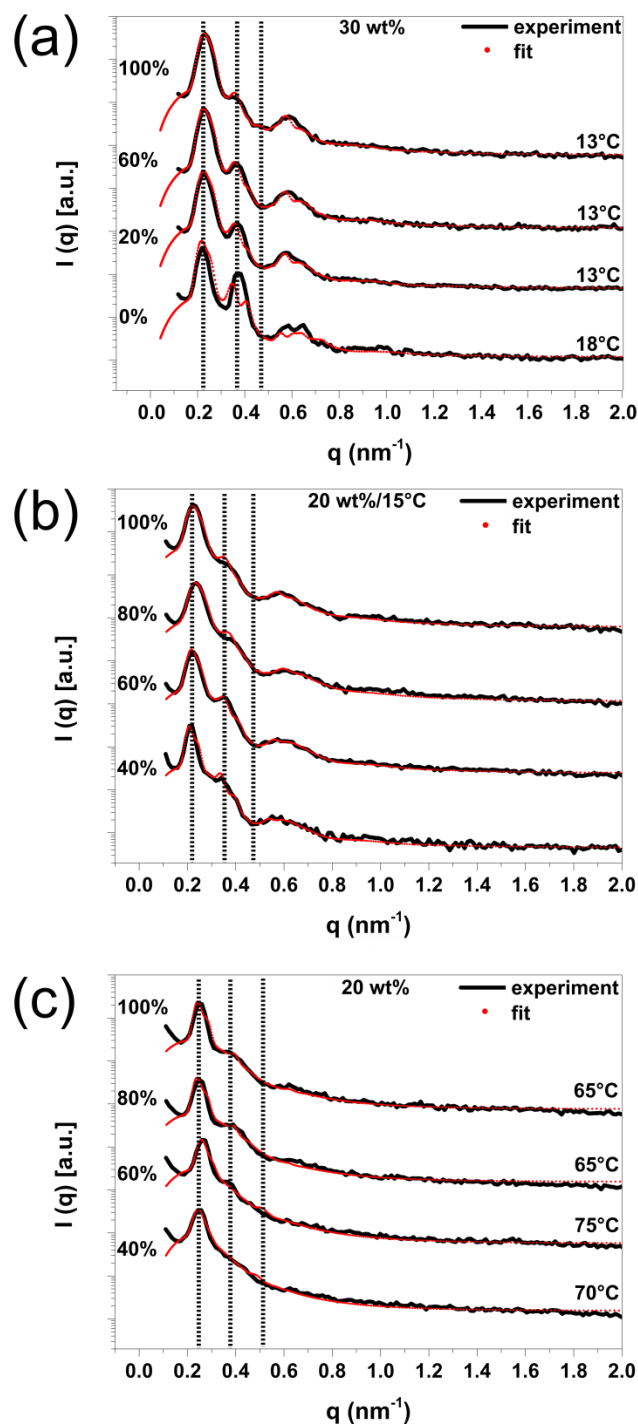


Figure 4.6: SAXS curves with corresponding fits (red dots) of selected micellar samples: (a) micelles in 30 wt.% DEP and (b) 20 wt.% in DEP with increasing number of UPy units at ambient temperatures; (c) micelles in 20 wt.% DEP at elevated temperatures close to the order-disorder transition.

For the 30 wt% solutions there is a pronounced first-order peak at $q = 0.22 \text{ nm}^{-1}$ with a higher-order reflection at $q = 0.37 \text{ nm}^{-1}$ and a form factor minimum at $q = 0.48 \text{ nm}^{-1}$. As shown by the vertical lines an increase of UPy-content does neither affect the position of the peaks, nor the position of the form factor minimum, thus showing the structure of the micelles and their ordered assembly are not altered by introducing the UPy-groups. This is also the case for the 20 wt% solution, where the position of the first-order reflection is at $q = 0.21 \text{ nm}^{-1}$ with a weak higher-order reflection at $q = 0.35 \text{ nm}^{-1}$ and a form factor minimum at $q = 0.48 \text{ nm}^{-1}$.

For a quantitative analysis, the scattering curves were fitted to an analytical expression describing the scattered intensity of ordered crystalline structures:^{23,24}

$$I(q) = (b_1 - b_2)^2 \rho_N \langle P(q, R) \rangle S(q) \quad (4.1)$$

where the b_j are the contrast factors of micelles and solvent, ρ_N is the number density of the micelles, and $P(q, R)$ is the form factor of the micellar core having spherical shape. $\langle \dots \rangle$ denotes the average over the particle size distribution, for which a Schulz-Zimm distribution is used. The sphere form factor is given by

$$P(q, R) = \frac{9}{(qR)^6} [\sin(qR) - qR \cos(qR)]^2 \quad (4.2)$$

The structure factor $S(q)$ which describes the spatial arrangement of the micelles is given by

$$S(q) = \frac{(2\pi)^3}{n_n \nu} \sum_{h,k,l} f_{hkl}^2 L_{hkl}(q, g_{hkl}) \quad (4.3)$$

where n_n is the number of micelles per unit cell, ν the unit cell volume, hkl the miller indices, L_{hkl} the peak shape function, and g_{hkl} the reciprocal lattice vector. Fits to **equation (4.1)** yield the space group, the unit cell dimension a , the mean crystalline domain size, the mean relative deviation of the micelles from the ideal lattice points (Debye-Waller factor), the mean micellar core radius, and the polydispersity of the micelles.

Figure 4.6 shows the measured SAXS-curves together with fits to **equation (4.1)** for concentrations of $\phi = 30 \text{ wt\%}$ (**Figure 4.6a**) and $\phi = 20 \text{ wt\%}$ (**Figure 4.6b**). We observe

pronounced Bragg peaks with higher order reflections, whose positions can be indexed on an *fcc*-lattice (space group *Fm3m*) in agreement with the study of Lodge *et al.*^{12,13} The determined unit cell dimensions a are in a range of 50-53 nm, depending on the concentration and temperature, but not on UPy-content. The micellar core radii R are 9.9-10.2 nm, which are also independent of the UPy-content. The unit cell dimension and the core radii will be used below for quantitative calculations of the fraction of elastically active chains. Typical domain sizes D are in the range 120-190 nm, thermal deviations δ (Debye-Waller factor) are between 2.5-5 nm, and the relative polydispersity σ of the micelles are all around 10%. The measured values are summarized in **Table 4.1**.

Table 4.1: Structural parameters determined from the SAXS-experiments: UPy-content x , unit cell dimension a , domain size D , Debye-Waller factor δ , micellar core radius R , relative standard deviation (polydispersity) of the micelles σ .

	$\phi = 20$ wt%			
x / wt%	40	60	80	100
a / nm	53	52	52	53
D / nm	192	154	121	128
δ / nm	4.8	4.3	3.8	3.9
R / nm	10.2	9.9	9.9	10.3
σ / nm	0.12	0.11	0.13	0.12
	$\phi = 30$ wt%			
x / wt%	0	20	60	100
a / nm	50	50	51	52
D / nm	167	146	143	137
δ / nm	3.0	2.8	2.7	2.6
R / nm	10.0	10.0	10.1	10.2
σ / nm	0.10	0.10	0.10	0.11

According to the rheological experiments the organogels melt above 55 °C for the 20 wt% solution and above 65 °C for the 30 wt% solution. As observed from the SAXS-curves measured for 20 wt% at temperatures above 55 °C (**Figure 4.6c**), we still observe scattering peaks, but with very weak second-order peaks, and more characteristic for liquid like order, indicating that the micelles undergo an order-disorder transition (ODT) into the disordered micellar phase upon heating above 55 °C.

For a more quantitative analysis of the dynamic-mechanical experiments we consider the shear-modulus of a gel as a function of the number of elastically connected junctions, *i.e.*

$$G' = n_{el}kT \quad (4.4)$$

where G' is the shear (storage) modulus, n_{el} the number density of elastically active chains, k Boltzmann's constant and T the temperature. From **equation (4.4)** we can calculate n_{el} for a micellar gel from the measured storage moduli at a given temperature, and compare this calculated value to the actual number density of polymer chains n_{ch} in the gel, which can be calculated from the dimension of the *fcc* unit cell a which is given by

$$n_{ch} = \frac{4Z}{a^3} \quad (4.5)$$

where Z is the number of block copolymer chains per micelle (association number). The factor 4 appears because there are four micelles per *fcc* unit cell. The association number Z can be calculated from the measured micellar core radius R , the degree of polymerization of the polyisoprene block N and the volume of an isoprene unit v_0 as

$$Z = \frac{4\pi R^3}{3Nv_0} \quad (4.6)$$

The volume of the polyisoprene repeat unit can be calculated from the molar mass $M = 68.12 \text{ g mol}^{-1}$ and the bulk density $\rho = 0.91 \text{ g cm}^{-3}$ as

$$v_0 = \frac{M}{\rho N} \quad (4.7)$$

By combining **equations (4.4-4.7)** the fraction of elastically active chains in the gels can be calculated as

$$\frac{n_{el}}{n_{ch}} = \frac{3G'Nv_0a^3}{16\pi kTR^3} \quad (4.8)$$

The calculated values are given in **Table 4.2**.

Table 4.2: Relative number of elastically active chains derived from two different theoretical models: UPy content x and f , relative number of active chains n_{el}/n_{ch} derived from **equation (4.8)** and Z_{el}/Z derived from **equation (4.11)**.

	$\phi = 20 \text{ wt\%}$			
$x / \text{wt\%}$	40	60	80	100
$f / \text{wt\%}$	32	49	65	81
n_{el} / n_{ch}	0.10	0.15	0.15	0.18
Z_{el} / Z	0.17	0.22	0.23	0.24
	$\phi = 30 \text{ wt\%}$			
$x / \text{wt\%}$	0	20	60	100
$f / \text{wt\%}$	0	16	49	81
n_{el} / n_{ch}	0.30	0.37	0.63	0.80
Z_{el} / Z	0.35	0.41	0.58	0.68

We observe that for the 20 wt% solution the fraction of active chains is relatively low, increasing from 11-17 % with increasing UPy-content. For the 30 wt% solution there is a more pronounced increase from 30-80% active chains. The near quantitative agreement between the calculated value of active chains based on the chemical UPy-content (81%) and on the rheological data (80%) for the 30 wt% concentration would mean that all PI-PS-UPy-chains are active, but has to be considered with some caution as the analysis of the rheological data are based on a quite simple model.

An alternative approach to quantify the influence of the UPy-content on the shear modulus is based on theoretical considerations of the intermicellar interaction potential $u(r)$, which is related to the shear modulus G' via its second derivative

$$G' = b \frac{n_n \varphi}{r} \frac{\partial^2 u(r)}{\partial r^2} \quad (4.9)$$

where n_n is the number of nearest neighbours (12 for *fcc*), φ is the close-packing fraction (*fcc*: $\varphi = \frac{\pi}{3\sqrt{2}} \approx 0.74$ for *fcc*), b a numerical prefactor of the order of 0.03, and r the distance between adjacent micelles. As an appropriate interaction potential we use the one derived by Witten and Pincus for spherical polymer brushes, which describes the block copolymer micellar systems quite well, *i.e.*

$$u(r) = \nu k T Z^{3/2} \ln\left(\frac{r}{2}\right) \quad (4.10)$$

where ν is Flory's exponent which for polymers in good solvents is $\nu = 0.6$. G' can then be calculated by taking the second derivative of $u(r)$ as

$$G' = b \frac{n_n \varphi}{r^3} \nu k T Z_{el}^{3/2} \quad (4.11)$$

With all geometric factors (b , n_n , r) being equal for varying UPy-contents, the association number Z_{el} derived from **equation (4.11)** using measured values of G' reflect the number of elastically active chains and their influence on the storage modulus G' . The ratio Z_{el}/Z is then a measure of the fraction of elastically active chains and is also summarized in **Table 4.2**. We observe very similar trends as for the ratio n_{el}/n_{ch} , *i.e.* for the 20 wt% solution there are rather small values, in the range of 17-24%, which increase only slightly with UPy-content. For the 30 wt% solution the values are higher, increasing from 35 to 68% (see **Figure 4.7**).

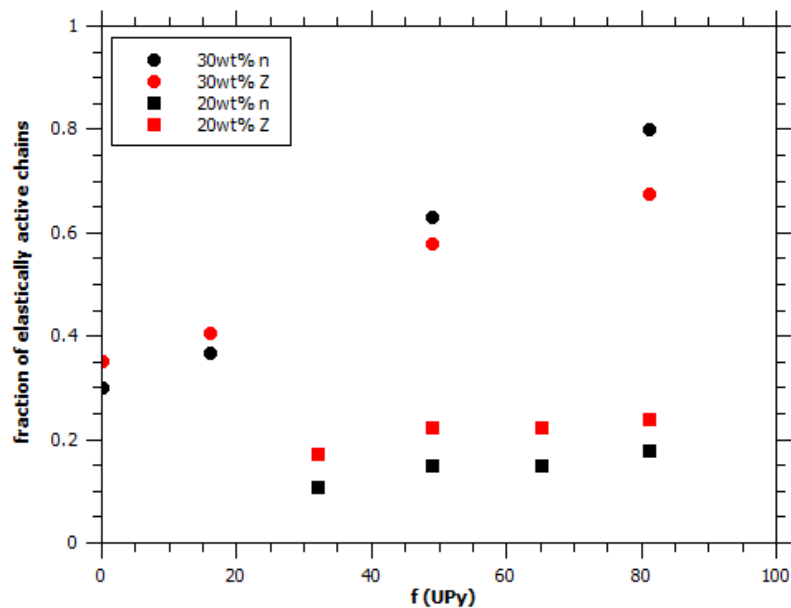


Figure 4.7: Fraction of elastically active chains as a function of the UPy-content calculated from two different models for concentrations of 20 and 30 wt%.

Both models show that the presence of the UPy-groups significantly increases the number of elastically active chains of the organogels. The calculations in particular show that the well-defined structure of the micellar organogels and their UPy-content can be well related *via* quantitative models to the observed macroscopic viscoelastic properties.

Since the organogels can be reversibly molten and solidified, similar to polymers, standard polymer molding techniques can be used to create well-defined organogel shapes. As the organogels have quite low viscosity in their molten state, we expected that micromolding should be possible to produce structural features in the micrometer range. To test this idea we mold-casted the molten liquid organogel using a fluoropolymer master featuring a parallel micron-sized channel structure, which was manufactured by soft lithography. The low adhesion of the fluoropolymer helped to remove the solidified organogel from the mold. **Figure 4.8** shows a transmission optical micrograph of the replicated channels in the organogel.

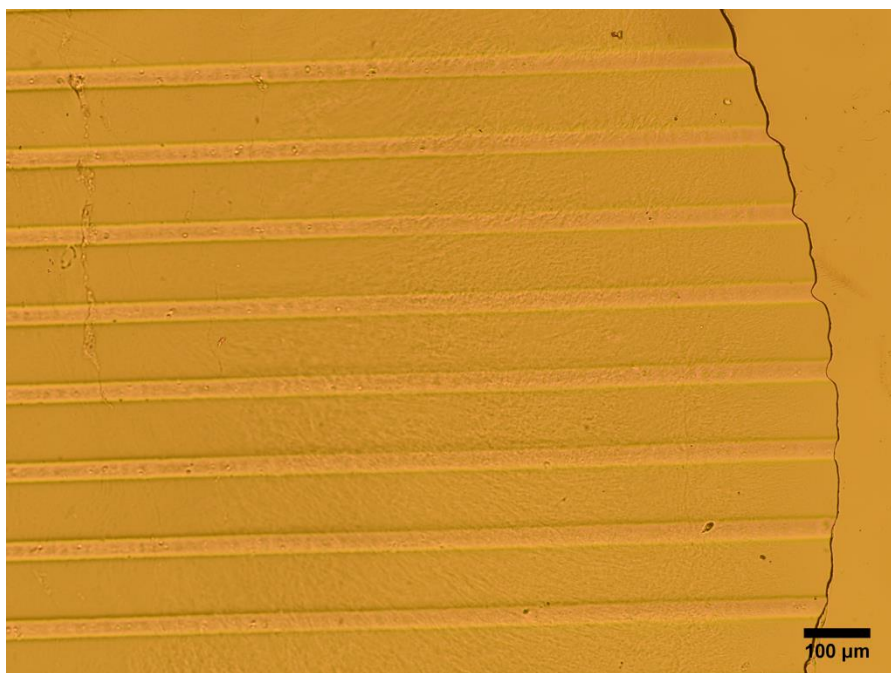


Figure 4.8: Optical micrograph of a channel array structure imprinted into the organogel by mold-casted from a fluoropolymer master, which was manufactured by soft lithography. The distance between the channels is 87 μm .

The distance between adjacent channels is 87 μm , the channel width is 32 μm , demonstrating that organogels can be well structured by micromolding.

Conclusions

We have developed organogels based on hydrogen-bond reinforced ordered micellar assemblies, having a very well-defined nanoscale structure and dynamic behaviour, which can nearly quantitatively related to their macroscopic viscoelastic properties. The organogels consist of block copolymer micelles with covalently linked hydrogen bonding UPy-group on their periphery, mediating transient attractive interactions between adjacent micelles *via* the reversible association/dissociation of dimers. An increasing UPy-content increases the storage modulus and the melting temperature. UPy-functionalized organogels show yielding behaviour with the maximum yield stress at shear rates, that correspond to the inverse of the UPy-dimer lifetime. Using two simple mechanical models we show that the molecular-/nano-scale properties of the micellar organogels can well be directly related to their macroscopic viscoelastic properties making them an interesting model system for a general study of such relationships. At temperatures above the order-disorder transition (55-65 $^{\circ}\text{C}$) the organogels melt into low-viscous solutions.

As the melting transition is reversible, they can thus be mold-casted at moderate temperatures into structures with micron-size precision, which is an interesting additional feature of these high-modulus, transparent, non-volatile organogels.

Acknowledgements

This work was supported by the ERC-Advanced Grant “Stream” #291211. We thank the Electron Microscopy Keylab facility of the University of Bayreuth for experimental support.

Supporting Information

Polymer and Precursor Characterisation

¹H-NMR:

2(6-Isocyanatohexylaminocarbonylamino)-6-methyl-4[1H]pyrimidinone

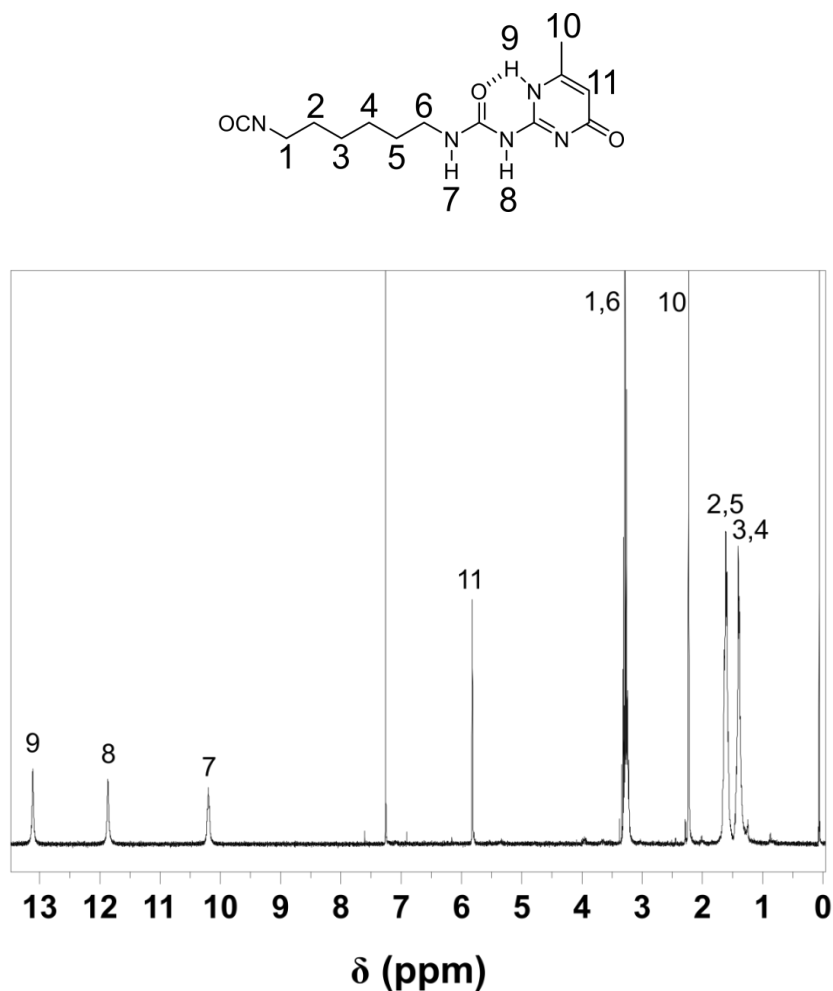


Figure S4.1 ¹H-NMR of 2(6-isocyanatohexylaminocarbonylamino)-6-methyl-4[1H]pyrimidinone in CDCl₃ (300 MHz).

¹H-NMR (300 MHz, CDCl₃): δ (ppm) = 1.23-1.49 (m, 4H, H_{3,4}), 1.50-1.70 (m, 4H, H_{2,5}), 2.23 (s, 3H, H₁₀), 3.20-3.34 (m, 4H, H_{1,6}), 5.82 (s, 1H, H₁₁), 10.20 (s, 1H, H₇), 11.87 (s, 1H, H₈), 13.11 (s, 1H, H₉).

PI-PS-OH

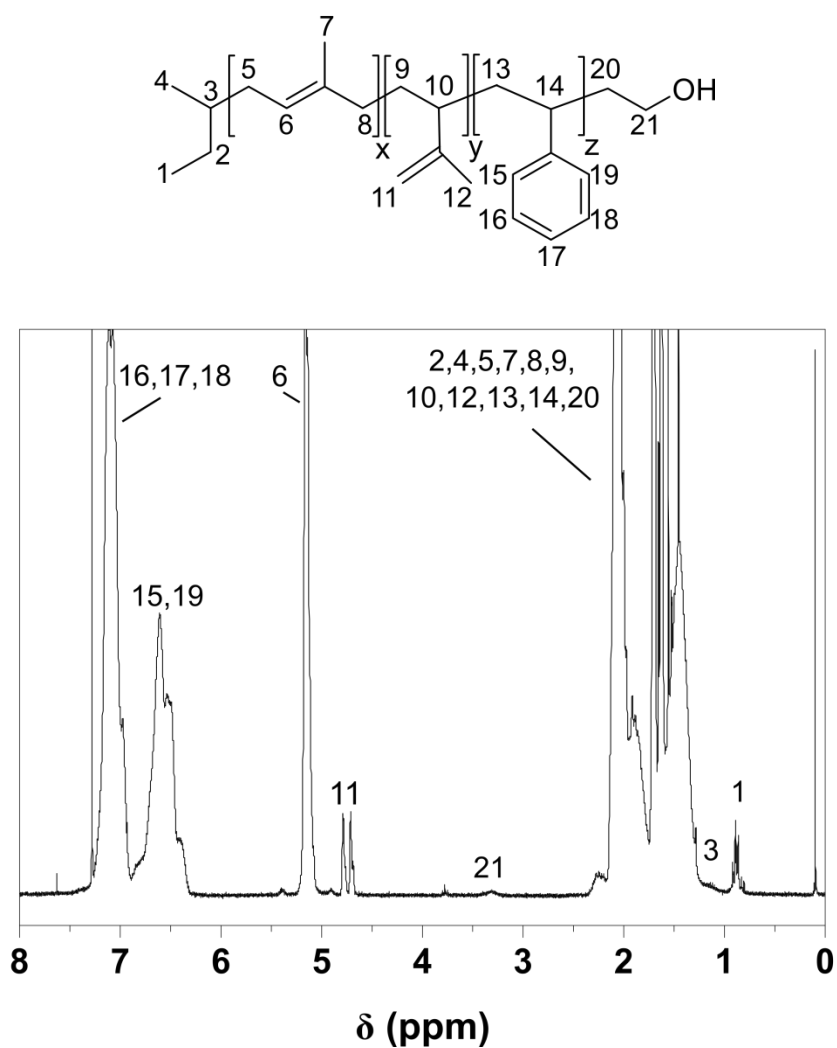


Figure S4.2: $^1\text{H-NMR}$ of poly(isoprene-*block*-styrene) in CDCl_3 .

$^1\text{H-NMR}$ (300 MHz, CDCl_3): δ (ppm) = 0.76-0.90 (m, 3H, H_1), 1.00-1.19 (m, 1H, H_3), 1.20-2.35 (m, 23H, $\text{H}_{2,4,5,7,8,9,10,12,13,14,20}$), 3.60 (m, 2H, H_{21}), 4.62-4.81 (m, 2H per unit 3,4-PI, H_{11}), 5.00-5.21 (m, 1H per unit 1,4-PI, H_6), 6.29-7.24 (m, 5H per unit PS, $\text{H}_{15,16,17,18,19}$).

PI-PS-UPy

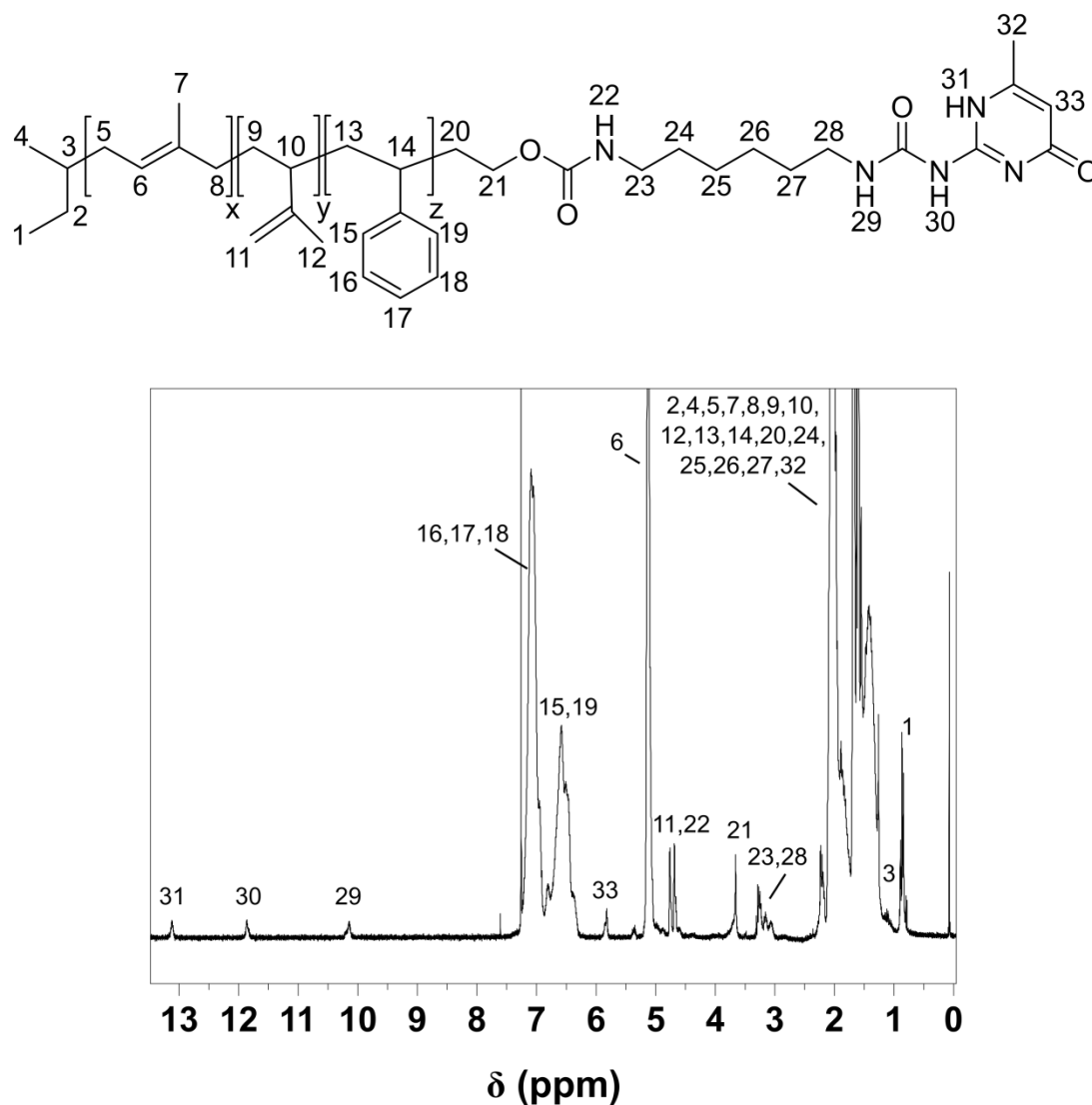


Figure S4.3: ¹H-NMR of poly(isoprene-*block*-styrene)-UPy in CDCl₃.

¹H-NMR (300 MHz, CDCl₃): δ (ppm) = 0.76-0.90 (m, 3H, H₁), 1.00-1.19 (m, 1H, H₃), 1.20-2.35 (m, 34H, H_{2,4,5,7,8,9,10,12,13,14,20,24,25,26,27,32}), 2.97-3.31 (m, 4H, H_{23,28}), 3.63-3.73 (m, 2H, H₂₁), 4.62-4.81 (m, 2H per unit 3,4-PI, H₁₁ + s, 1H, H₂₂), 5.00-5.21 (m, 1H per unit 1,4-PI, H₆), 5.28 (s, 1H, H₃₃) 6.29-7.24 (m, 5H per unit PS, H_{15,16,17,18,19}), 10.20 (s, 1H, H₂₉), 11.87 (s, 1H, H₃₀), 13.11 (s, 1H, H₃₁).

GPC:

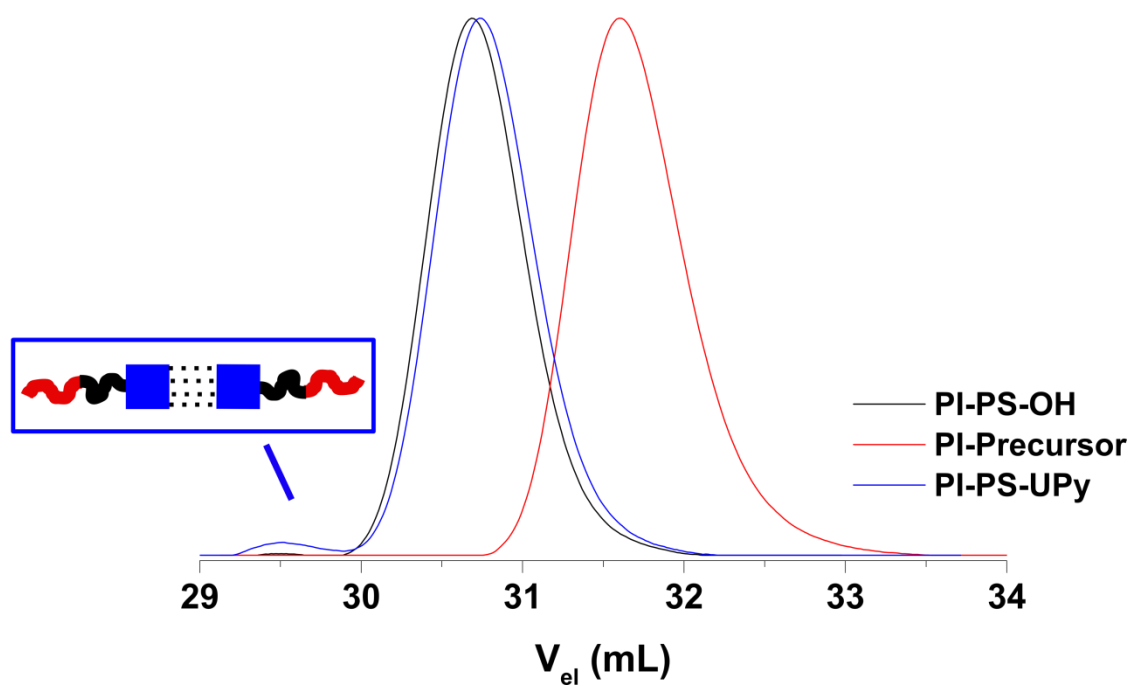


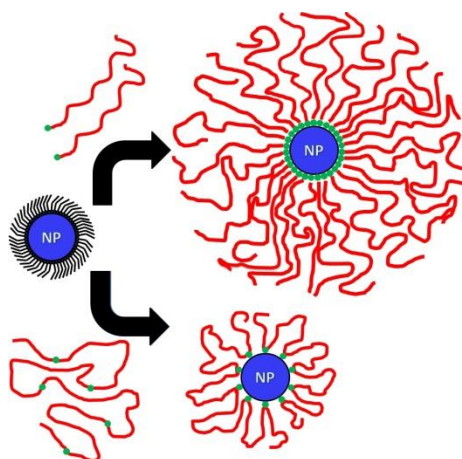
Figure S4.4: GPC measurements of poly(isoprene-*block*-styrene) (PI-PS), PI precursor, and PI-PS-UPy in THF at room temperature with a flow rate of 1 mL/min ($c \approx 1$ mg/mL).

References

1. A. R. Hirst, B. Escuder, J. F. Miravet, and D. K. Smith, “High-Tech Applications of Self-Assembling Supramolecular Nanostructured Gel-Phase Materials: From Regenerative Medicine to Electronic Devices,” *Angew. Chem. Int. Ed.* **47** (42), 8002–8018 (2008).
2. A. Banerjee, G. Palui, and A. Banerjee, “Pentapeptide Based Organogels: The Role of Adjacently Located Phenylalanine Residues in Gel Formation,” *Soft Matter* **4** (7), 1430–1437 (2008).
3. I. W. Hamley, *The Physics of Block Copolymers* (Oxford University Press, Oxford, New York, 1998).
4. L. Zhang and A. Eisenberg, “Multiple Morphologies of "Crew-Cut" Aggregates of Polystyrene-*b*-poly(acrylic acid) Block Copolymers,” *Science* **268** (5218), 1728–1731 (1995).
5. B. Lindman and P. Alexandridis, *Amphiphilic Block Copolymers. Self-Assembly and Applications*, 1st ed. (Elsevier, Amsterdam, New York, 2000).
6. S. Förster and T. Plantenberg, “From Self-Organizing Polymers to Nanohybrid and Biomaterials,” *Angew. Chem. Int. Ed.* **41** (5), 688–714 (2002).
7. S. Fischer, A. Exner, K. Zielske, J. Perlich, S. Deloudi, W. Steurer, P. Lindner, and S. Förster, “Colloidal Quasicrystals with 12-fold and 18-fold Diffraction Symmetry,” *Proc. Natl. Acad. Sci. U.S.A.* **108** (5), 1810–1814 (2011).
8. G. Wanka, H. Hoffmann, and W. Ulbricht, “Phase Diagrams and Aggregation Behavior of Poly(oxyethylene)-Poly(oxypropylene)-Poly(oxyethylene) Triblock Copolymers in Aqueous Solutions,” *Macromolecules* **27** (15), 4145–4159 (1994).
9. Z. Zhou and B. Chu, “Phase Behavior and Association Properties of Poly(oxypropylene)-Poly(oxyethylene)-Poly(oxypropylene) Triblock Copolymer in Aqueous Solution,” *Macromolecules* **27** (8), 2025–2033 (1994).

10. D. A. Hajduk, M. B. Kossuth, M. A. Hillmyer, and F. S. Bates, “Complex Phase Behavior in Aqueous Solutions of Poly(ethylene oxide)–Poly(ethylene) Block Copolymers,” *J. Phys. Chem. B* **102** (22), 4269–4276 (1998).
11. T. P. Lodge, J. Bang, K. J. Hanley, J. Krocak, S. Dahlquist, B. Sujan, and J. Ott, “Origins of Anomalous Micellization in Diblock Copolymer Solutions,” *Langmuir* **19** (6), 2103–2109 (2003).
12. T. P. Lodge, B. Pudil, and K. J. Hanley, “The Full Phase Behavior for Block Copolymers in Solvents of Varying Selectivity,” *Macromolecules* **35** (12), 4707–4717 (2002).
13. K. J. Hanley, T. P. Lodge, and C.-I. Huang, “Phase Behavior of a Block Copolymer in Solvents of Varying Selectivity,” *Macromolecules* **33** (16), 5918–5931 (2000).
14. H. Bagger-Jørgensen, L. Coppola, K. Thuresson, U. Olsson, and K. Mortensen, “Phase Behavior, Microstructure, and Dynamics in a Nonionic Microemulsion on Addition of Hydrophobically End-Capped Poly(ethylene oxide),” *Langmuir* **13** (16), 4204–4218 (1997).
15. M. Odenwald, H.-F. Eicke, and W. Meier, “Transient Networks by ABA Triblock Copolymers and Microemulsions: A Rheological Study,” *Macromolecules* **28** (14), 5069–5074 (1995).
16. J. B. Beck and S. J. Rowan, “Multistimuli, Multiresponsive Metallo-Supramolecular Polymers,” *J. Am. Chem. Soc.* **125** (46), 13922–13923 (2003).
17. A. Eisenberg, B. Hird, and R. B. Moore, “A New Multiplet-Cluster Model for the Morphology of Random Ionomers,” *Macromolecules* **23** (18), 4098–4107 (1990).
18. R. P. Sijbesma, F. H. Beijer, L. Brunsveld, Folmer, Brigitte J. B., Hirschberg, J. H. K. Ky, Lange, Ronald E. F. M., Lowe, Jimmy K. L., and E. W. Meijer, “Reversible Polymers Formed from Self-Complementary Monomers Using Quadruple Hydrogen Bonding,” *Science* **278** (5343), 1601–1604 (1997).
19. L. Brunsveld, Folmer, B. J. B., E. W. Meijer, and R. P. Sijbesma, “Supramolecular Polymers,” *Chem. Rev.* **101** (12), 4071–4098 (2001).

20. B. Folmer, R. P. Sijbesma, R. M. Versteegen, van der Rijt, Joost A. J., and E. Meijer, “Supramolecular Polymer Materials: Chain Extension of Telechelic Polymers Using a Reactive Hydrogen-Bonding Synthon,” *Adv. Mater.* **12** (12), 874–878 (2000).
21. Söntjens, Serge H. M., R. P. Sijbesma, van Genderen, Marcel H. P., and E. W. Meijer, “Stability and Lifetime of Quadruply Hydrogen Bonded 2-Ureido-4[1 H]-pyrimidinone Dimers,” *J. Am. Chem. Soc.* **122** (31), 7487–7493 (2000).
22. H. M. Keizer, R. van Kessel, R. P. Sijbesma, and E. Meijer, “Scale-up of the Synthesis of Ureidopyrimidinone Functionalized Telechelic Poly(ethylenebutylene),” *Polymer* **44** (19), 5505–5511 (2003).
23. S. Förster, A. Timmann, M. Konrad, C. Schellbach, A. Meyer, S. S. Funari, P. Mulvaney, and R. Knott, “Scattering Curves of Ordered Mesoscopic Materials,” *J. Phys. Chem. B* **109** (4), 1347–1360 (2005).
24. S. Förster, S. Fischer, K. Zielske, C. Schellbach, M. Sztucki, P. Lindner, and J. Perlich, “Calculation of Scattering-Patterns of Ordered Nano- and Mesoscale Materials,” *Adv. Colloid Interface Sci.* **163** (1), 53–83 (2011).



5

Polymer Ligand Exchange to Control Stabilization and Compatibilization of Nanocrystals

Sascha Ehlert,[†] Sara Mehdizadeh Taheri,[†] Daniela Pirner,[†] Markus Drechsler,[§] Hans-
Werner Schmidt,^{‡§} Stephan Förster^{*†§}

[†] Physical Chemistry I, University of Bayreuth, Germany

[‡] Macromolecular Chemistry I, University of Bayreuth, Germany

[§] Bayreuther Institut für Makromolekülforschung and Bayreuther Zentrum für Kolloide
Grenzflächen, University of Bayreuth, Germany

Published in: ACS Nano, **2014**, 8 (6), 6114–6122

Reprinted with permission from Ehlert, S.; Mehdizadeh Taheri, S.; Pirner, D. *et al* ACS
Nano, 2014, 8 (6), pp 6114–6122. © 2014 American Chemical Society.

Abstract

We demonstrate polymer ligand exchange to be an efficient method to control steric stabilization and compatibilization of nanocrystals. A rational design of polymer binding groups and ligand exchange conditions allows to attach polymer brushes with grafting densities $>1 \text{ nm}^{-2}$ to inorganic nanocrystals for nearly any nanocrystal/polymer combination using only a few types of binding groups. We demonstrate the potential of the method as an alternative to established grafting-from and grafting-to routes in considerably increasing the stabilization of inorganic nanocrystals in solution, to prepare completely miscible polymer nanocomposites with a controllable distance between nanoparticles, and to induce and control aggregation into percolation networks in polymeric matrices for a variety of different nanocrystal/polymer combinations. A dense attachment of very short polymer ligands is possible enabling to prepare ordered nanoparticle monolayers with a distance or pitch of only 7.2 nm, corresponding to a potential magnetic storage density of 12.4 Tb/in². Not only end-functionalized homopolymers, but also commercially available copolymers with functional comonomers can be used for stable ligand exchange, demonstrating the versatility and broad potential of the method.

Introduction

Nanocrystals and polymer nanocomposites are of immense interest in fundamental research as well as in a large variety of industrial applications. As an example, semiconductor nanocrystals (quantum dots) are used in medical applications as fluorescent tags,^{1,2} as LEDs³ or tunable lasers^{4,5} in optical applications, or for energy conversion in photovoltaic cells.⁶⁻⁸ Magnetic nanocrystals find applications as contrast agents in magnetic resonance imaging,⁹ or metal nanoparticles in catalytic applications.¹⁰ The stability of nanocrystals in solution is crucial to prevent agglomeration with loss of functionality. The combination of nanocrystals and a polymer matrix leads to nanocomposites. These composites could have enhanced mechanical,¹¹ optical¹² or electrical¹³ properties, but uncontrolled agglomeration often prevents the enhancement

and even deteriorates many useful properties. Therefore, it is of great importance to avoid or, even better, to control the agglomeration of nanocrystals.

The most common way to efficiently stabilize nanocrystals against agglomeration is to cover them with a polymeric brush. Such sterically stabilized particles are known to form stable colloidal solutions¹⁴ or, if the polymer brush is compatible with a polymer matrix, to form well dispersed nanocomposites.¹⁵ There are two established approaches to form a polymer brush on a surface. The first approach is the grafting-from method. By this method the polymer is grown from initiator groups which have been covalently linked to the nanocrystal surface¹⁶ to obtain a covalently bound polymer layer. The polymer density depends on the grafting density of the initiator groups. The grafting-from method allows a variety of different polymerization types such as radical, anionic and cationic polymerization. Because of the covalent bond of the polymer a grafting density of 0.4 nm^{-2} is sufficient to stabilize nanocrystals.¹⁷ A drawback of this method is the need to develop a new initiator coupling reaction scheme for each new nanocrystal-polymer combination. Further, there is no straightforward way to control nanocrystal agglomeration, if this would be desired.

The second approach is the grafting-to method. This method has the advantage that polymers could be presynthesized with established polymerization procedures for a state-of-the-art control of composition, architecture, and polydispersity. The preformed polymer will be covalently bound to the nanocrystals by a chemical reaction between a functional end group of the polymer and a functional group at the nanocrystal surface.¹⁸ Again, a drawback is the need to establish new functional group linking schemes for each new nanocrystal-polymer combination. In addition, a control of agglomeration cannot easily be achieved, and due to steric repulsion of the attached polymer chains, high grafting densities are hard to reach.

A concept to work around establishing new covalent linker chemistries is to coat nanocrystals with a shell of silica, for which covalent attachment schemes for initiators and covalent binding groups have been well established.¹⁹⁻²¹ However, this requires to develop and optimize new nanocrystal-silica core/shell-growth procedures, which is not a trivial task. Therefore, a versatile method that would allow stable, high-density polymer attachment for a large variety of nanocrystal-polymer combinations would be highly desirable.

A possible approach could be based on the exchange of nanocrystal surface ligands. State-of-the-art methods to prepare inorganic nanocrystals²² yield nanoparticles that are

stabilized by alkyl phosphines, amines or carboxylic acids. These groups have proven to be most efficient in controlling nanocrystal growth during synthesis, and to provide stability of the final particles in solution. The exchange of these surface ligands with polymers could be an attractive route for a flexible and versatile polymer attachment. So far, the exchange of coordinating surfactants has been only reported for short organic molecules²³ and thiol-functionalized polymers.^{24,25} The exchange with short organic molecules is mostly used to attach new functional groups to the nanocrystal surface or to transfer the nanocrystals into another solvent.^{26–28} The exchange with thiol groups is specifically used for gold nanocrystals because of the high affinity of gold to thiols, providing bonding that is nearly as strong as a covalent bond.

Here, we outline a polymer ligand exchange method which is broadly applicable to stabilize a large variety of different nanocrystal-polymer combinations. It is based on coordinative surface binding, which is successfully used in nanocrystal synthesis. We demonstrate the versatility of this ligand exchange method for the preparation of a variety of different polymer brush stabilized nanocrystals and show the potential for solution stabilization, nanocomposite compatibility, nanoparticle distance control to sub-10 nm pitch structures, and the controlled agglomeration to form percolation networks.

Results and discussion

Thermodynamic considerations

The coordinative ligand exchange can be thermodynamically described by a reaction $NP - L1 + L2 \rightleftharpoons NP - L2 + L1$, where $NP - L1$ are the nanocrystals (NP) coated with the original low-molecular weight ligand $L1$, and $NP - L2$ are the nanocrystals coated with the desired polymer ligand $L2$. From the law of mass action it follows that the concentration of the desired polymer-coated nanocrystal is given by

$$[NP \cdot L2] = K \frac{[NP \cdot L1][L2]}{[L1]} \quad (5.1)$$

where K is the equilibrium binding constant. In order to achieve a high yield of $[NP \cdot L2]$, one has to choose ligands with a large binding constant K , work with a large excess of polymer ligand $[L2]$, and remove the originally bound low-molecular weight ligand $[L1]$.

Ligands with suitable binding constants for ligand exchange procedures can be identified in a rational way by using Pearson's hard/soft acid/base (HSAB) principle. Most of the metals or metal ions in nanocrystals can be characterized as soft acids (Cd^{2+} , Ag^0 , Au^0) or as borderline acids (Fe^{2+} , Pb^{2+} , Zn^{2+}). Oxidic nanoparticles (ZnO , Fe_2O_3) can be considered as hard bases. Accordingly, the metals would best be coordinated by soft bases such as thiols, phosphines or phosphonates, or borderline bases such as pyridine. Hard bases would be best stabilized by hard acids, such as carboxylic acids. For a given ligand, the binding strength could be further increased by using multidentate ligands.

Not surprisingly, the above choice of ligands corresponds to the set of ligands which are used in the currently most efficient synthetic procedures of nanocrystals, *e.g.*, by hot injection routes, where alkyl oleates (*e.g.*, oleic acid), phosphines (*e.g.*, trioctyl phosphine (TOP)), phosphonates (*e.g.*, trioctylphosphine oxide (TOPO)) are commonly used to stabilize nanoparticles during synthesis.²²

An important issue when using polymeric ligands is to *not* use the ligands having the highest binding strength, but somewhat more moderate binding. A certain reversibility of surface coordination and decoordination is needed to obtain dense brush layers for sufficient steric stabilization of the nanocrystals in solution or compatibilization in polymer nanocomposites. This reversibility allows polymer chains to relocalize on the nanoparticle surface to facilitate attachment of further polymer chains to increase the brush density. The importance of chain relocalization on nanocrystal surfaces has been recently shown by HRTEM, and has a pronounced effect on the colloidal stability and aggregation.²⁹

In line with these considerations we observe that optimal for polymer ligand exchange procedures are (1) combinations of PbS-, Fe_3O_4 -, ZnO- (borderline acids Pb^{2+} , Fe^{2+} , Zn^{2+}) and CdSe-, Ag-nanoparticles (soft acids Cd^{2+} , Ag^0) with multidentate amines (hard bases) such as diethylenetriamine (DETA) or pentaethylenhexamine (PEHA), or (2) Fe_3O_4 -, ZnO-nanoparticles (hard bases) with the hard acid RCOOH. PEHA can nearly be considered a general purpose ligand, since it also very well stabilizes oxidic, hard base nanocrystals such as ZnO and Fe_3O_4 where it coordinates to the metal centers. The structure of the respective polymer ligands are shown in **Figure 5.1**.

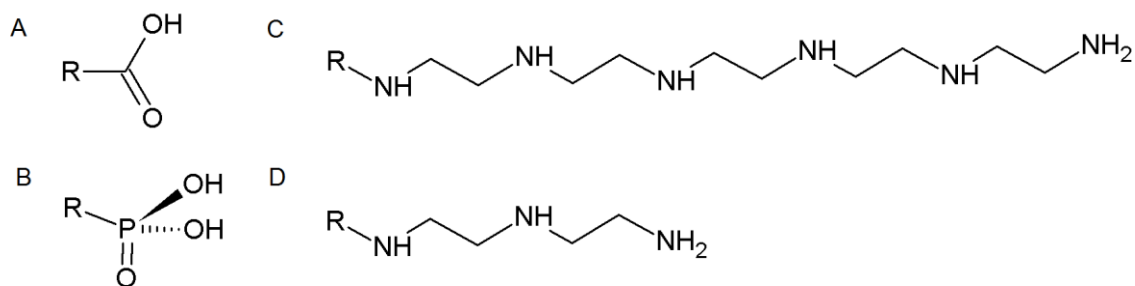


Figure 5.1: Suitable coordinating groups for polymer ligand exchange: (A) carboxylic acid (-COOH), (B) phosphonic acid (-PO(OH)₂), (C) pentaethylenhexamine (-PEHA), and (D) diethylenetriamine (-DETA). R represents the polymer chain, which in the present study comprises polystyrene (PS), poly(methyl methacrylate) (PMMA), and polyisoprene (PI).

Polymers used as examples in the present work include polystyrene (PS), polyisoprene (PI), and poly(methyl methacrylate) (PMMA) in combination with the coordinating groups -COOH, -PEHA, or -DETA to act as polymeric ligands *L2*. Many other polymers such as polyethylene (PE), poly-3-hexylthiophene (P3HT), and poly(ethylene oxide) will work as well.³⁰ In principle, nearly every polymer which could be functionalized with one of the coordinating groups above should be suitable for the ligand exchange procedure. The same holds for the choice of nanocrystals, where in this work Ag-, Au-, CdSe-, PbS-, Fe₃O₄-, and ZnO-nanoparticles are investigated.

The nanocrystals used in the present study were originally coated with oleic acid, since they were synthesized by thermal decomposition of their oleate complexes, an established state-of-the art procedure to prepare highly crystalline monodisperse nanocrystals in large quantities.²² For the ligand exchange procedures described below, the oleic acid *L1*-coated nanocrystals were dissolved in a common solvent (THF) together with a large excess of the polymeric ligand *L2*. Generally we find that just mixing the components in dilute solution is insufficient to achieve complete polymer ligand exchange. We attribute this to the good steric stabilization provided by oleic acid (*L1*), which was chosen to bind sufficiently strong to limit the growth and stabilize the nanocrystals during their synthesis. Thus, in the sense of **equation 5.1** the concentrations [*NP – L1*] and [*L2*] must be considerably increased to achieve complete ligand exchange. We find that this can be accomplished by precipitating the nanoparticles and polymeric ligands *via* the addition of a common nonsolvent (ethanol) to bring nanoparticles (NP) and polymer ligands (*L2*) in direct contact thereby considerably increasing the local polymer segment density. This step is in the following termed quantitative precipitation. As oleic acid (*L1*) is soluble in ethanol, this will simultaneously deplete ligand *L1* from the mixture which further

promotes ligand exchange. In a second step, the precipitate, a mixture of $NP - L2$, free polymeric ligand $L2$, and remaining amounts of oleic acid ($L1$), is redissolved in THF. To subsequently remove excess free polymeric ligand and remaining oleic acid, the $NP - L2$ nanoparticles undergo a selective precipitation by the stepwise addition of small amounts of the nonsolvent ethanol. The selective precipitation of $NP - L2$ in the presence of free polymeric ligand $L2$ is possible due to the low entropy of mixing of high molecular weight polymers. The entropy of mixing of polymers in solution is proportional to $1/N$, where N is the degree of polymerization. In our context, polymer-coated nanoparticles can be considered as very high molecular weight polymers with a much lower solubility compared to the free polymer chains. Thus, they precipitate at much less nonsolvent content compared to the free polymer. This principle is the basis of established procedures for polymer fractionation. Depending on the desired purity of the $NP - L2$, each of the quantitative and selective precipitation can be repeated. The progress in removing ligands $L1$ and excess $L2$ can be monitored by thermo gravimetric analysis (TGA). The stability against aggregation in solution can be assessed by dynamic light scattering (DLS), and in the dry state by transmission electron microscopy (TEM).

Ligand exchange monitoring

As a first example for the ligand exchange procedure we describe the preparation of polystyrene (PS) brush coated CdSe nanocrystals with PS-PEHA as a polymer ligand ($L2$) starting from oleic acid coated nanocrystals. Grafting-from or grafting- to procedures to coat CdSe-nanocrystals with polystyrene have been published, but are synthetically challenging.^{26,31} The polymer ligand exchange can conveniently be followed by thermo gravimetric analysis.

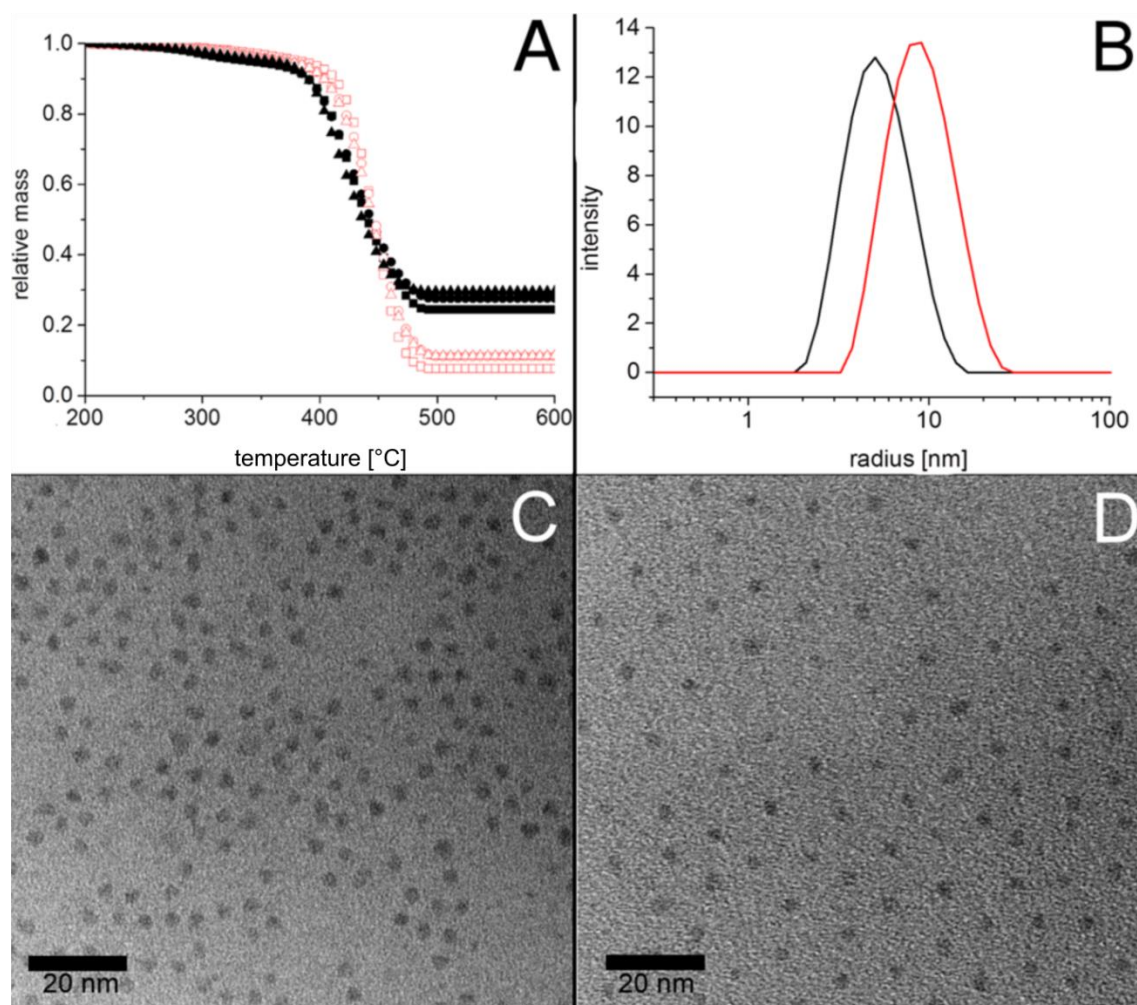
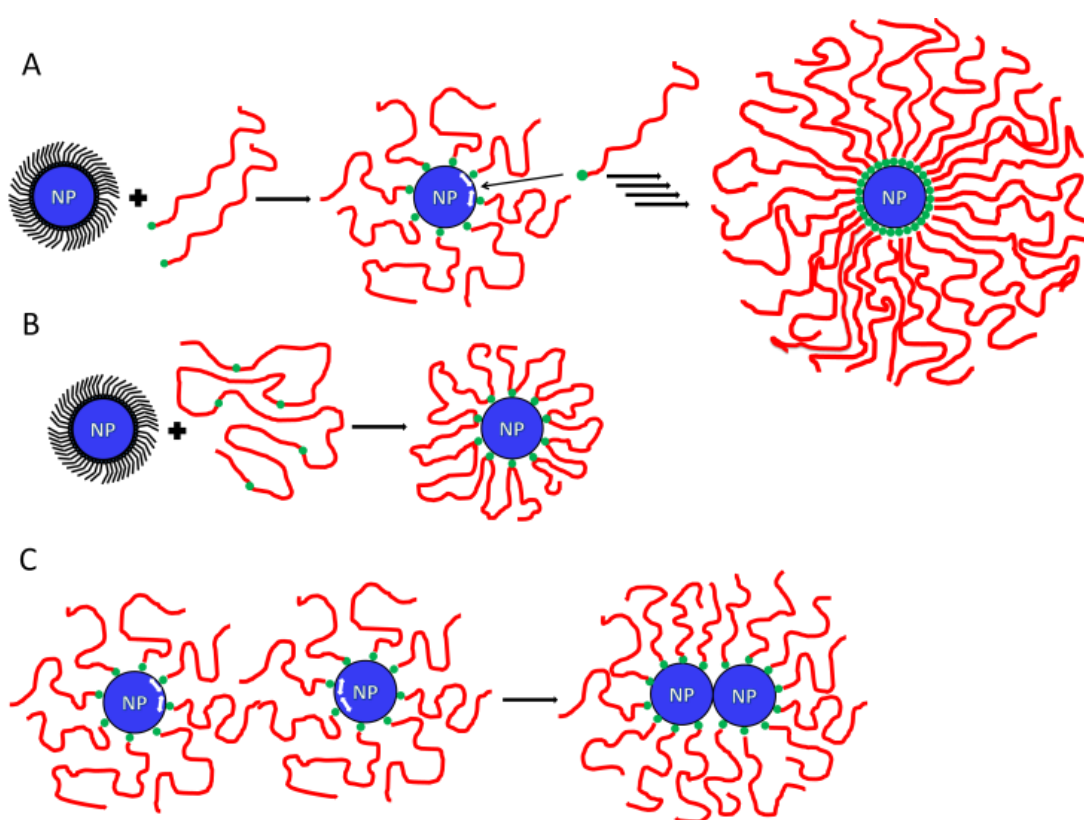


Figure 5.2: (A) TGA measurements of the ligand exchange steps (red = quantitative steps; black = selective steps; squares = step 1; circles = step 2; triangles = step 3). (B) Particle size distribution measured by DLS measurements in THF of 3 nm CdSe nanocrystals stabilized with oleic acid (black) and after ligand exchange with polystyrene-PEHA 2700 g/mol (red). TEM images of the CdSe nanocrystals with oleic acid (C) and with polystyrene-PEHA 2700 g/mol (D). The increased interparticle distance after coating with polystyrene is a clear indication of stable polymer brush binding.

The TGA-curves in **Figure 5.2(A)** show that already after the first quantitative precipitation the amount of oleic acid in the mixture has reduced to below 3 wt% as deduced from the small decrease of the relative mass from 1.00 at 250 °C to 0.97 at 350 °C. The drop of the relative mass between 380 and 480 °C is due to the thermal degradation of the polystyrene chains. This is supported by reference measurements of pure oleic-acid coated nanocrystals and pure polystyrene in the Supporting Information (**Figure 5.S1**). As seen in **Figure 5.2(A)**, the solid nanoparticle content is 8 % after the first quantitative precipitation, increasing to 13 wt% after the second and to 14 wt% after the third quantitative precipitation due to the removal of free unbound polystyrene chains. The excess of free polymer chains is considerably further reduced by selective

precipitation, where the solid content increases to 22 and 28 wt%, finally nearly saturating at 30 wt%, indicating an almost complete removal of free polymer ligand.

With the mean diameter and the bulk density of the nanocrystals, the molecular weight of the polymer, and the ratio of polymer to nanocrystals from the TGA measurement a grafting density of 1.2 nm^{-2} can be calculated for the CdSe-polystyrene particles shown in **Figure 5.2**. This grafting density is much higher than the grafting densities reported for the covalent grafting-to and grafting-from methods.¹⁷ These high grafting densities can be explained with the mobility of the polymer chains on the particle surface due to the reversible coordinating and decoordination of the ligands, as illustrated in **Scheme 5.1**.



Scheme 5.1: A) Nanocrystal coated with oleic acid (black), which is exchanged against a polymer (red) with a coordinating end-group (green). Because of the surface mobility of the end groups, bound polymer chains can relocate on the surface to facilitate attachment of further polymer chains to yield very high brush densities. (B) The possibility to employ copolymers as polymer ligands to obtain dense polymer brushes. (C) Relocalization of surface-bound polymer to allow controlled agglomeration into nanoparticle dimers, and subsequently chains and networks.

The obtained polymer-brush coated nanoparticles are well stabilized in solution and in bulk. The measured particle size distributions of oleic acid- and polystyrene-coated CdSe-nanoparticles dispersed in solution (**Figure 5.2(B)**) show the increase of the hydrodynamic radius expected for the attachment of a spherical polymer brush, and no signs of agglomeration. TEM-images (**Figure 5.2(C,D)**) show the increase of the interparticle distance after attachment of the polymer chains.

Increased solution stability

Also metal nanocrystals can be polymer brush-coated *via* the ligand exchange procedure. We investigated silver nanocrystals which are relevant for many applications where their unique plasmonic properties or their antibacterial properties are exploited. A specific issue for small (5 nm) silver nanoparticles is the lack of long-term stability in solution³² as shown in **Figure 5.3**. After 2 weeks in THF solution the nanocrystals have become polydisperse due to aggregation and fusion into larger nanoparticles. We found that the ligand exchange with PS(16k)-DETA yielded silver nanocrystals coated with a dense polystyrene brush which considerably improved steric stabilization. Even after several months there was no noticeable change of the size distribution of the silver nanocrystals.

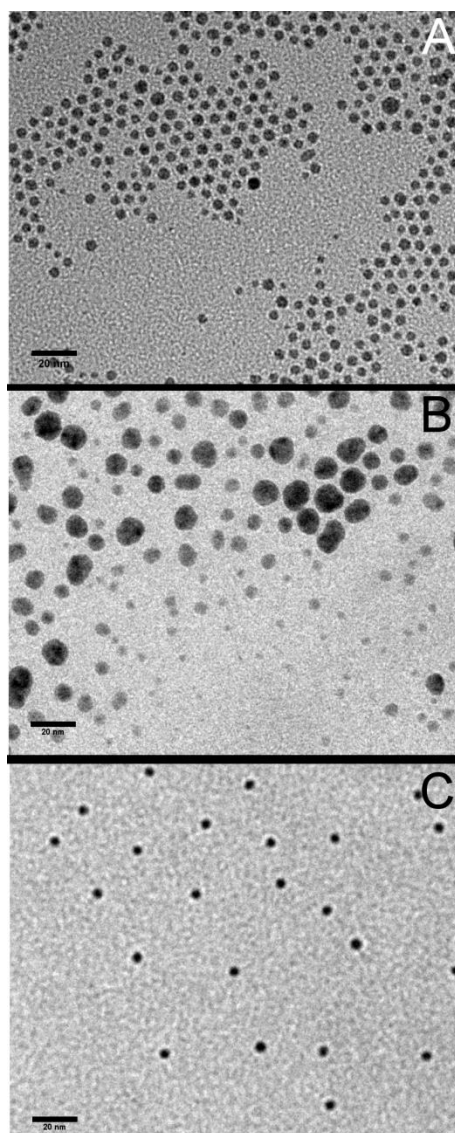


Figure 5.3: TEM images of silver nanocrystals (A) after synthesis with oleic acid as surfactant, (B) after 2 weeks in THF with oleic acid as surfactant and (C) after 2 weeks with a polystyrene (PS-DETA) brush in THF solution, prepared by the ligand exchange method (scale bars are 20 nm).

Nanoparticle distance control

For many applications it is important to control the distance between nanocrystals on surfaces or in bulk, *e.g.*, in magnetic storage layers to achieve high storage densities, or in the active matrix of hybrid solar cells to adjust the nanoparticle distance to the exciton diffusion length. Because of the high grafting density achievable by the ligand exchange method the polymer brushes are dense and homogeneous, resulting in a well-defined and controllable interparticle distance. The distance can be varied *via* the molecular weight of the polymer ligands. **Figure 5.4** shows the example of iron oxide nanocrystals which were coated with PS-DETA and PS-PEHA with different molecular weights.

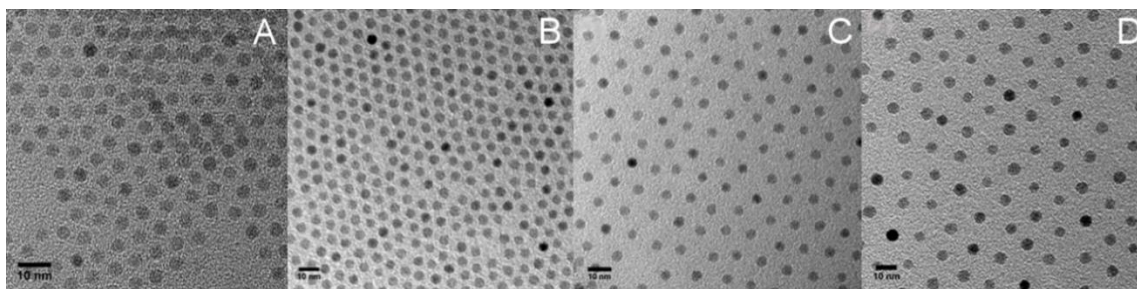


Figure 5.4: TEM images of 5 nm Fe_3O_4 nanocrystals coated with (A) oleic acid, and polystyrene ligands of different molecular weights, *i.e.*, (B) 1000, (C) 3450, and (D) 8450 g/mol (scale bars are 10 nm). We note the interparticle distance in (B) is smaller than that of oleic acid, with a distance below 10 nm (7.2 nm), which is relevant for magnetic storage layers.

For iron oxide nanoparticles also a covalent grafting-to/grafting-from method has been developed, which, however, is quite involved.³³ As shown in **Figure 5.4**, we demonstrate that by adjusting the PS molecular weight, the center-to-center distances between the nanocrystals can not only be increased, but also decreased compared to the distance resulting from the original oleic acid layer. The smaller distance is remarkable, since it demonstrates the possibility to prepare polymer-stabilized nanocrystal assemblies with a distance or pitch smaller than 10 nm, in our case 7.2 nm, corresponding to a potential magnetic storage density of 12.4 Tb/inch², which is very high, and not possible with current state-of-the-art block copolymer templating procedures.³⁴ This control over the distance is a very useful tool for the generation of nanocrystal superlattices.³⁵

As an example for a further nanocrystal-polymer combination we show in **Figure 5.5A** polyisoprene-coated PbS-nanocrystals obtained by ligand exchange with PI-PEHA.

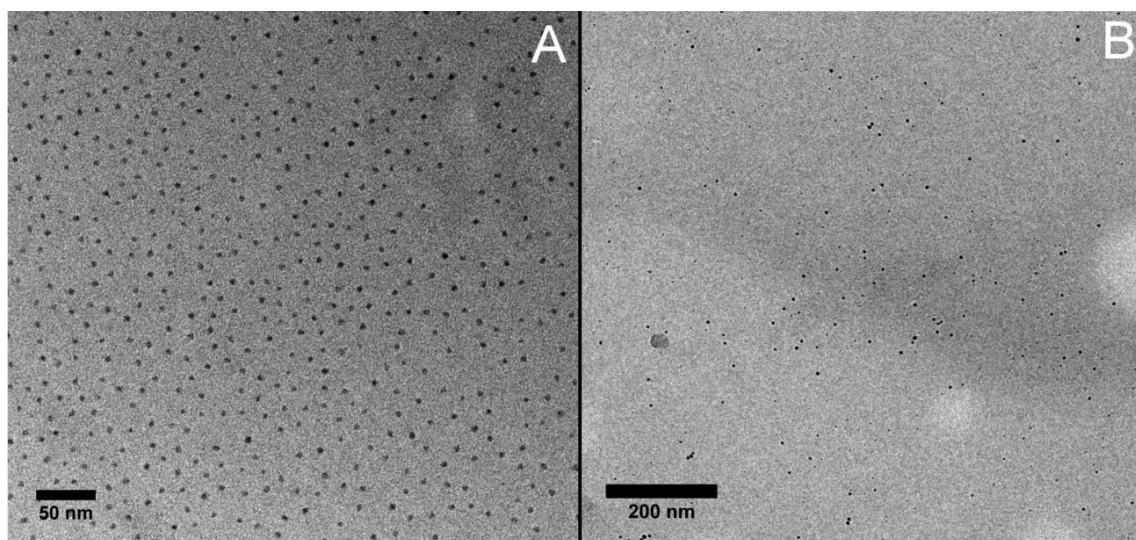


Figure 5.5: TEM images of 7 nm PbS nanocrystals coated with polyisoprene (PI-PEHA) 15 000 g/mol (A) and 15 nm Ag-nanocrystals coated with PMMA-co-polymethacrylic acid (Aldrich, Mw 34 000 g/mol, 1.6 % methacrylic acid) in a PMMA matrix (2 wt%) (B).

Polyisoprene is a viscous liquid, but the PI-coated nanocrystals are solid, indicating strong reinforcement of the nanocomposite due to the nanocrystals.

Extension to copolymer ligands

So far we used endfunctionalized homopolymers as polymeric ligands for the ligand exchange procedure. However, also copolymers can be used as ligands, which considerably broadens the variability of available polymeric ligands and provides a route for up-scaling, since many functional copolymers are commercially available.

Scheme 5.1(B) shows how copolymers can similarly coordinate to the nanocrystal surface *via* functional comonomers to form flower-like, dense polymer brushes. Here the brush thickness depends on the molar fraction of binding groups. In **Figure 5.5(B)** we show the example of Ag-nanocrystals coated with poly(methyl methacrylate) (PMMA) by ligand exchange with a commercially available PMMA-*co*-polymethacrylic acid copolymer (Aldrich, M_w 34 000 g/mol, 1.6 % methacrylic acid), incorporated into a PMMA-homopolymer. Also in this case, high ligand densities for sufficient stabilization in solution and compatibilization with PMMA-matrices can be achieved. Using these copolymers we could prepare up to 20 g of PMMA-coated ZnO-nanoparticles for reinforcement and surface hardening for PMMA-ZnO-nanocomposites on the kg-scale.

Controlled nanocrystal aggregation

For nanocomposites it is often desired to not have singly dispersed nanocrystals, but to rather have aggregated nanocrystal assemblies to increase, *e.g.*, electrical or thermal conductivity. Examples are hybrid solar cells where the semiconductor nanocrystals should form a percolation network to provide sufficient electrical conductivity. Here, nanocrystals with coordinatively bound polymers, attached *via* ligand exchange, open a route for a controlled aggregation into percolation networks.

The stabilization of the nanocrystals depends on the binding strength of the ligand and the density of the polymer brush. By using a ligand with lower binding strength and/or reducing the excess of polymer ligand [L2] in the ligand exchange procedure, the stability of the polymer-coated nanocrystals against aggregation can be reduced in a controlled fashion. Upon aggregation, polymer ligands can relocalize on the nanoparticle surface (see **Scheme 5.1(C)**) to stabilize extended string-like assemblies that form cross-links and thus efficiently percolate into a continuous network.^{29,36} Such a controlled aggregation

would not be possible with covalently bound polymers. With the example of polystyrene-stabilized CdSe-nanocrystals we show that by variation of the ligand excess in the ligand exchange procedure it is possible to tune the stability and aggregation of the nanocrystals from a stable, singly dispersed, well-separated state (**Figure 5.2**) to slightly aggregated, string-like multiplet assemblies (**Figure 5.6(A,B)**), and eventually to a continuous percolation network, as shown in **Figure 5.6(C)**.

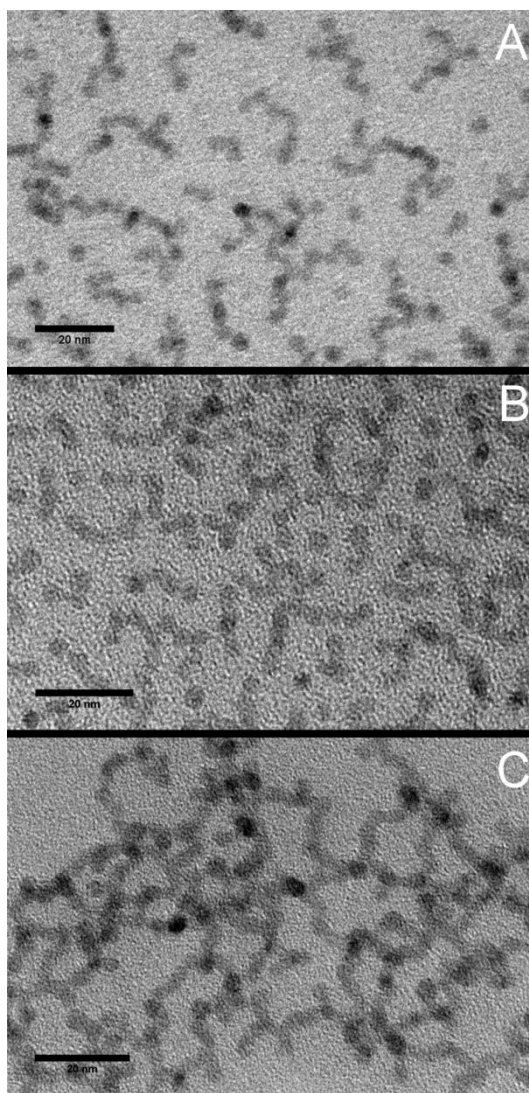


Figure 5.6: TEM images of 4 nm CdSe nanocrystals with a polystyrene brush forming (A) single crystals and short multiplet chains; (B) short chains and networks; (C) a percolating branched network (scale bars are 20 nm).

This can be favorably employed, *e.g.*, in active matrices of solar cells, where in a first step well-stabilized nanocrystals can be incorporated at high volume fractions with good homogeneous dispersion and no clustering, and then aggregated into a dense percolation network by, *e.g.*, thermal destabilization in the polymer matrix.

Conclusions

We show that polymer ligand exchange is a very versatile method to coat nanocrystals densely with a spherical polymer brush, shown for a variety of nanocrystal/polymer combinations including PS-PEHA@CdSe, PS-DETA@Ag, PS-PEHA@Fe₃O₄, PI-PEHA@PbS, and PMMA-co-PMAc@ZnO, for which otherwise suitable linker chemistries involving covalent attachment of initiators for grafting-from or functional groups for grafting-to would have to be developed. A rational design of the coordinating groups for polymer ligand exchange is possible and a set of a few different ligands is sufficient to apply this procedure to nearly every nanocrystal/polymer combination. We show the excellent solution stability of the polymer-coated nanocrystal, the possibility to adjust interparticle distances, the possibility to aggregate the particles in a controlled way into percolation networks, and the use of commercially available copolymers to broaden the scope of the method.

Materials and methods

Chemicals

Cyclohexane (Aldrich) and tetrahydrofuran (THF, Aldrich) were purified by distillation from a sodium-potassium alloy and from the benzophenone-potassium adduct. Isoprene (Aldrich) was purified successively by distillation from CaH₂ (Aldrich) and di-*n*-butyl magnesium (Aldrich). Ethylene oxide (AirLiquide) was purified by distillation from CaH₂ and *n*-butyl lithium (Aldrich). All other chemicals were used as received, which include sodium oleate (TCI Europe, >97.0 %), *sec*-butyl lithium (1.4 M in cyclohexane; Aldrich), tetrahydrofuran (THF, Sigma-Aldrich, 99,9 %), cadmium acetate dihydrate (Sigma-Aldrich, 98 %), octadecene (Sigma-Aldrich, tech.), methanol (AppliChem, tech.), silver nitrate (Sigma-Aldrich, ≥ 99 %), trimethylamine (Sigma-Aldrich, ≥ 99 %), acetone (AppliChem, tech.), iron chloride hexahydrate (Sigma-Aldrich, > 98 %), hexane (Sigma-Aldrich, 95 %), oleic acid (Alfa Aesar, 90 %), *sec*-butyl lithium (Sigma-Aldrich, 1,4 M in cyclohexane), ethylene oxide (Sigma-Aldrich, 99,5 %), 1,1'-carbonyldiimidazole (CDI, Sigma-Aldrich, reagent grade), chloroform (Aldrich, anhydrous, amylene stabilized), pentaethylenhexamine (PEHA, Sigma-Aldrich, tech.).

Nanocrystal synthesis

Cadmium selenide nanocrystals were synthesized by the method of Cao³⁷ *via* the thermal decomposition of cadmium oleate. Silver nanocrystals were synthesized after Nakamoto³² *via* the reduction of silver oleate. Iron oxide nanocrystals were synthesized after Hyeon³⁸ *via* thermal decomposition of iron oleate. The lead sulfide nanocrystals were synthesized as reported by Hines.³⁹ Zinc oxide nanocrystals were synthesized by hydrolysis of zinc oleate in organic solvent as reported by our group.⁴⁰ Detailed procedures are described in the Supporting Information.

Polymer ligand synthesis

Polystyrene (PS) was synthesized by living anionic polymerization with *sec*-butyl lithium as initiator at -70 °C in THF. The polymerization was terminated either with ethylene oxide to obtain a hydroxyl end group or with CO₂ to obtain a carboxylic acid end group. The hydroxyl end group was subsequently activated by CDI and reacted with PEHA or DETA to create a multivalent amine function.

Polyisoprene (PI) was synthesized by living anionic polymerization in cyclohexane. The polymerization was initiated with *sec*-butyl lithium at 30 °C and terminated with ethylene oxide to obtain hydroxyl terminated PI. The hydroxyl end group was subsequently activated by CDI and reacted with PEHA or DETA to create a multivalent amine function. Detailed procedures are described in the Supporting Information.

Ligand exchange

The ligand exchange consists of two phases. In the first phase the nanocrystals in solution were mixed with an excess of the polymer followed by three cycles of quantitative precipitation, centrifugation and dissolving. The excess of polymer was removed in the second phase composed of three cycles of selective precipitation, centrifugation and dissolving. In a typical exchange 100 mg of 3 nm CdSe nanocrystals were dissolved in 5 mL of THF. To the nanocrystal solution 1 g of polystyrene ligand (PS-X) in 10 mL of THF was added. After the two solutions were completely mixed 50 mL of ethanol was added for quantitative precipitation. The precipitate was separated by centrifugation at 3250 g. The supernatant was discarded and the precipitate was dissolved in 10 mL of THF. This procedure was repeated two times. Subsequently ethanol was added slowly until precipitation occurs. The precipitate was separated by centrifugation at 3250 g. After

centrifugation the supernatant was checked for remaining nanocrystals by fluorescence or color. If there were remaining nanocrystals more ethanol was added and the precipitate was separated again. This was repeated until no nanocrystals remain in the supernatant. The supernatant was discarded and the precipitate was dissolved in 10 mL of THF. This procedure was repeated two times.

Characterization

The nanocrystals were characterized by transmission electron microscopy (TEM) and dynamic light scattering (DLS). The coated nanocrystals were characterized by TEM, DLS and thermo gravimetric analysis (TGA). TEM images were obtained on a Zeiss 922 Omega microscope. For the DLS measurements a Malvern Zetasizer Nano SZ were used. The TGA measurements were performed with a Mettler Toledo TGA1 with alumina pans, under nitrogen flow and a heating rate of 20 K/min.

Conflict of interest

The authors declare no competing financial interest.

Acknowledgment

Financial support for S.E. and D.P. by the German Science Foundation (collaborative research center SFB840, project TPB09 and SPP 1369) is gratefully acknowledged.

Supporting Information

Materials and Methods

Chemicals

Cyclohexane (Aldrich) and tetrahydrofuran (THF, Aldrich) were purified by distillation from a sodium-potassium alloy and from the benzophenone-potassium adduct. Isoprene (Aldrich) was purified successively by distillation from CaH_2 (Aldrich) and di-*n*-butyl magnesium (Aldrich). Ethylene oxide (AirLiquide) was purified by distillation from CaH_2 and *n*-butyl lithium (Aldrich). All other chemicals were used as received, which include sodium oleate (TCI Europe, > 97.0 %), *sec*-butyl lithium (1.4 M in cyclohexane; Aldrich), tetrahydrofuran (THF, Sigma-Aldrich, 99,9 %), cadmium acetate dihydrate (Sigma-Aldrich, 98 %), octadecene (Sigma-Aldrich, tech.), bis(trimethylsilyl) sulfide (TMS, Aldrich), methanol (AppliChem, tech.), silver nitrate (Sigma-Aldrich, ≥ 99 %), selenium (Aldrich), trimethylamine (Sigma-Aldrich, $\geq 99\%$), acetone (AppliChem, tech.), iron chloride hexahydrate (Sigma-Aldrich, > 98 %), hexane (Sigma-Aldrich, 95 %), oleic acid (Alfa Aesar, 90 %), 1,1' carbonyldiimidazole (CDI, Sigma-Aldrich, reagent grade), chloroform (Aldrich, anhydrous, amylene stabilized), pentaethylenehexamine (PEHA, Sigma-Aldrich, tech.), tetrabutylammonium hydroxide (TBAH, Alfa Aesar, 1 M in methanol), ethanol (AppliChem, tech.), triethylamine (Aldrich, 99 %), lead-(II)-nitrate (Aldrich, 99 %), zinc chloride (Aldrich, 99 %), styrene (Aldrich, 99 %).

Nanocrystal synthesis

Cadmium selenide nanocrystals were synthesized *via* the thermal decomposition of cadmium oleate.³⁷ In a typical synthesis 1.6 g (2.5 mmol) of cadmium oleate were dissolved in 35 ml octadecene and added to 45 ml of selenium (0.1 M) in octadecene solution. The mixture was degassed by 100 °C under vacuum for 1h and subsequent heated to 240 °C under a nitrogen atmosphere. According to the requirements the solution was kept at this temperature for 1 to 30 minutes and then cooled to room temperature. The nanocrystals were purified by at least 3 precipitation dissolving cycles with ethanol/methanol and THF.

Silver nanocrystals were synthesized *via* the reduction of silver oleate.³² In a typical synthesis 1 g of silver oleate were mixed with 20 ml of triethylamine and heated to 80 °C

for 3h. The nanocrystals were purified by precipitation with acetone and dissolving in THF two times.

Iron-oxide nanoparticles were synthesized by thermal decomposition of an iron oleate complex according to the procedure of Park *et al.*³⁸ The iron oleate complex was synthesized from a reaction mixture of iron(III) chloride and sodium oleate at 70 °C. The viscous and brownish iron oleate compound (31.89 g) was dissolved in octadecene and as a stabilizing agent oleic acid (5.04 g) was added to the solution. The reaction mixture was heated under reflux at a rate of 2 °C/min up to 110 °C in vacuum, and after that in a nitrogen atmosphere with the same heating rate up to 317 °C. The reaction mixture was stirred under reflux at 317 °C for 20 min. After the solution was cooled down at RT, 50 % THF was added to the nanoparticle-solution to avoid the formation of separated phases. The work up was carried out by precipitation of the nanoparticles in acetone. The particles could be easily redispersed in toluene or THF.

The lead sulfide nanocrystals were synthesized as reported by Hines.³⁹ In a typical synthesis 0.3 g of lead oleate were dissolved in 200 ml of octadecene and degassed at 100 °C under vacuum for 1h. The solution was heated to 150 °C under nitrogen atmosphere and 20 ml of a TMS octadecene solution was injected subsequently the mixture was cooled to 90 °C and kept there for 1h. The nanocrystals were purified by two precipitation dissolving cycles with methanol and THF. Zinc oxide nanocrystals were synthesized by hydrolysis of zinc oleate in organic solvent.⁴⁰ In a typical synthesis 16 ml of TBAH solution (1 M) were added to 15 g zinc oleate in 300 ml THF and kept at 50 °C for 16h. The nanocrystals were purified by at least 3 precipitation dissolving cycles with methanol and THF.

Polymer synthesis

Polystyrene (PS) was synthesized by living anionic polymerization in THF using high vacuum techniques and argon as inert atmosphere. The polymerization of styrene was initiated with *sec*-butyl lithium at -70 °C. The polymerization was terminated either with ethylene oxide to obtain a hydroxyl end group or with CO₂ to obtain a carboxylic acid end group. The mixture was stirred for at least 12 hours at room temperature and terminated with degassed acetic acid. The polymer was precipitated in cold (-20 °C) methanol.

Polyisoprene (PI) was synthesized *via* living anionic polymerization in cyclohexane using high vacuum techniques and dry nitrogen as inert atmosphere. The polymerization of isoprene was initiated with *sec*-butyl lithium at 30 °C. After complete conversion of

isoprene a small amount of THF was condensed into the reactor. Then ethylene oxide in an at least 10-fold excess over the initiator concentration was added to the solution to cap the living PI chain ends. The mixture was stirred for at least 12 hours at 40 °C and terminated with degassed acetic acid. The polymer was precipitated in cold (-20 °C) methanol.

The narrow distributed, hydroxyl functionalized polymer was further functionalized by a following two-step reaction to attach a multidentate amine group to the polymer. In the first step, the hydroxyl group was activated with 1,1'-carbonyldiimidazole (CDI) in chloroform. Therefore the polymer solution in chloroform was added drop-wise to a CDI (25-fold excess) solution in chloroform. After stirring the reaction for 24 hours at room temperature, the solution was extracted three times with water to remove residual CDI and dried under vacuum. In the next step, pentaethylenehexamine (PEHA, 25-fold excess) was dissolved in chloroform and the CDI activated polymer solution in chloroform was added drop-wise to the amine solution. After a reaction time of 24 hours the solution was extracted three times with water and dried under vacuum.

Characterization

The grafting density D was calculated with the formula:

$$D = \frac{4 \cdot r_n^3 \cdot \rho_n \cdot N_A \cdot (100 - X_n)}{3 \cdot d_n^2 \cdot M_p \cdot X_n}$$

Were r_n and d_n are the nanocrystal radius respectively the diameter, ρ_n is the material density in bulk, N_A is the Avogadro constant, M_p is the molecular mass of the polymer and X_n is the weight fraction of the nanocrystals in percent derived from the TGA measurements. This formula is for spherical particles, under the assumptions that the density of the particles is similar to the density of the bulk material and that no free polymer is present.

Figure 5.S1 shows the ability of the TGA method to characterize the coated nanocrystals regarding the amount of ligand on the surface.

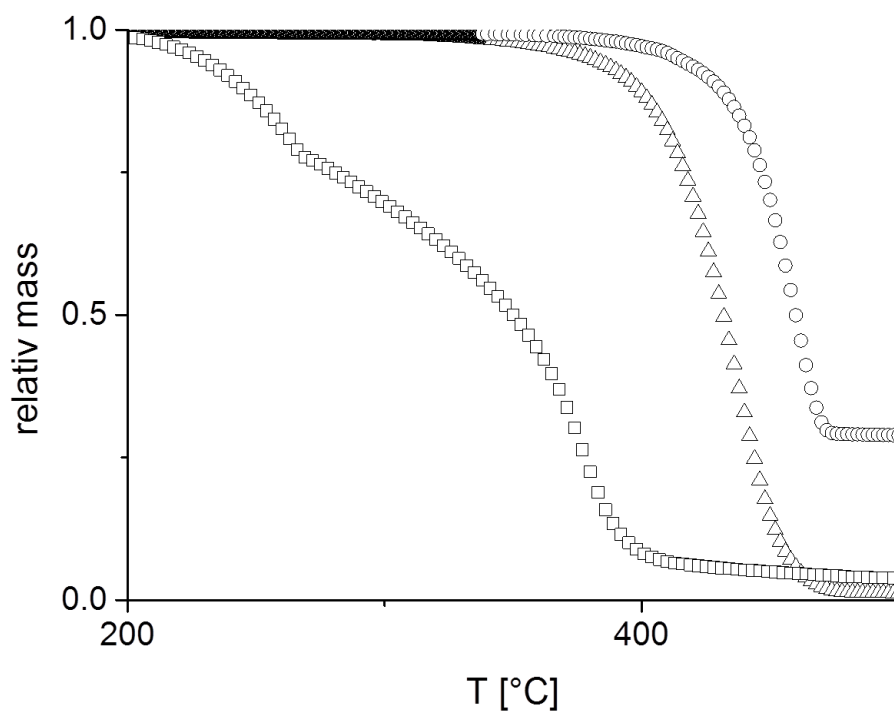


Figure 5.S1: TGA measurements of technical oleic acid (squares), polystyrene (9k PS, triangles) and ZnO nanocrystals coated with 9kPS (circles).

Figure 5.S2 show another example for the controlled aggregation followed by TGA measurements. The derived grafting density for the coated nanocrystals decreases significant with increasing aggregation.

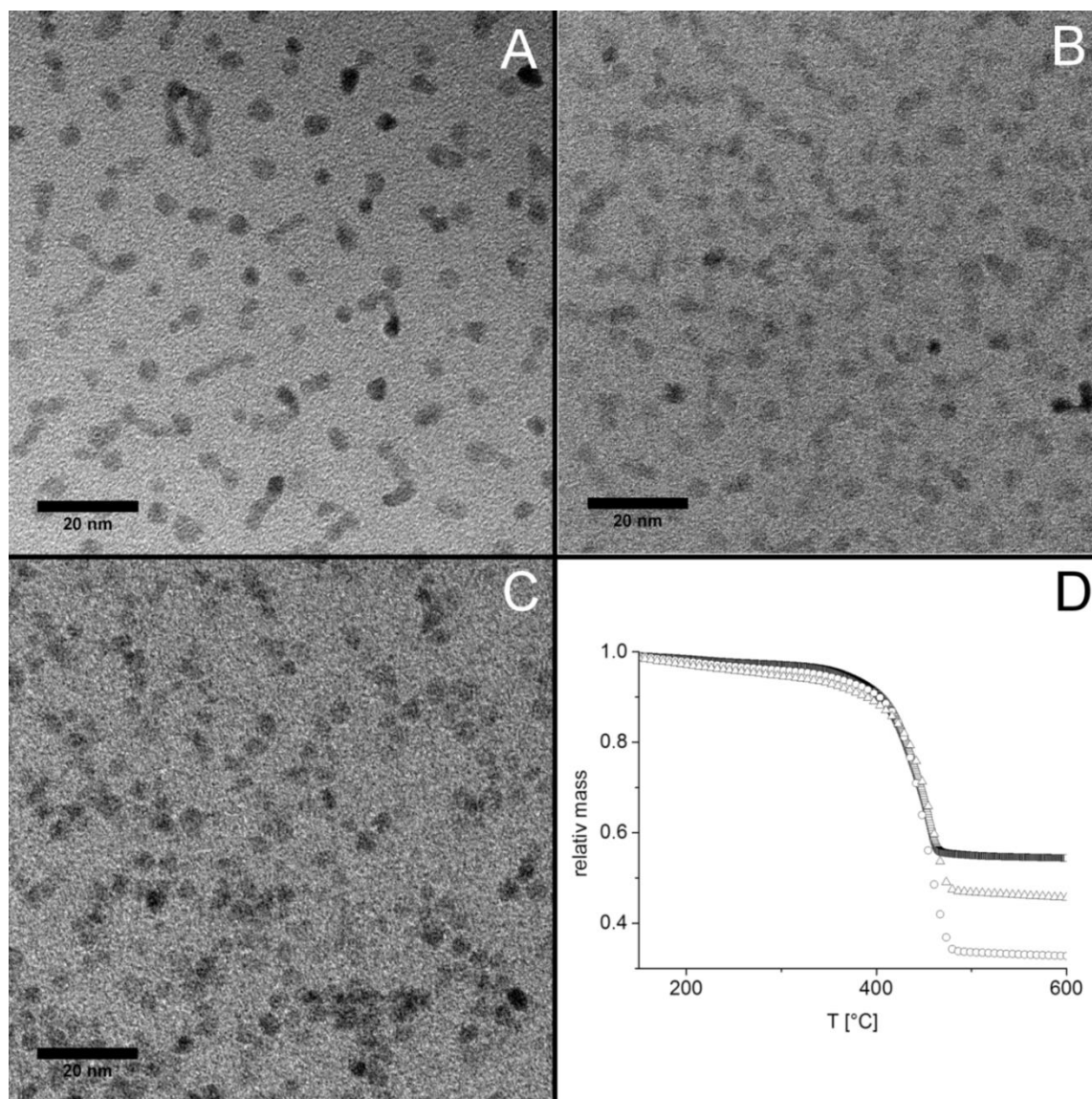


Figure 5.S2: TEM images of polystyrene (2700 g/mol) coated ZnO nanocrystals (4 nm) with different grafting densities A: $1,35 \text{ nm}^{-2}$, B: $0,98 \text{ nm}^{-2}$, C: $0,68 \text{ nm}^{-2}$ and the TGA measurements (D) for the three composites (A: circles, B: triangles, C: squares).

References

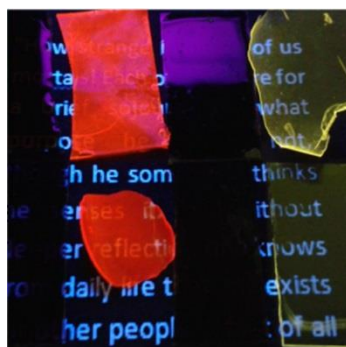
1. S. Pathak, S.-K. Choi, N. Arnheim, and M. E. Thompson, “Hydroxylated Quantum Dots as Luminescent Probes for In Situ Hybridization,” *J. Am. Chem. Soc.* **123** (17), 4103–4104 (2001).
2. H. Mattoussi, J. M. Mauro, E. R. Goldman, T. M. Green, G. P. Anderson, V. C. Sundar, and M. G. Bawendi, “Bioconjugation of Highly Luminescent Colloidal CdSe-ZnS Quantum Dots with an Engineered Two-Domain Recombinant Protein,” *Phys. Status Solidi B* **224** (1), 277–283 (2001).
3. J. Lee, V. C. Sundar, J. R. Heine, M. G. Bawendi, and K. F. Jensen, “Full Color Emission from II-VI Semiconductor Quantum Dot-Polymer Composites,” *Adv. Mater.* **12** (15), 1102–1105 (2000).
4. V. I. Klimov, A. A. Mikhailovsky, S. Xu, A. Malko, J. A. Hollingsworth, C. A. Leatherdale, H. J. Eisler, and M. G. Bawendi, “Optical Gain and Stimulated Emission in Nanocrystal Quantum Dots,” *Science* **290** (5490), 314–317 (2000).
5. H. J. Eisler, V. C. Sundar, M. G. Bawendi, M. Walsh, H. I. Smith, and V. Klimov, “Color-Selective Semiconductor Nanocrystal Laser,” *Appl. Phys. Lett.* **80** (24), 4614–4616 (2002).
6. Y. Tachibana, M. Nazeeruddin, M. Grätzel, D. R. Klug, and J. R. Durrant, “Electron Injection Kinetics for the Nanocrystalline TiO₂ Films Sensitised with the Dye (Bu₄N)₂Ru(dcbpyH)₂(NCS)₂,” *Chem. Phys.* **285** (1), 127–132 (2002).
7. E. Stathatos, P. Lianos, S. M. Zakeeruddin, P. Liska, and M. Grätzel, “A Quasi-Solid-State Dye-Sensitized Solar Cell Based on a Sol-Gel Nanocomposite Electrolyte Containing Ionic Liquid,” *Chem. Mater.* **15** (9), 1825–1829 (2003).
8. W. U. Huynh, J. J. Dittmer, and A. P. Alivisatos, “Hybrid Nanorod-Polymer Solar Cells,” *Science* **295** (5564), 2425–2427 (2002).

9. A. Masotti, A. Pitta, G. Ortaggi, M. Corti, C. Innocenti, A. Lascialfari, M. Marinone, P. Marzola, A. Daducci, A. Sbarbati, E. Micotti, F. Orsini, G. Poletti, and C. Sangregorio, “Synthesis and Characterization of Polyethylenimine-Based Iron Oxide Composites as Novel Contrast Agents for MRI,” *Mag. Reson. Mater. Phys., Biol. Med.* **22** (2), 77–87 (2009).
10. D. Wang, Y. Wang, X. Li, Q. Luo, J. An, and J. Yue, “Sunlight Photocatalytic Activity of Polypyrrole–TiO₂ Nanocomposites Prepared by ‘In Situ’ method,” *Catal. Commun.* **9** (6), 1162–1166 (2008).
11. van Zyl, W. E., M. García, Schrauwen, B. A. G., B. J. Kooi, De Hosson, J. Th. M., and H. Verweij, “Hybrid Polyamide/Silica Nanocomposites: Synthesis and Mechanical Testing,” *Macromol. Mater. Eng.* **28** (2), 106–110 (2002).
12. C.-H. Hung and W.-T. Whang, “Effect of Surface Stabilization of Nanoparticles on Luminescent Characteristics in ZnO/Poly(hydroxyethyl methacrylate) Nanohybrid Films,” *J. Mater. Chem.* **15** (2), 267–274 (2005).
13. S. Singha and M. Thomas, “Dielectric Properties of Epoxy Nanocomposites,” *IEEE Trans. Dielect. Electr. Insul.* **15** (1), 12–23 (2008).
14. D. H. Napper, *Polymeric Stabilization of Colloidal Dispersions* (Academic Press, London, New York, 1983).
15. S. Fischer, A. Salcher, A. Kornowski, H. Weller, and S. Förster, “Completely Miscible Nanocomposites,” *Angew. Chem. Int. Ed.* **50** (34), 7811–7814 (2011).
16. N. Tsubokawa, A. Kogure, and Y. Sone, “Grafting of Polyesters from Ultrafine Inorganic Particles: Copolymerization of Epoxides with Cyclic Acid Anhydrides Initiated by COOK Groups Introduced onto the Surface,” *J. Polym. Sci. A Polym. Chem.* **28** (7), 1923–1933 (1990).
17. K. Ohno, K. Koh, Y. Tsujii, and T. Fukuda, “Fabrication of Ordered Arrays of Gold Nanoparticles Coated with High-Density Polymer Brushes,” *Angew. Chem. Int. Ed.* **42** (24), 2751–2754 (2003).

18. P. Mansky, Y. Liu, E. Huang, T. P. Russell, and C. Hawker, “Controlling Polymer-Surface Interactions with Random Copolymer Brushes,” *Science* **275** (5305), 1458–1460 (1997).
19. G. Li, D. L. Zeng, L. Wang, Baoyu, Zong, K. G. Neoh, and E. T. Kang, “Hairy Hybrid Nanoparticles of Magnetic Core, Fluorescent Silica Shell, and Functional Polymer Brushes,” *Macromolecules* **42** (21), 8561–8565 (2009).
20. W. He, L. Cheng, L. Zhang, X. Jiang, Z. Liu, Z. Cheng, and X. Zhu, “Bifunctional Nanoparticles with Magnetism and NIR Fluorescence: Controlled Synthesis from Combination of AGET ATRP and 'Click' Reaction,” *Nanotechnology* **25** (4), 045602 (2014).
21. H. Awada, H. Medlej, S. Blanc, M.-H. Delville, R. C. Hiorns, A. Bousquet, C. Dagron-Lartigau, and L. Billon, “Versatile Functional Poly(3-hexylthiophene) for Hybrid Particles Synthesis by the Grafting Onto Technique: Core@Shell ZnO Nanorods,” *J. Polym. Sci. Part A: Polym. Chem.* **52** (1), 30–38 (2014).
22. J. Park, J. Joo, S. G. Kwon, Y. Jang, and T. Hyeon, “Synthesis of Monodisperse Spherical Nanocrystals,” *Angew. Chem. Int. Ed.* **46** (25), 4630–4660 (2007).
23. M. Karg, N. Schelero, C. Oppel, M. Gradzielski, T. Hellweg, and R. von Klitzing, “Versatile Phase Transfer of Gold Nanoparticles from Aqueous Media to Different Organic Media,” *Chem.-Eur. J.* **17** (16), 4648–4654 (2011).
24. H. Pletsch, L. Peng, F. Mitschang, A. Schaper, M. Hellwig, D. Nette, A. Seubert, A. Greiner, and S. Agarwal, “Ultrasound-Mediated Synthesis of High-Molecular Weight Polystyrene-Grafted Silver Nanoparticles by Facile Ligand Exchange Reactions in Suspension,” *Small* **10** (1), 201–208 (2014).
25. M. K. Corbierre, N. S. Cameron, M. Sutton, K. Laaziri, and R. B. Lennox, “Gold Nanoparticle/Polymer Nanocomposites: Dispersion of Nanoparticles as a Function of Capping Agent Molecular Weight and Grafting Density,” *Langmuir* **21** (13), 6063–6072 (2005).

-
26. H. Skaff and T. Emrick, “Reversible Addition Fragmentation Chain Transfer (RAFT) Polymerization from Unprotected Cadmium Selenide Nanoparticles,” *Angew. Chem.* **116** (40), 5497–5500 (2004).
27. T. Zhang, J. Ge, Y. Hu, and Y. Yin, “A General Approach for Transferring Hydrophobic Nanocrystals into Water,” *Nano Lett.* **7** (10), 3203–3207 (2007).
28. D. Celik, M. Krueger, C. Veit, H. F. Schleiermacher, B. Zimmermann, S. Allard, I. Dumsch, U. Scherf, F. Rauscher, and P. Niyamakom, “Performance Enhancement of CdSe Nanorod-Polymer Based Hybrid Solar Cells Utilizing a Novel Combination of Post-Synthetic Nanoparticle Surface Treatments,” *Sol. Energy Mater. Sol. Cells* **98**, 433–440 (2012).
29. M. S. Nikolic, C. Olsson, A. Salcher, A. Kornowski, A. Rank, R. Schubert, A. Frömsdorf, H. Weller, and S. Förster, “Micelle and Vesicle Formation of Amphiphilic Nanoparticles,” *Angew. Chem. Int. Ed.* **48** (15), 2752–2754 (2009).
30. Tobias Honold, *Nanoparticle Polymer Hybrids for Sandwich Solar Cells*, M. Sc. Thesis, University of Bayreuth, 2013.
31. Esteves, Ana C C, L. Bombalski, T. Trindade, K. Matyjaszewski, and A. Barros-Timmons, “Polymer Grafting from CdS Quantum Dots *via* AGET ATRP in Miniemulsion,” *Small* **3** (7), 1230–1236 (2007).
32. M. Yamamoto, Y. Kashiwagi, and M. Nakamoto, “Size-Controlled Synthesis of Monodispersed Silver Nanoparticles Capped by Long-Chain Alkyl Carboxylates from Silver Carboxylate and Tertiary Amine,” *Langmuir* **22** (20), 8581–8586 (2006).
33. Y. Wang, X. Teng, J.-S. Wang, and H. Yang, “Solvent-Free Atom Transfer Radical Polymerization in the Synthesis of Fe₂O₃@Polystyrene Core–Shell Nanoparticles,” *Nano Lett.* **3** (6), 789–793 (2003).
34. S. Kim, P. F. Nealey, and F. S. Bates, “Directed Assembly of Lamellae Forming Block Copolymer Thin Films Near the Order-Disorder Transition,” *Nano Lett.* **14** (1), 148–152 (2014).

35. S. Mehdizadeh Taheri, S. Fischer, and S. Förster, “Routes to Nanoparticle-Polymer Superlattices,” *Polymers* **3** (4), 662–673 (2011).
36. P. Akcora, H. Liu, S. K. Kumar, J. Moll, Y. Li, B. C. Benicewicz, L. S. Schadler, D. Acehan, A. Z. Panagiotopoulos, V. Pryamitsyn, V. Ganesan, J. Ilavsky, P. Thiyagarajan, R. H. Colby, and J. F. Douglas, “Anisotropic Self-Assembly of Spherical Polymer-Grafted Nanoparticles,” *Nat. Mater.* **8** (4), 354–359 (2009).
37. Y. A. Yang, H. Wu, K. R. Williams, and Y. C. Cao, “Synthesis of CdSe and CdTe Nanocrystals without Precursor Injection,” *Angew. Chem.* **117** (41), 6870–6873 (2005).
38. J. Park, K. An, Y. Hwang, J.-G. Park, H.-J. Noh, J.-Y. Kim, J.-H. Park, N.-M. Hwang, and T. Hyeon, “Ultra-Large-Scale Syntheses of Monodisperse Nanocrystals,” *Nat. Mater.* **3** (12), 891–895 (2004).
39. M. A. Hines and G. D. Scholes, “Colloidal PbS Nanocrystals with Size-Tunable Near-Infrared Emission: Observation of Post-Synthesis Self-Narrowing of the Particle Size Distribution,” *Adv. Mater.* **15** (21), 1844–1849 (2003).
40. S. Ehlert, T. Lunkenbein, J. Breu, and S. Förster, “Facile Large-Scale Synthetic Route to Monodisperse ZnO Nanocrystals,” *Colloids Surf., A* **444**, 76–80 (2014).



6

A General Route to Optically Transparent Highly Filled Polymer Nanocomposites

Sascha Ehlert, Corinna Stegelmeier, Daniela Pirner, and Stephan Förster

Physical Chemistry I, University of Bayreuth, Germany

Published in: *Macromolecules*, **2015**, 48 (15), 5323-5327

Reprinted with permission from Ehlert, S.; Stegelmeier, C.; Pirner, D. *et al*
Macromolecules, **2015**, **48** (15), pp 5323–5327. © 2015 American Chemical Society.

Abstract

Polymer nanocomposites for optical applications require high optical transparency at high filling ratios of nanoparticles. The nanoparticles provide optical functionality but unfortunately have a strong tendency to aggregate in polymer matrices leading to strong turbidity and reduced optical transmission, particularly at high filling ratios. We report a general route to non-aggregated highly filled, optically transparent polymer nanocomposites. It is based on using nanoparticles that have been coated with polymers forming spherical brushlike layers providing thermodynamic miscibility with the polymer matrix over the complete range of nanoparticle volume fractions. The polymers are attached *via* a versatile ligand exchange procedure which enables to prepare a wide range of optically transparent polymer nanocomposites up to weight fractions of 45%. This is demonstrated for a broad range of metal and semiconductor nanoparticles in optically transparent polymer matrices relevant for selective light/UV absorption, photoluminescence, and high/low refractive index polymer materials.

Introduction

Polymer nanocomposites are currently of immense interest in fundamental research as well as in a large variety of industrial applications. Nanoparticles provide new or largely enhanced material properties, but unfortunately their agglomeration mostly prevents these enhancements and often deteriorates material properties. Therefore, generally less than 5-10 wt% of nanoparticles can be dispersed into polymer matrices without sacrificing material properties by aggregation.¹ Promising experimental studies² and theoretical investigations³ have been reported to understand or control nanoparticle aggregation. This is a critical issue especially for optical applications that take advantage of the optical properties of nanoparticles. These are integrated into transparent polymers for ease of processing and protection,⁴ but often at the cost of agglomeration which causes turbidity and strongly reduces optical transmission and efficiency.

Since the first reports of polymer-gold nanocomposites for optical applications,^{5,6} nanocomposites consisting of inorganic metal or semiconducting nanoparticles and transparent polymer matrices have been continuously investigated toward applications

based on selective light absorption in the UV/vis range, photoluminescence, and high/low refractive index polymeric materials. For nanocomposites used as UV-photo-protective materials, high transparency in the visible range and steep absorption in the near UV-range ($\lambda < 400$ nm) are required. The most promising inorganic materials are ZnO and TiO₂ nanoparticles, which have bulk band gap energies of around 3 eV. These nanoparticles are preferably incorporated into poly(methyl methacrylate) (PMMA) or other transparent polymer matrices.⁷⁻⁹ For photoluminescent materials, semiconductor nanoparticles are particularly attractive, since they show wavelength-tunable light emission due to the quantum size effect and possess high photostability and a narrow emission bandwidth. Semiconductor nanoparticles can cover a large range of light emission wavelengths from 400 to 1400 nm. Preferred materials for polymer nanocomposites have been CdSe, CdTe, and CdSe core/shell nanoparticles, which have been integrated into poly(lauryl methacrylate),¹⁰ polystyrene,¹¹ PMMA,^{12,13} and poly(butyl methacrylate)¹⁴ matrices for electro-optical applications. Optical applications of polymers are often limited by their relatively narrow range of the refractive index (RI), which is typically only in the range between 1.3 and 1.7. The introduction of inorganic nanoparticles into polymer matrices can result in materials with much larger variations in their RI, which would enable applications as lenses, optical filters, reflectors, optical waveguides, optical adhesives, or antireflection films.¹⁵ For high-RI materials, TiO₂, ZrO₂, ZnS, and Si nanoparticles are mostly studied because of their transparency in the visible (TiO₂, ZrO₂, and ZnS) or red part (Si) of the spectrum,¹⁶ but also PbS nanoparticles are investigated for application in the NIR. For low-RI materials Au nanoparticles have been used within polymer nanocomposites.¹⁷⁻²⁰

For all the reported examples optical transparency was limited, particularly at high filling ratios where nanoparticles aggregate, such that only very thin micrometer-sized films could be used for optical applications. Exceptions are epoxy/SiO₂ or TiO₂ nanocomposites, where favorable R-OH...O-Si/Ti interactions provide interfacial stability that largely suppresses nanoparticle aggregation. An optical transmittance of up to 82% for 10 wt% TiO₂ and of up to 70% for 30 wt% TiO₂ nanocomposites could be achieved for these materials.²¹ Here we report a general route to nonaggregated highly filled, optically transparent polymer nanocomposites. The method is based on a spherical polymer brush coating of the nanoparticles which provides thermodynamic miscibility of the nanoparticles with the polymer matrix over the complete range of nanoparticle volume fractions as we have recently shown.²²⁻²⁴ This prevents nanoparticle aggregation

in the polymer matrix that can cause turbidity. We here apply this methodology to prepare optically transparent nanocomposites with an optical transmittance of up to 90% for nanoparticle weight fractions of up to 45 wt% with examples covering a large variety of chemically different nanoparticle/polymer combinations reaching from noble metal (Au, Ag), semiconductor (ZnO, CdSe, PbS), to magnetic nanoparticles (Fe_2O_3) in transparent polymer matrices including poly(methyl methacrylate) (PMMA), polystyrene (PS), polyisoprene (PI), and poly(2-vinylpyridine) (P2VP).

Experimental part

Nanoparticle synthesis

The gold nanoparticles were synthesized by the method of Yu *et al.* via reduction of chloroauric acid by oleylamine.²⁵ Cadmium selenide nanocrystals were synthesized by the method of Yang *et al.* via thermal decomposition of cadmium oleate.²⁶ Silver nanocrystals were synthesized after Yamamoto *et al.* via reduction of silver oleate.²⁷ Iron oxide nanocrystals were synthesized after Park *et al.* via thermal decomposition of iron oleate.²⁸ The lead sulfide nanocrystals were synthesized as reported by Hines.²⁹ Zinc oxide nanocrystals were synthesized by hydrolysis of zinc oleate in organic solvent as reported recently by our group.³⁰

Polymer synthesis

Polystyrene (PS) was synthesized by living anionic polymerization with *sec*-butyllithium as initiator at $-70\text{ }^\circ\text{C}$ in THF. The polymerization was terminated either with ethylene oxide to obtain a hydroxyl end group (PS-OH) or with CO_2 to obtain a carboxylic acid end group (PS-COOH). Polyisoprene (PI) was synthesized by living anionic polymerization in cyclohexane. The polymerization was initiated with *sec*-butyllithium at $30\text{ }^\circ\text{C}$ and terminated with ethylene oxide to obtain hydroxyl-terminated PI (PI-OH). Poly-2-vinylpyridine (P2VP) was synthesized by living anionic polymerization in THF at $-70\text{ }^\circ\text{C}$ with *sec*-butyllithium as initiator. The polymerization was terminated with ethylene oxide to obtain a hydroxyl end group (P2VP-OH). Poly(methyl methacrylate-*co*-methacrylic acid) (PMMA-*co*-PMAc) with 1% PMAc was purchased from Sigma-Aldrich and used as received.

The OH end groups of the narrowly distributed, hydroxyl-functionalized polymers (PS-OH, PI-OH, P2VP-OH) were subsequently converted into multidentate amine end groups *via* a two-step reaction. In the first step, the hydroxyl end group was activated with 1,1'-carbonyldiimidazole (CDI) in chloroform. Therefore, the polymer solution in chloroform was added dropwise to a CDI (25-fold excess) solution in chloroform. After stirring the reaction for 24 h at room temperature, the solution was extracted three times with water to remove residual CDI and dried under vacuum. In the next step, pentaethylenehexamine (PEHA, 25-fold excess) was dissolved in chloroform, and the CDI activated polymer solution in chloroform was added dropwise to the amine solution. After a reaction time of 24 h the solution was extracted three times with water and dried under vacuum. The properties of the polymer ligands are summarized in **Table 6.1**.

Table 6.1: Molecular weights M_w , polydispersity, and type of end groups of the polymer ligands used for the stabilization of the Nanoparticles

polymer	M_w (g/mol)	PDI	coordinating end group
PS	2500	1.19	PEHA
PS	8600	1.08	COOH
PI	16000	1.12	PEHA
P2VP	3825	1.07	PEHA
PMMA	34000	2.26	<i>co</i> -MAA (\approx 1%)

Polymer grafted nanoparticles by ligand exchange

The polymer brush on the nanoparticle surface was prepared by the ligand exchange method developed in our group *via* subsequent precipitation dissolution cycles.²⁴ The procedure generally consists of two steps. In the first step a solution of nanoparticles is mixed with a solution containing an excess of polymer ligand. Then the nanoparticles together with the polymer ligand are quantitatively precipitated by addition of an excess of a nonsolvent to remove the original nanoparticle surface ligand (oleic acid). The precipitant containing the nanoparticles and the excess polymer ligand is collected by

centrifugation, redissolved, and in the second step the nanoparticles selectively precipitated by addition of a defined amount of nonsolvent to remove excess polymer ligand from the polymer-coated nanoparticles. If necessary, each step can be repeated to fully separate excess ligands (oleic acid, polymer ligand), which can be checked by thermogravimetric analysis.

Nanocomposite preparation

The nanocomposites were prepared by mixing the brush grafted nanoparticle in the desired concentration with the matrix polymer in solution, followed by evaporation and drying under vacuum.

Characterization

The nanocomposites were characterized by transmission electron microscopy (TEM), thermogravimetric analysis (TGA), and UV/vis spectroscopy. TEM images were obtained on a Zeiss 922 Omega microscope. The TGA measurements were performed with a Mettler Toledo TGA1 with alumina pans, under nitrogen flow and a heating rate of 20 K/min. The UV/vis spectra were measured using an Agilent 8453. The films for photos and UV/vis measurements were solvent cast on glass slides. The samples for TEM were either cast on Cu grids from diluted solution or put on the Cu grid after cutting the films with a microtome. For the TGA measurements parts of the films were used.

Results and discussion

Theoretical considerations

The intensity loss due to scattering of light passing through a polymer matrix with refractive index n_p , filled with spherical particles with radius R and refractive index n_{NP} , can be calculated from Rayleigh's law

$$I = I_0 \exp \left[-\frac{3\phi l R^3}{4\lambda^4} \left(\frac{n_{NP}}{n_p} - 1 \right) \right] \quad (6.1)$$

where I is the intensity of the transmitted light, I_0 the intensity of the incident light, ϕ the volume fraction of the particles, l the optical path length or film thickness, and λ the wavelength of the light. From **equation 6.1** it is evident that the particle size has a very strong effect, much stronger than the film thickness, and that scattering and the resulting turbidity strongly increase with increasing particle size. Generally, 40 nm is considered as an upper limit for nanoparticle diameters to avoid intensity loss of transmitted light due to scattering. In our study we investigate very small nanoparticles with radii $R < 10$ nm. With the refractive index of the used polymers (PS, PMMA, and P2VP) in the range of $n_p \sim 1.5$, typical nanoparticle refractive indices $n_p \sim 3$, a film thickness of $l \sim 100 \mu\text{m}$, and a quite high volume fraction of $\phi \sim 0.2$, only a fraction of 0.02% of the incident light is lost due to scattering for a particle radius of 10 nm. For a radius of 40 nm this value increases to 1.5% and for a radius of 100 nm already to 21%. Thus, agglomeration of nanoparticles will cause a quite considerable increase of turbidity.

Polymer nanocomposite preparation

Polymer nanocomposites for optical applications are commonly prepared by either directly incorporating the nanoparticles into a polymer matrix by mechanical or physicochemical methods,^{31–36} chemical methods based on in situ polymerization,^{7–9} or sol/gel routes.³⁷ These methods kinetically trap the nanoparticles in the dispersed state to suppress aggregation and to obtain a homogeneous dispersion of nanoparticles in the polymer matrix. As the nanoparticles are immiscible with the polymer matrix, these are nonequilibrium states and as such are not long-term stable. Their aggregation state and distribution may change by subsequent processing and may delicately depend on the sample preparation conditions.

For our study the nanoparticles were stabilized with a polymer brush of the same polymer as the matrix polymer to afford complete thermodynamic miscibility and thus to avoid nanoparticle agglomeration. For complete miscibility up to the highest volume fractions of nanoparticles the grafting density of the polymer brush must be sufficiently high to overcome attractive interparticle forces. Since for this work high grafting densities are required and many different nanoparticle-polymer combinations are considered, we used the ligand exchange method for the end attachment of the polymer chains.²⁴ This method employs functional groups on the polymer chain ends to coordinatively bind to the nanoparticle surface. With a set of a few polymers with the same coordination groups

(-COOH and -PEHA; see **Table 6.1**) and several different nanoparticles it is thus possible to create a broad range of different polymer nanocomposites using the same methodology.

Optical properties and dispersion states

Figure 6.1 shows a variety of different nanocomposites as 100-250 μm thick films prepared *via* solvent casting on glass slides (Ag-PMMA, CdSe-PMMA, PbS-PI, Au-PS, Fe_2O_3 -P2VP, ZnO-PS) or as free-standing films (ZnO-PMMA, CdSe-PS). All are optically transparent at filling ratios of up to 45 wt% of nanoparticles.

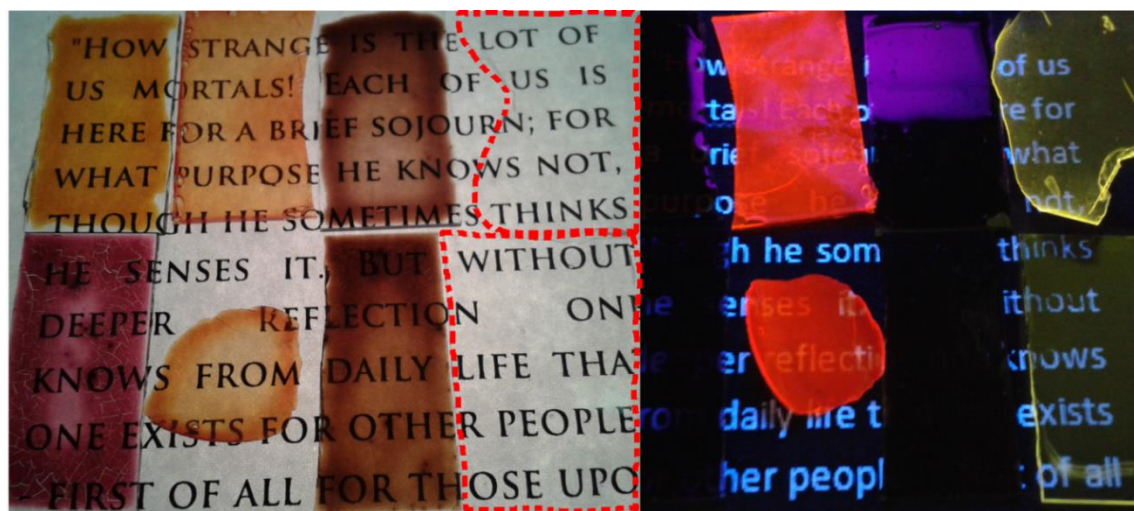


Figure 6.1: Left panel: photographs of transparent nanocomposites films (150 μm) on glass. Upper row: Ag-PMMA (100 μm , 2 wt%), CdSe-PMMA (200 μm , 10 wt%), PbS-PI (10 wt%), and free-standing ZnO-PMMA (250 μm , 10 wt%). Lower row: Au-PS (100 μm , 2 wt%), freestanding CdSe-PS (100 μm , 29%), Fe_2O_3 -P2VP (5 wt%), and ZnO-PS (150 μm , 45 wt%). The dashed red lines indicate the sample positions of the ZnO-PMMA and ZnO-PS films. Right panel: fluorescence of the same nanocomposites at UV illumination.

For the Au and Ag nanocomposites with their strong plasmon absorption we kept the weight fractions at lower values (2 wt%) to keep the visible optical transparency. All weight fractions were determined by thermogravimetric analysis (TGA) (see **Figure 6.S1** in the Supporting Information). The CdSe and ZnO semiconductor nanocomposites show the expected characteristic fluorescence upon UV illumination. The UV/vis spectra in **Figure 6.2** show for all nanocomposites transmissions of 90-95% except for the wavelength range within which the nanoparticles absorb light.

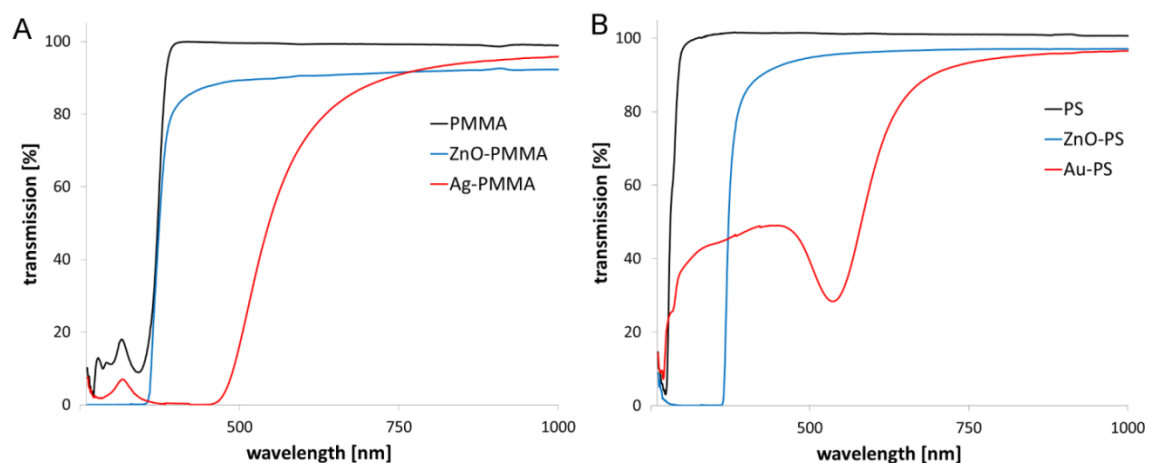


Figure 6.2: UV/vis spectra for nanocomposites with (A) PMMA and (B) PS matrices and different nanoparticles (Ag 5 wt%, Au 10 wt%, ZnO 10 wt% in PMMA, and 45 wt% in PS) showing 90-95% transparency at high loading ratios in the wavelength range above the absorptions edges of ZnO or above the plasmon resonance of Ag and Au. Film thickness is 250 μm for all except Ag-PMMA and Au-PS which are 100 μm .

Further examples for prepared optically transparent nanocomposites (PbS-PI, Fe_2O_3 -P2VP, CdSe-PMMA) are shown in **Figure 6.S2** of the Supporting Information.

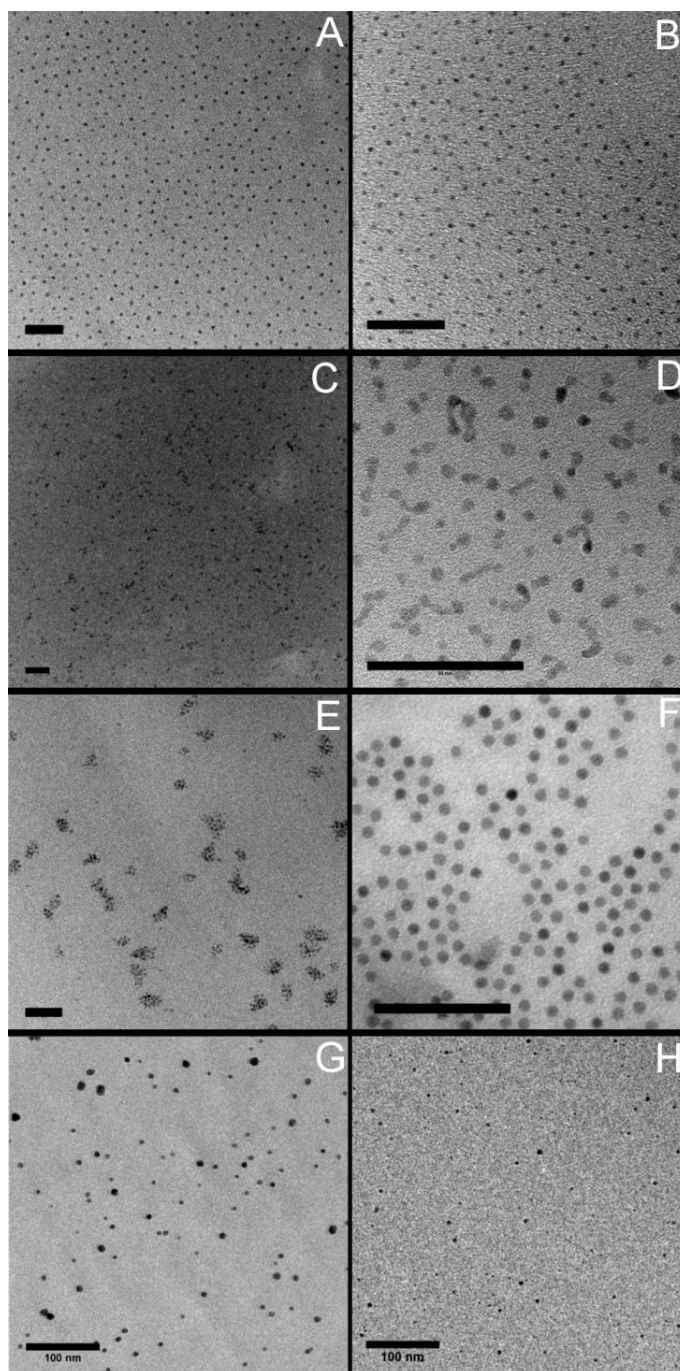


Figure 6.3: (A–F) TEM images of solvent-cast nanocomposites: (A) PbS-polyisoprene nanocomposite (7 nm, 10 wt%); (C and E) PMMA nanocomposites with CdSe nanoparticles (4 nm, 10 wt%) and ZnO nanoparticles (4 and 22 nm multiplets, 10 wt%); (B and D) polystyrene nanocomposites with CdSe nanoparticles (3 nm, 29 wt%) and ZnO nanoparticles (4 nm, 45 wt%); (F) poly(2-vinylpyridine) nanocomposite with Fe₂O₃ nanoparticles (6 nm, 10 wt%). Scale bars are all 50 nm. (G, H) TEM images of thin microtomed sections of a 10 wt% Au-polystyrene (G) and 2.5 wt% Ag-PMMA (H) nanocomposite (scale bars are 100 nm).

In **Figure 6.3**, TEM images of the nanocomposites are shown. We observe for PbS, CdSe, Fe₂O₃, Ag, and Au homogeneously dispersed single nanoparticles, where the mean interparticle distance is determined (1) by the thickness of the polymer brush, as has been demonstrated recently²¹ and observed in the TEM images (**Figure 6.S3** and **6.S4**) and DLS measurements (**Figure 6.S5**), and (2) the amount of free matrix polymer which

dilutes the nanoparticle system leading to an increase of the mean interparticle distance $D \sim \phi^{-1/3}$, where ϕ is the volume fraction of the nanoparticles in the polymer matrix. For the ZnO nanoparticles (**Figure 6.3D,E**) we observe the formation of small multiplets due to a slightly lower polymer ligand density. Still, also for these nanoparticles we obtained highly transparent nanocomposites up to weight fractions of 45%. In **Figure 6.3G,H** we show TEM images of microtomed thin sections of bulk nanocomposites proving the absence of aggregation in thicker sections.

The miscibility of nanoparticles and polymer matrix not only provides transparent nanocomposites for optical applications but also increases the mechanical properties of the nanocomposites. As an example, nanoindentation measurements show a considerable increase of the elastic modulus for the ZnO/PMMA nanocomposites, increasing from 10 GPa for pure PMMA over 23 GPa for a weight fraction of 5% reaching 35 GPa for the 10 wt% nanocomposite as shown in **Figure 6.4**, demonstrating the improved scratch resistance of these materials which is also important for optical applications.

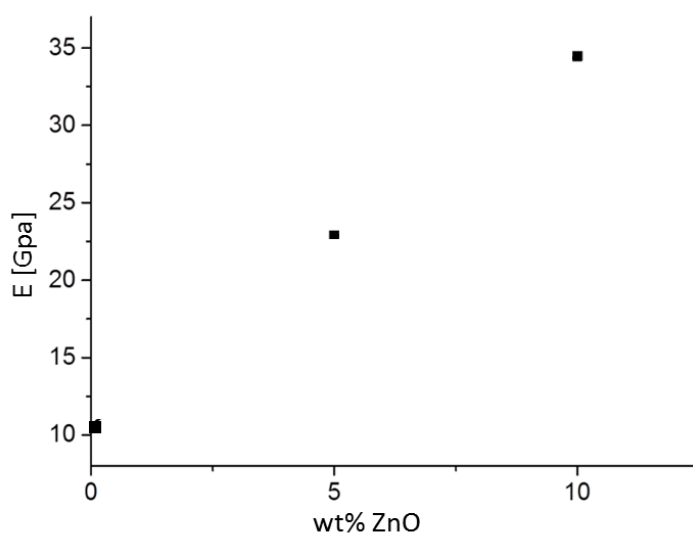


Figure 6.4: Nanoindentation measurements of ZnO-PMMA composites with different ZnO contents indicating a significantly increasing E-modulus with increasing ZnO content and thus considerably improved scratch resistance.

Conclusions

We report a general route to nonaggregated highly filled, optically transparent polymer nanocomposites for a large variety of different nanoparticle/polymer matrix combinations including Ag, Au, CdSe, ZnO, Fe₂O₃, PbS in poly(methyl methacrylate) (PMMA),

polyisoprene (PI), polystyrene (PS), and poly(2-vinylpyridine) (P2VP) as examples. The incorporation of nanoparticles not only provides high optical transparency but also improves mechanical properties to improve scratch resistance.

Notes

The authors declare no competing financial interest.

Acknowledgements

Financial support by the collaborative research center SFB840 (project TPB09) is gratefully acknowledged.

Supporting Information

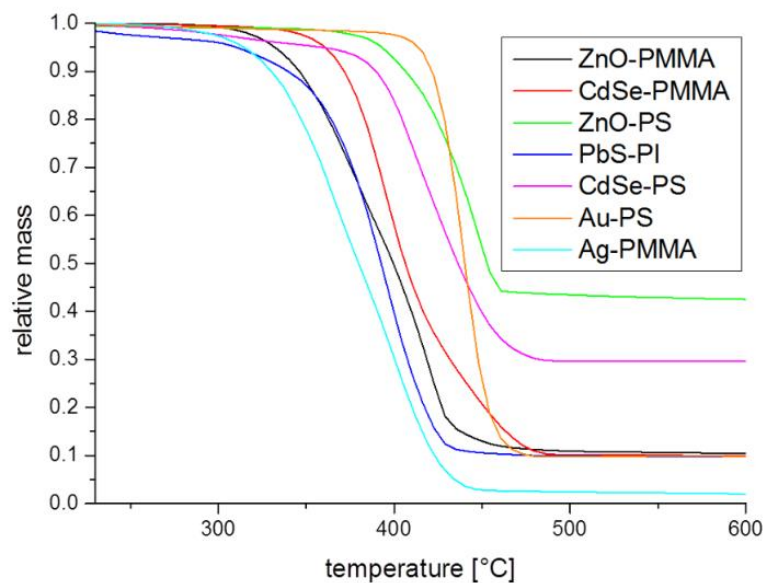


Figure 6.S1: TGA measurements of all investigated nanocomposites.

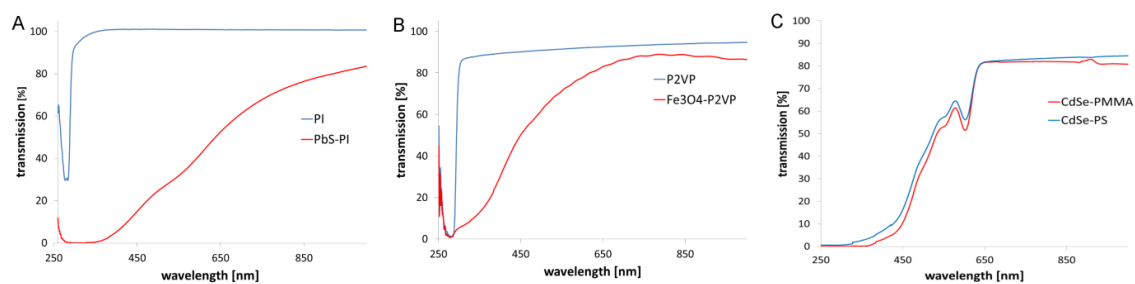


Figure 6.S2: UV-vis spectra of PbS-PI (A), iron oxide Fe₂O₃-P2VP (B), and CdSe-PMMA (C) nanocomposites with high transmission.

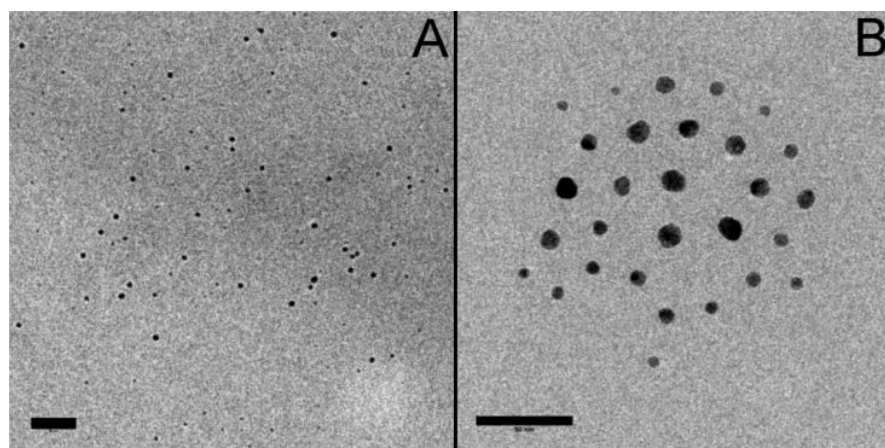


Figure 6.S3: TEM-images of solvent cast Ag-PMMA (A, 15 nm, 2%) and Au-PI (B, 15 nm, 10%) nanocomposites (scale bars are 50 nm).

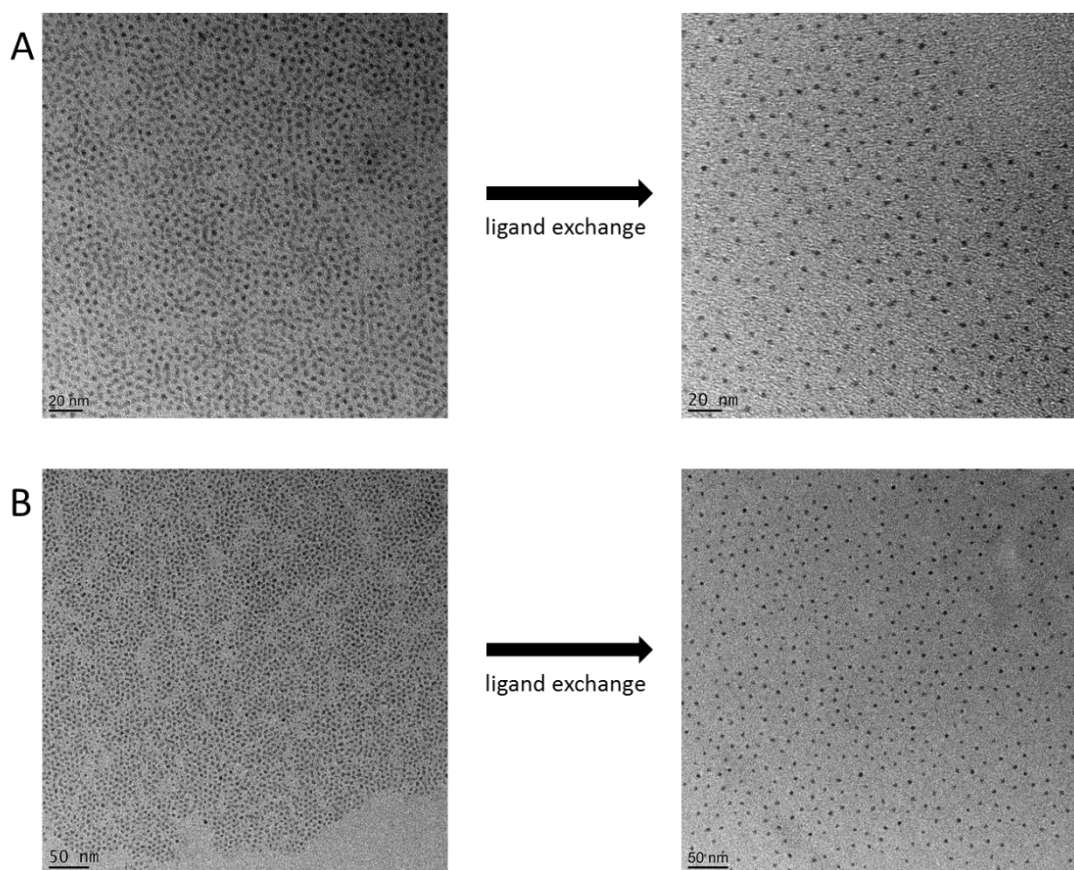


Figure 6.S4: TEM-images of CdSe-nanoparticles (A) and PbS-nanoparticles (B) before (left) and after the ligand exchange (right) with polystyrene (A) and polyisoprene (B).

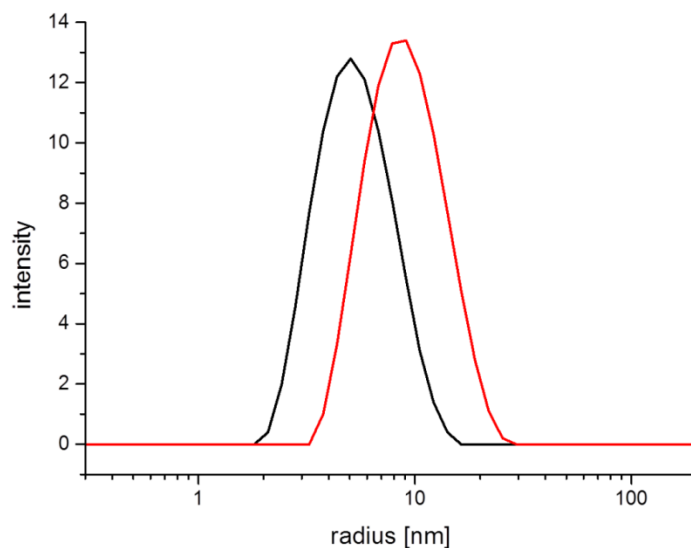


Figure 6.S5: Size distribution of CdSe-nanoparticles (black) and CdSe-nanoparticles coated with a PS-polymer brush (red) as measured by dynamic light scattering (DLS).



Figure 6.S6: Photo of a 10 wt% ZnO/PS-nanocomposite thin film where the ZnO nanoparticles were coated with oleic acid instead of a polystyrene brush layer. The incompatibility and aggregation of the nanoparticles in the PS (8600 g/mol) matrix are causing pronounced turbidity.

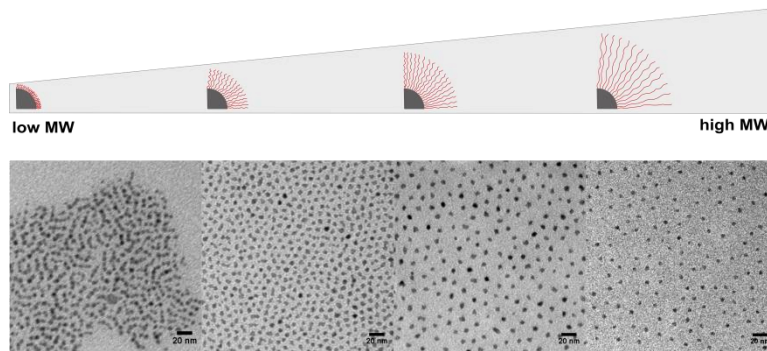
References

1. R. K. Gupta, E. Kennel, and K.-J. Kim, *Polymer Nanocomposites Handbook* (CRC Press, Boca Raton, 2010).
2. P. Akcora, H. Liu, S. K. Kumar, J. Moll, Y. Li, B. C. Benicewicz, L. S. Schadler, D. Acehan, A. Z. Panagiotopoulos, V. Pryamitsyn, V. Ganesan, J. Ilavsky, P. Thiyagarajan, R. H. Colby, and J. F. Douglas, “Anisotropic Self-Assembly of Spherical Polymer-Grafted Nanoparticles,” *Nat. Mater.* **8** (4), 354–359 (2009).
3. J. Liu, Y. Gao, D. Cao, L. Zhang, and Z. Guo, “Nanoparticle Dispersion and Aggregation in Polymer Nanocomposites: Insights from Molecular Dynamics Simulation,” *Langmuir* **27** (12), 7926–7933 (2011).
4. S. Li, M. Meng Lin, M. S. Toprak, D. K. Kim, and M. Muhammed, “Nanocomposites of Polymer and Inorganic Nanoparticles for Optical and Magnetic Applications,” *Nano Rev.* **1**, 5214 (2010).
5. W. Caseri, “Inorganic Nanoparticles as Optically Effective Additives for Polymers,” *Chem. Eng. Commun.* **196** (5), 549–572 (2008).
6. W. Caseri, “Nanocomposites of Polymers and Metals or Semiconductors: Historical Background and Optical Properties,” *Macromol. Rapid Commun.* **21** (11), 705–722 (2000).
7. J. Zhang, S. Luo, and L. Gui, “Poly(methyl methacrylate)-Titania Hybrid Materials by Sol-Gel Processing,” *J. Mater. Sci.* **32** (6), 1469–1472 (1997).
8. A. H. Yuwono, B. Liu, J. Xue, J. Wang, H. I. Elim, W. Ji, Y. Li, and T. J. White, “Controlling the Crystallinity and Nonlinear Optical Properties of Transparent TiO₂–PMMA Nanohybrids,” *J. Mater. Chem.* **14** (20), 2978–2987 (2004).
9. C.-H. Hung and W.-T. Whang, “Effect of Surface Stabilization of Nanoparticles on Luminescent Characteristics in ZnO/Poly(hydroxyethyl methacrylate) Nanohybrid Films,” *J. Mater. Chem.* **15** (2), 267–274 (2005).

10. J. Lee, V. C. Sundar, J. R. Heine, M. G. Bawendi, and K. F. Jensen, “Full Color Emission from II-VI Semiconductor Quantum Dot-Polymer Composites,” *Adv. Mater.* **12** (15), 1102–1105 (2000).
11. L. Erskine, T. Emrick, A. P. Alivisatos, and J. M. Fréchet, “Preparations of Semiconductor Nanocrystal-Polystyrene Hybrid Materials,” *Polym. Prepr.* **41**, 593 (2000).
12. S. C. Farmer and T. E. Patten, “Photoluminescent Polymer/Quantum Dot Composite Nanoparticles,” *Chem. Mater.* **13** (11), 3920–3926 (2001).
13. H. Zhang, Z. Cui, Y. Wang, K. Zhang, X. Ji, C. Lü, B. Yang, and M. Gao, “From Water-Soluble CdTe Nanocrystals to Fluorescent Nanocrystal–Polymer Transparent Composites Using Polymerizable Surfactants,” *Adv. Mater.* **15** (10), 777–780 (2003).
14. G. G. Yordanov, G. D. Gicheva, and C. D. Dushkin, “Optical Memory Based on Photo-Activated Fluorescence of Core/Shell CdSe/CdS Quantum Dots Embedded in Poly(butylmethacrylate),” *Mater. Chem. Phys.* **113** (2-3), 507–510 (2009).
15. H. Althues, J. Henle, and S. Kaskel, “Functional Inorganic Nanofillers for Transparent Polymers,” *Chem. Soc. Rev.* **36** (9), 1454–1465 (2007).
16. G. Zhang, H. Zhang, H. Wei, S. Zhu, Z. Wu, Z. Wang, F. Jia, J. Zhang, and B. Yang, “Creation of Transparent Nanocomposite Films with a Refractive Index of 2.3 Using Polymerizable Silicon Nanoparticles,” *Part. Part. Syst. Charact.* **30** (8), 653–657 (2013).
17. L. Zimmermann, M. Weibel, W. Caseri, and U. W. Suter, “High Refractive Index Films of Polymer Nanocomposites,” *J. Mater. Res.* **8** (07), 1742–1748 (1993).
18. M. Weibel, W. Caseri, U. W. Suter, H. Kiess, and E. Wehrli, “Preparation of Polymer Nanocomposites with “Ultrahigh” Refractive Index,” *Polym. Adv. Technol.* **2** (2), 75–80 (1991).
19. C. Lü, C. Guan, Y. Liu, Y. Cheng, and B. Yang, “PbS/Polymer Nanocomposite Optical Materials with High Refractive Index,” *Chem. Mater.* **17** (9), 2448–2454 (2005).

-
20. L. Zimmermann, M. Weibel, W. Caseri, U. W. Suter, and P. Walther, “Polymer Nanocomposites with “Ultralow” Refractive Index,” *Polym. Adv. Technol.* **4** (1), 1–7 (1993).
21. P. Tao, A. Viswanath, Y. Li, R. W. Siegel, B. C. Benicewicz, and L. S. Schadler, “Bulk Transparent Epoxy Nanocomposites Filled with Poly(glycidyl methacrylate) Brush-Grafted TiO₂ Nanoparticles,” *Polymer* **54** (6), 1639–1646 (2013).
22. M. Bieligmeyer, S. M. Taheri, I. German, C. Boisson, C. Probst, W. Milius, V. Altstädt, J. Breu, H.-W. Schmidt, F. D’Agosto, and S. Förster, “Completely Miscible Polyethylene Nanocomposites,” *J. Am. Chem. Soc.* **134** (44), 18157–18160 (2012).
23. S. Fischer, A. Salcher, A. Kornowski, H. Weller, and S. Förster, “Completely Miscible Nanocomposites,” *Angew. Chem. Int. Ed.* **50** (34), 7811–7814 (2011).
24. S. Ehlert, S. M. Taheri, D. Pirner, M. Drechsler, H.-W. Schmidt, and S. Förster, “Polymer Ligand Exchange to Control Stabilization and Compatibilization of Nanocrystals,” *ACS Nano* **8** (6), 6114–6122 (2014).
25. H. Yu, M. Chen, P. M. Rice, S. X. Wang, R. L. White, and S. Sun, “Dumbbell-Like Bifunctional Au-Fe₃O₄ Nanoparticles,” *Nano Lett.* **5** (2), 379–382 (2005).
26. Y. A. Yang, H. Wu, K. R. Williams, and Y. C. Cao, “Synthesis of CdSe and CdTe Nanocrystals without Precursor Injection,” *Angew. Chem.* **117** (41), 6870–6873 (2005).
27. M. Yamamoto, Y. Kashiwagi, and M. Nakamoto, “Size-Controlled Synthesis of Monodispersed Silver Nanoparticles Capped by Long-Chain Alkyl Carboxylates from Silver Carboxylate and Tertiary Amine,” *Langmuir* **22** (20), 8581–8586 (2006).
28. J. Park, K. An, Y. Hwang, J.-G. Park, H.-J. Noh, J.-Y. Kim, J.-H. Park, N.-M. Hwang, and T. Hyeon, “Ultra-Large-Scale Syntheses of Monodisperse Nanocrystals,” *Nat. Mater.* **3** (12), 891–895 (2004).
29. M. A. Hines and G. D. Scholes, “Colloidal PbS Nanocrystals with Size-Tunable Near-Infrared Emission: Observation of Post-Synthesis Self-Narrowing of the Particle Size Distribution,” *Adv. Mater.* **15** (21), 1844–1849 (2003).

30. S. Ehlert, T. Lunkenbein, J. Breu, and S. Förster, “Facile Large-Scale Synthetic Route to Monodisperse ZnO Nanocrystals,” *Colloids Surf., A* **444**, 76–80 (2014).
31. J. Zheng, R. W. Siegel, and C. G. Toney, “Polymer Crystalline Structure and Morphology Changes in Nylon-6/ZnO Nanocomposites,” *J. Polym. Sci. B Polym. Phys.* **41** (10), 1033–1050 (2003).
32. V. Khrenov, M. Klapper, M. Koch, and K. Müllen, “Surface Functionalized ZnO Particles Designed for the Use in Transparent Nanocomposites,” *Macromol. Chem. Phys.* **206** (1), 95–101 (2005).
33. M. Xiong, G. Gu, B. You, and L. Wu, “Preparation and Characterization of Poly(styrene butylacrylate) Latex/Nano-ZnO Nanocomposites,” *J. Appl. Polym. Sci.* **90** (7), 1923–1931 (2003).
34. D. Sun, N. Miyatake, and H.-J. Sue, “Transparent PMMA/ZnO Nanocomposite Films Based on Colloidal ZnO Quantum Dots,” *Nanotechnology* **18** (21), 215606 (2007).
35. N. S. Allen, M. Edge, A. Ortega, G. Sandoval, C. M. Liauw, J. Verran, J. Stratton, and R. B. McIntyre, “Degradation and Stabilisation of Polymers and Coatings: Nano versus Pigmentary Titania Particles,” *Polym. Degrad. Stab.* **85** (3), 927–946 (2004).
36. S. H. Stelzig, M. Klapper, and K. Müllen, “A Simple and Efficient Route to Transparent Nanocomposites,” *Adv. Mater.* **20** (5), 929–932 (2008).
37. J. Noack, L. Schmidt, H.-J. Gläsel, M. Bauer, and E. Kemnitz, “Inorganic-Organic Nanocomposites Based on Sol-Gel Derived Magnesium Fluoride,” *Nanoscale* **3** (11), 4774–4779 (2011).



7

Rheological Study of Polymer Nanocomposites: Influence of Nanoparticles on Polymer Chain Dynamics

Daniela Pirner, Martin Dulle, and Stephan Förster

Physical Chemistry I, University of Bayreuth, Germany

To be submitted

Abstract

We investigate polymer nanocomposites made of narrow disperse spherical nanoparticles that are coated with end-functionalized polymers to form a spherical polymer brush layer. These nanoparticles can be homogeneously dispersed in the corresponding polymer matrix. The structure of the polymer-coated nanoparticles was examined by using small angle X-ray scattering (SAXS) and transmission electron microscopy (TEM), and was related to the viscoelastic properties of the nanocomposites. We observe a systematic retardation of the polymer relaxation dynamics with increasing particle loading. Nanoparticle aggregation leads to the formation of chain-like structures causing a strong reinforcement effect.

Introduction

In the last decades, nanocomposites have gained a lot of attention and were in the focus of many studies.¹⁻⁴ The use of nanocomposites, meaning the addition of inorganic nano-fillers to a polymeric matrix, is a prominent tool to trigger the properties of polymers and opened up a bright field of applications. They provide both the flexibility of the lightweight polymer matrix and the specificities of nanoparticles leading to an improvement in mechanical,^{5,6} electrical,⁷ optical⁸ and barrier⁹ properties of polymer materials. A good dispersibility of the nano-fillers in the matrix is essential to achieve unique material properties. However, especially nano objects tend to aggregate,¹⁰ due to large interfacial areas, and therefore many methods to stabilize the fillers in order to make them miscible in the matrix were investigated. Nearly, all proposed methods deal with surface modification of the nano-fillers to overcome the strong particle-particle interactions, which favor agglomeration of particles. Either surface modification with low molecular weight ligands or with polymeric ligands, usually of the same type as the matrix polymer, is applied.¹¹ It has been shown that the more promising route to get a good dispersion of nano-fillers is the use of polymeric ligands. Here, two main approaches were developed: “grafting-from” and “grafting-to” attachment of polymer chains on particle surfaces. The grafted polymer layer sterically stabilizes the nanoparticles by complete shielding of the attractive forces. The grafting-from method

often results in higher grafting densities of polymer chains, since the polymer chains are directly grown from the nanoparticle surface.¹² In the case of grafting-to techniques the polymer chains are pre-synthesized and are attached to the nanoparticle surface in a second preparation step. Usually, steric repulsions limit the grafting density. Recently, we introduced a grafting-to approach, which results in high grafting densities and thus to a brush-like polymer layer surrounding the particles by using coordinative interactions, instead of covalent bonds, to attach the polymer chains on the nanoparticles.¹³ A great advantage of the grafting-to method is that the polymer chains can be synthesized in controlled manner and characterized previously the attachment, which is important for fundamental understanding of structure-property relationship in nanocomposites.

For an optimal design of nanocomposites the understanding of the impact of the interfacial layer on macroscopic properties is essential and therefore many parameters have to be considered. The main parameters which have to be controlled are polymer-particle interactions, the polymer dynamics and the mechanism responsible for the retardation of the polymer dynamics. In many studies, a reinforcement of the mechanical properties is observed in nanocomposites. This effect is mainly attributed to the formation of interconnected structures,¹⁴ which lead to a solid-like mechanical response at low frequency mechanical deformations. Usually, polymer stabilized nanoparticles exhibit a much lower level of reinforcement compared to nanoparticles with low molecular weight ligands.

Although nanocomposites with uniform fillers are desired for many applications, recently many studies focus on controlled particle aggregation which has additional advantages.^{14–16} These nanoparticle aggregates can form different intermediate structures in the polymer matrix such as ramified or elongated objects. Several approaches were developed to control the hierarchical formation of these structures and to tune the final material properties. In general, a stronger reinforcement is obtained due to network formation and stronger interactions between the fillers and matrix polymer compared to isolated nanoparticles.

In this work, we investigate polyisoprene nanocomposites formed by narrow disperse spherical PbS nanoparticles, which are coated with a polyisoprene brush layer. The surface modification of the nanoparticles is carried out with the previous introduced grafting-to approach.¹³ Here, the focus is on the investigation of the influence of the grafted chain length on the viscoelastic properties. In addition, the loading of particles is varied at a fixed molecular weight of the brush layer. In addition, we study the

mechanical properties of “primary” nanoparticle aggregates, which consist of a sequence of nanoparticles being coated with polyisoprene. The results allow one to develop a route towards prediction and triggering of nanocomposite mechanical properties.

Material and Methods

Preparation of Nanocomposites

Polyisoprene-coated PbS nanoparticles, PbS@PI were used. The synthesis of the polymeric ligands, as well as the nanoparticles, was reported previously.¹³ The polymer chains were attached to the nanoparticle surface by a ligand-exchange technique to form stable and densely coated nanoparticles.¹³

Characterization Methods

Polymer Characterization. The end-functionalization and the structure of the polymers are determined by ¹H-NMR spectroscopy in CDCl₃, using a 300 MHz Bruker Ultrashield 300-spectrometer. The molecular weight distributions of the polymers are determined by gel permeation chromatography (GPC) in tetrahydrofuran (THF) by using *cis*-1,4-polyisoprene calibration standards. Four SDplus MZ columns with a porosity range from 10⁶ to 100 Å at a flow rate of 1 mL/min are used. Signals are detected with a Shodex RI-71 detector and a UV-detector. In **Table 7.1** the molecular characteristics of the polymers are listed. All used polymers are well-defined and have a narrow molecular weight distribution (PDI ≤ 1.08).

Table 7.1: Molecular characterization of polymers.

Sample	M_n (g·mol ⁻¹) ^a	M_w (g·mol ⁻¹) ^a	M_w/M_n	DP
PI-58k	58022	58731	1.01	850
PI-15k	15338	15660	1.02	224
PI-4.3k	4314	4506	1.04	62
PI-1.7k	1677 ^b	1761 ^b	1.05	23

^aThe molecular weight distribution is determined by GPC (THF, RT, 1 mL/min flow rate) using 1,4-polyisoprene. ^bThe molecular weight distribution is obtained by MALDI-ToF.

Characterization of Nanocomposites. The coated nanoparticles are characterized by transmission electron microscopy (TEM), thermogravimetric analysis (TGA), dynamic light scattering (DLS), small-angle X-ray scattering (SAXS) and rheology. Bright-field TEM observations are performed to characterize the nanocomposite structure and to exclude the formation of aggregates. The samples are prepared from drop casting in solution and examined on a Zeiss CEM 902 electron microscope operated at 80 kV. TGA measurements are obtained with a Netzsch TG 209 F1 Libra under nitrogen flow and a heating rate of 10 K/min to generate information about the grafting densities on the particle surface. The grafting densities are found in **Table 7.S1** (Supporting Information) and are calculated under the assumption of spherical particles using the density of the bulk material and that no free polymer is present. The hydrodynamic radii of the coated nanoparticles are determined by DLS and are carried out with a Malvern Instruments Zetasizer Nano Series device in dilute solutions in THF. All SAXS data reported here were measured using the small-angle X-ray system “Double Ganesha AIR” (SAXSLAB, Denmark). The X-ray source of this laboratory-based system is a rotating anode (copper, MicoMax 007HF, Rigaku Corporation, Japan) providing a micro-focused beam at $\lambda = 0.154$ nm. The data are recorded by a position sensitive detector (PILATUS 300K, Dectris). To cover the range of scattering vectors between 0.04-5.0 nm⁻¹ different detector positions are used. The measurements were done on a Kapton film at room temperature. Viscoelastic properties of the nanocomposites are studied by using a Malvern Instruments Bohlin Gemini HR Nano rheometer with a 25 or 8 mm stainless steel plate–plate setup. The oscillatory shear measurements were carried out from 0.01 Hz to 10 Hz in the linear response regime. The measured temperature range was between 6 °C to 60 °C. In **Table**

7.2 the compositions of the nanocomposites samples are listed, containing the weight fractions (wt%) and volume fraction of the polymer coated nanoparticles (ϕ composite) and the volume fraction of the bare nanoparticles (ϕ nanoparticle).

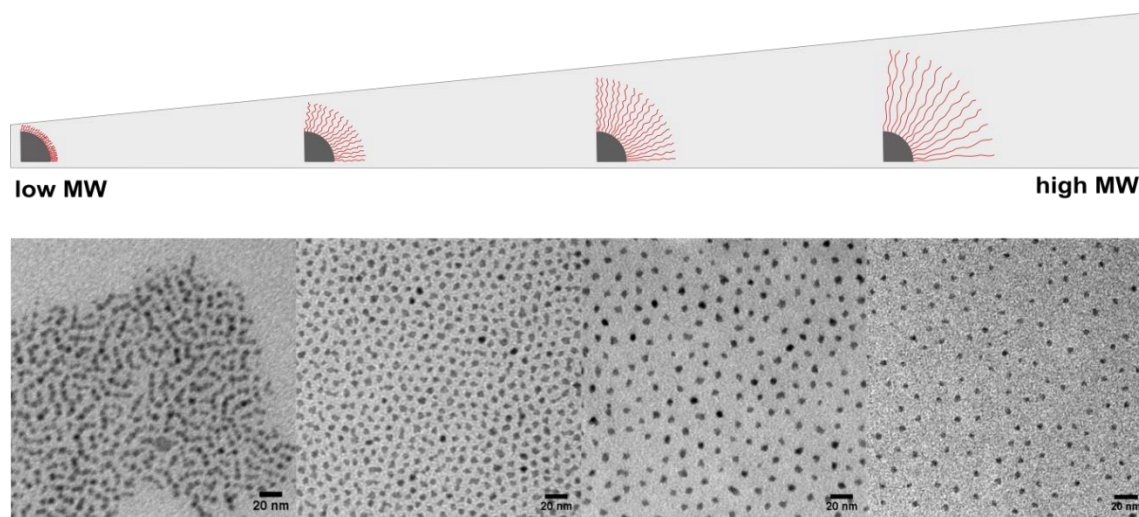
Table 7.2: Weight (wt%) and volume fraction (ϕ) of the polymer stabilized nanoparticles and the bare nanoparticles in the nanocomposites.

Sample	Composite (wt%)	ϕ Composite	ϕ Nanoparticle
PI-58k+PbS@PI-58k	0	0	0
PI-58k+PbS@PI-58k	20	0.18	$2 \cdot 10^{-3}$
PI-58k+PbS@PI-58k	40	0.36	$4 \cdot 10^{-3}$
PI-58k+PbS@PI-58k	60	0.56	$6 \cdot 10^{-3}$
PI-58k+PbS@PI-58k	80	0.77	$8 \cdot 10^{-3}$
PI-58k+PbS@PI-58k	100	1	0.01
PI-15k+PbS@PI-15k	100	1	0.012
PI-4.3k+PbS@PI-4.3k	100	1	0.024
PI-1.7k+PbS@PI-1.7k	100	1	0.186

Results and Discussion

Polyisoprene nanocomposites with polyisoprene stabilized PbS nanoparticles as fillers are chosen as a model system to study the influence of the polymer brush layer and the particle loading on the mechanical properties. The spherical PbS nanoparticles have a diameter of 7.5 nm. The molecular weight of the polyisoprene brush is varied from relatively low molecular weights (1.7 kg/mol) to high molecular weights (58 kg/mol). **Scheme 7.1** show the growing polymer chain length on the nanoparticle surface which is related to an increase in brush layer thickness. In addition, the corresponding TEM

images from each sample are presented. The applied ligand exchange approach results in densely grafted polymer chains forming a brush-like layer with highly stretched polymer chains due to the loss of conformational freedom.



Scheme 7.1: Concept of increasing molecular weight of the polymer brush on the nanoparticle surface and corresponding TEM images of the polyisoprene stabilized PbS nanoparticles with increasing molecular weight: 1.7 kg/mol, 4.3 kg/mol, 15 kg/mol, and 58 kg/mol.

The grafting densities of the polymer chains on the nanoparticle surface are listed in **Table 7.S1** (see Supporting Information) and are above or around 1 nm^{-2} , depending on the molecular weight of polymer chains. The grafting density is influenced by the chain length, which influences the steric repulsion and varies for each PbS@PI system.

With decreasing polymer chain length the distance between the nanoparticles is reduced which allows interparticle distance control. However, for very short polymer chains (1.7 kg/mol) “primary” aggregates are obtained. The spherical nanoparticles cannot be stabilized as isolated particles anymore. These primary aggregates consist of a linear sequence of nanoparticles (2 to 6 particles per aggregate), similar to pearl-necklace structures. This formation represents a controlled clustering which opens the way to new mechanical properties and applications.

SAXS measurements were performed to get information about the distance between the nanoparticles in bulk (**Figure 7.1**). In addition DLS measurements reveal the hydrodynamic diameter of the polymer stabilized nanoparticles in THF (**Figure 7.2**). In **Table 7.3** the structural parameters of the polyisoprene-coated nanoparticles are summarized.

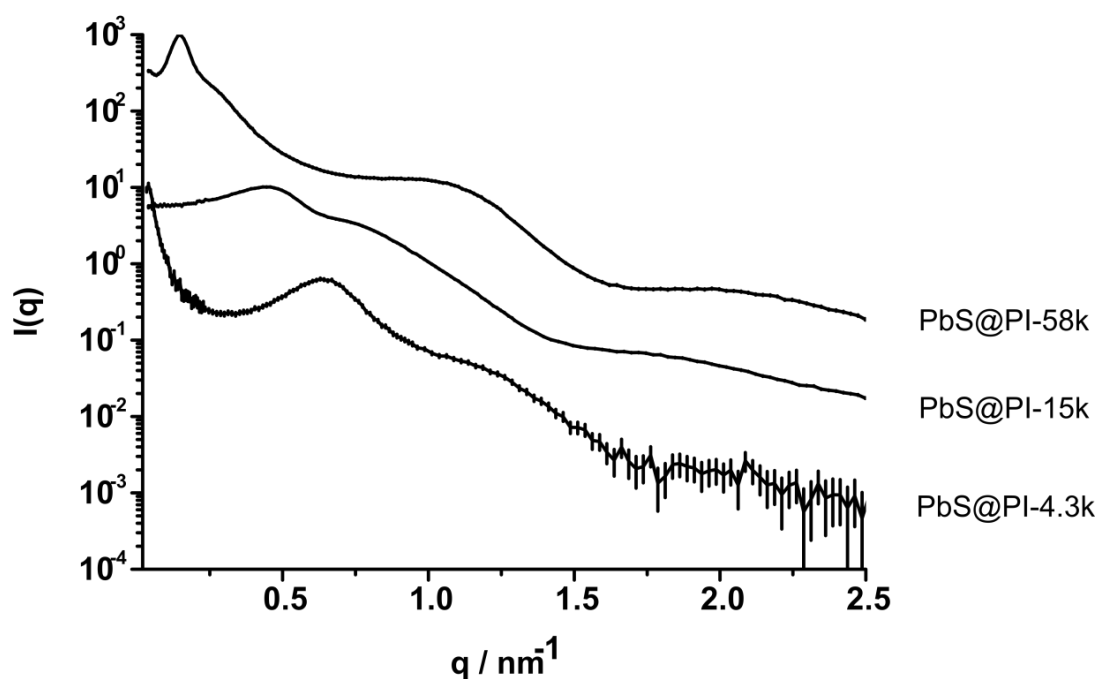


Figure 7.1: Measured SAXS curves for three different polymer-coated PbS-nanoparticle systems with different polymer chain length (4.3 kg/mol, 15 kg/mol, and 58 kg/mol).

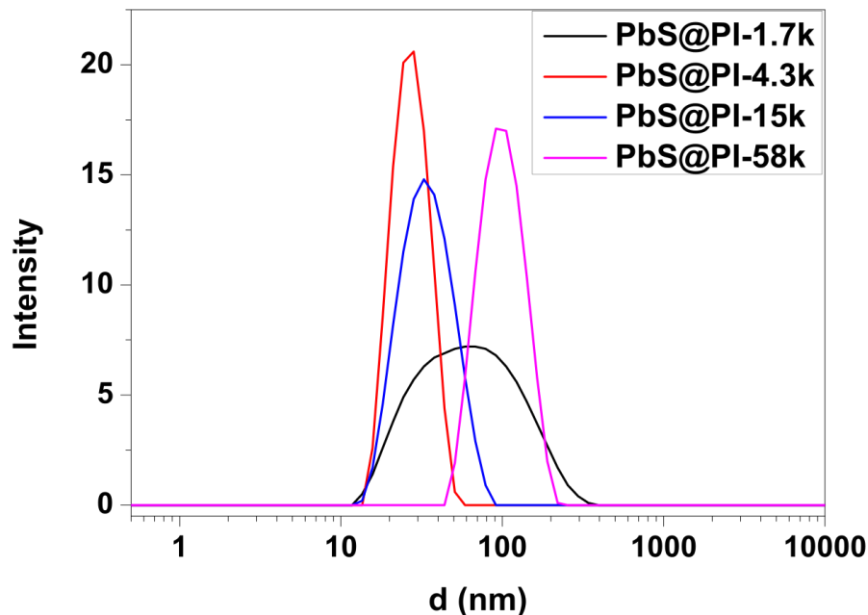


Figure 7.2: DLS measurements of the polymer stabilized nanoparticles in THF at 25 °C. PbS@PI1.7k $d=58.75$ nm (primary aggregates, broad size distribution); PbS@PI4.3k $d=27.05$ nm; PbS@PI15k $d=32.12$ nm; PbS@PI58k $d=97.82$ nm.

The diameter of the PbS nanoparticles was kept constant at 7.5 nm. The distance between the particles and the hydrodynamic diameters differ depending on the molecular weight of the grafted polymer chains. The coated nanoparticles with the highest molecular weight

(58 kg/mol) results in particle arrangements with a mean distance of 42 nm between the particles in bulk and a hydrodynamic radius of 97 nm in solution. The mean distance in bulk as well as the hydrodynamic diameter in solution decreases with decreasing molecular weight. The coated-nanoparticles with the 1.7 kg/mol polyisoprene forms primary aggregates as already demonstrated in the TEM images (**Scheme 7.1**). In addition, DLS measurements show a broad size distribution and no well-defined mean diameter could be obtained. There is no linear relationship between the molecular weight and the mean distance, since the polymer chains adopt a stretched non-Gaussian.

Table 7.3: Structural parameters of the polymer-coated nanoparticles in bulk and solution.

Sample	d_{PbS} (nm) ^a	Mean distance (nm) ^a	d_{H} (nm) ^b
PbS@PI-58k	7.5	42	97
PbS@PI-15k	7.5	12	33
PbS@PI-4.3k	7.5	10	28
PbS@PI-1.7k	7.5	-	-

^aThe diameter of the PbS nanoparticles and the mean distance of the polymer-coated nanoparticles were determined by SAXS measurements in bulk. ^bThe hydrodynamic diameter of the polymer-coated nanoparticles was determined by DLS measurements in dilute solutions in THF.

The influence of the polymer-coated nanoparticles on the mechanical properties of polyisoprene is presented in **Figure 7.3** and **7.4**. Nanocomposites were prepared by using polyisoprene with a molecular weight of 58 kg/mol for both, matrix and polymer brush. The neat polyisoprene was mixed with different weight fractions of polymer-coated nanoparticles ranging from 0 wt% (neat polymer) to 100 wt% (neat PbS@PI-58k). In **Figure 7.3(a)** a typical oscillatory dynamic-mechanical measurement is shown for 60 wt% PbS@PI58k in polyisoprene matrix for different temperatures (15 °C, 20 °C, 40 °C, and 60 °C). The individual curves can be combined to a master curve (**Figure 7.3(b)**) by horizontally shifting the curves with an a_T -factor by means of time-temperature superposition using the Williams-Landel-Ferry equation (**equation 7.1**).¹⁷

$$\log(a_T) = \log \frac{\tau(T)}{\tau(T_0)} = \frac{-C_1(T - T_0)}{C_2 + (T - T_0)} \quad (7.1)$$

The reference temperature T_0 was set to 20 °C. The obtained WLF-constants C_1 and C_2 are found to be 4.3 and 89.2 respectively.

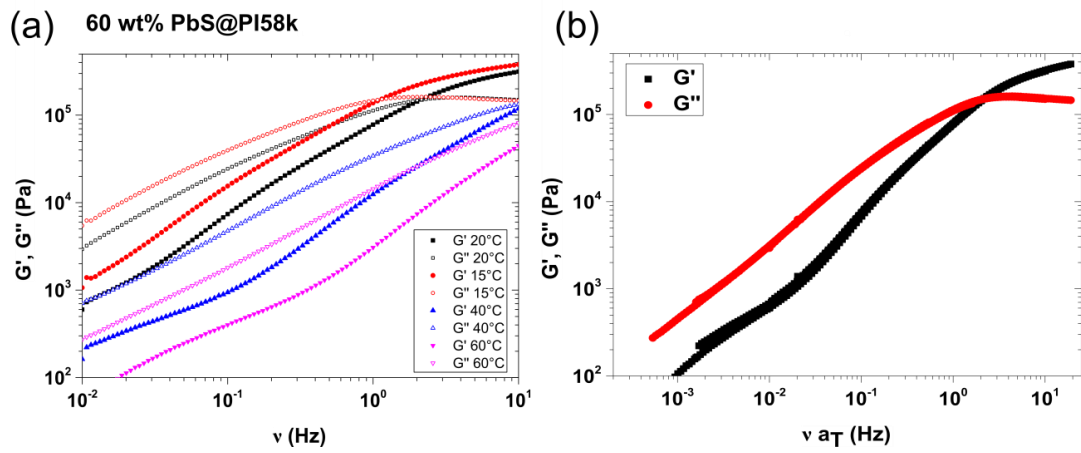


Figure 7.3: (a) Storage modulus G' (closed squares) and loss modulus G'' (open squares) of a 60 wt% PbS@PI58k nanocomposite in polyisoprene (58 kg/mol) at different temperatures and (b) the constructed master curve using the time-temperature superposition method with reference temperature $T_0=20$ °C.

In **Figure 7.4(a)** the loss modulus G' and **Figure 7.4(b)** storage modulus G'' of the generated master curves of each sample with different particle loadings are plotted separately as a function of frequency.

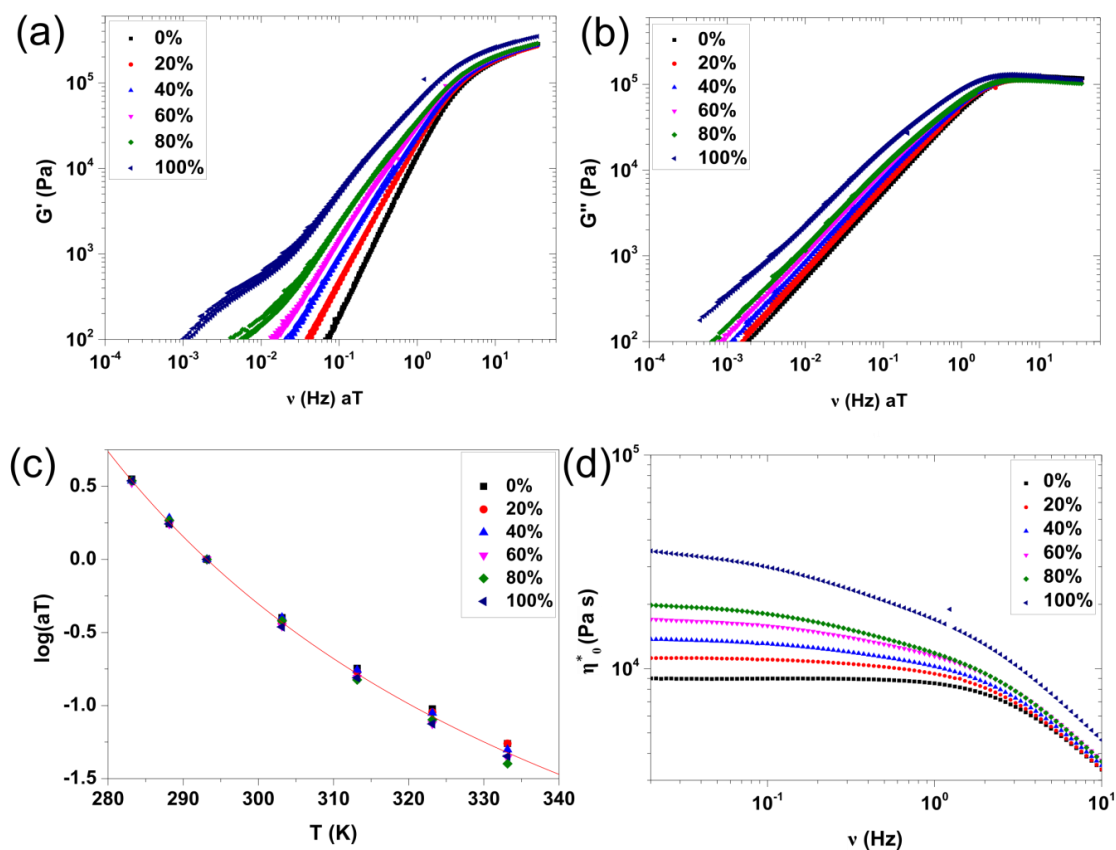


Figure 7.4: (a) Storage modulus G' and (b) loss modulus G'' of master curves of the different PI58k+PbS@PI58k nanocomposites weight fractions (0%, 20%, 40%, 60%, 80%, 100%) as a function of frequency using $T_0 = 20^\circ\text{C}$ as reference temperature and (c) the corresponding shift factors a_T plotted against the temperatures. (d) Complex viscosity η_0^* as a function of frequency for each sample at 20°C .

The dynamic mechanical measurement of the neat polyisoprene shows typical viscoelastic properties with a terminal regime of $G' \sim \omega^2$ and $G'' \sim \omega^1$.¹⁸ By adding the nanoparticles to the polymer matrix the storage modulus G' increases in the low frequency range. Consequently, the terminal flow of the nanocomposites is suppressed and steady reinforcement occurs. In contrary to other groups, who describe an almost solid-like behavior at high particle loadings, in our system only a slight increase of the storage modulus G' is achieved. This can be explained with the high grafting density of the polymer chains surrounding the particles. Hence, the particles are shielded and the formation of aggregates even at high particle loading is impeded. No rigid nanoparticle network is formed, which would lead to a strong reinforcement effect. Additionally, in **Figure 7.4(c)** the a_T -shift factors for generating the master curves are plotted as a function of temperature. The shift factors for each sample are almost identical considering all weight fractions of nanocomposites, which indicates that the relaxation times of the different nanocomposites have the same polymer-like temperature dependence.

In addition, the complex viscosity η_0^* provides information about the viscoelastic behavior as depicted in **Figure 7.4(d)**. The neat polyisoprene behaves typical viscoelastic, having a Newtonian-type flow at low frequencies and a decrease of viscosity with increasing frequencies (shear thinning). With increasing particle loading the samples become more viscous and the starting point of shear thinning is shifted towards lower frequencies. The viscosity curve of the neat polymer-coated nanoparticles (100%) becomes almost linear in the accessible frequency range. Concerning higher frequencies the value of η_0^* increases with higher particle loading, which indicates that the nanoparticles start to dominate the polymer melt and interact with each other that retard the motion of the polymer brush chains.

In order to investigate the polymer chain dynamics and the relaxation behavior of the polymer chains in to nanocomposites mixtures the measured oscillatory shear curves were fitted by using the Havriliak-Negami equation (**equation 7.2**).¹⁹

$$G^*(\omega) = \frac{G_\infty}{(1 + (i\omega\tau_{HN})^\alpha)^\gamma} \quad (7.2)$$

One can derive for the Havriliak-Negami equation a relaxation time distribution function $g_{HN}(\tau)$ (**equation 7.3**).

$$\tau g_{HN}(\tau) = \frac{1}{\alpha\Gamma(\gamma)} H_{22}^{11} \left(\frac{\tau}{\tau_{HN}} \left| \begin{matrix} (1, \alpha^{-1}) & (1,1) \\ (\gamma, \alpha^{-1}) & (1,1) \end{matrix} \right. \right) \quad (7.3)$$

Where $\Gamma(z)$ is the Gamma function and H_{22}^{11} is the Fox H-function. This allows one to numerically compute the relaxation time distribution function *via* a series expansion and an asymptotic expansion as

$$g_{HN}(\tau) = \sum_{n=0}^{\infty} \frac{(-1)^n \Gamma(\gamma + n)}{n! \Gamma(\gamma)} \frac{\sin[\pi\alpha(\gamma + n)]}{\pi} \left(\frac{\tau}{\tau_{HN}} \right)^{\alpha(\gamma+n)}, \quad \frac{\tau}{\tau_{HN}} < 1 \quad (7.4)$$

$$g_{HN}(\tau) = \sum_{n=1}^{\infty} \frac{(-1)^{n-1} \Gamma(\gamma + n) \sin[\pi n \alpha]}{n! \Gamma(\gamma) \pi} \left(\frac{\tau}{\tau_{HN}}\right)^{\alpha n}, \quad \frac{\tau}{\tau_{HN}} > 1 \quad (7.5)$$

The Havriliak-Negami fit were used to determine the distribution of relaxation times for each sample by using the plateau modulus G_{∞} , the mean relaxation time τ , and the two parameter α and γ that describe the width and shape of the distribution. In **Figure 7.5(a)** the observed time relaxation distributions are illustrated for each weight fraction ranging from 0% to 100% at a fixed temperature of 20 °C. With increasing particle loading the distribution alter from a narrow distribution (0%) to a very broad distribution (100%). Additionally, the mean time is slightly shifted from 0.22 s to 0.30 s towards longer relaxation times, which indicates a retardation of the polymer chain dynamics with increasing particle loading. The content of free polymer chains is decreasing until, in the case of 100%, only polymer-coated nanoparticles are present. Our experiments indicate that the interfacial polymer layer has a slower mobility compared to the free polymer chains. The observed relaxation time is related to the α -relaxation process which is associated to the glass transition and the mobility of the polymer segments enabling translational motion of the polymer chains.

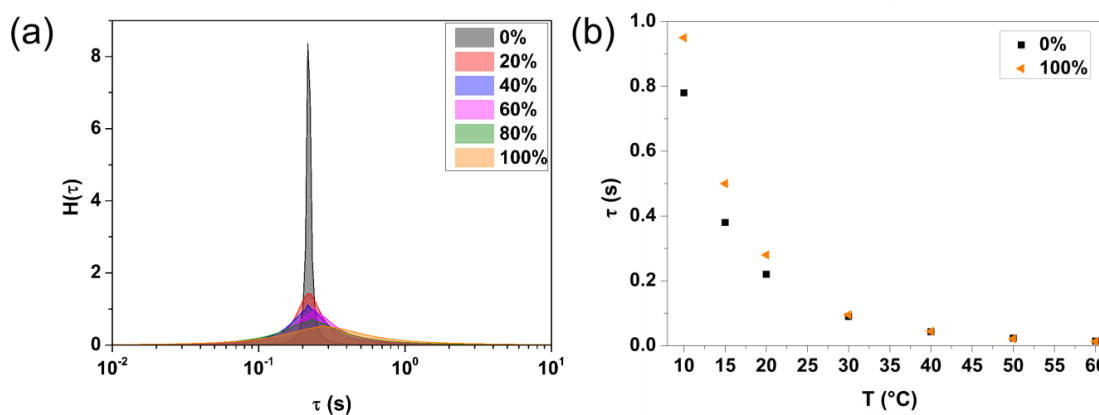


Figure 7.5: (a) Determined τ relaxation distribution of PI58k+PbS@PI58k nanocomposites of different weight fractions at 20 °C by fitting the rheological measurements with the Havriliak-Negami equation and (b) the corresponding mean relaxation times at different temperatures.

Figure 7.5(b) represents the mean relaxation times at different temperatures for the two extremes, the neat polymer (0%) and the polymer-coated nanoparticles (100%). The relaxation times of both samples are strongly dependent on temperature. At low temperatures the mean relaxation time of the grafted polymer chains is slower than the relaxation time of the free chains. Consequently, the polymer chain dynamics are much

more affected by the presents of particles at lower temperatures. At higher temperatures the retardation of polymer chain dynamics is less pronounced and the mean chain relaxation times are nearly identical. This effect could be explained by the interfacial polymer layer mobility. With decreasing temperatures the chain mobility of the coated polymer chains is reduced resulting in a reduction of the relaxation times of the matrix polymer.

Four different molecular weights of the grafted polymer chains were considered to analyze the effect of chain length and brush thickness on the mechanical and dynamic properties of the neat polymer-coated nanoparticles. Besides the already presented polyisoprene-PbS nanoparticles with a relative high molecular weight of 58 kg/mol polyisoprene with a molecular weight of 15 kg/mol, 4.3 kg/mol and 1.7 kg/mol were investigated. As mentioned above the nanoparticles coated with the shortest polymer chains (1.7 kg/mol) did not result in single isolated polymer-coated nanoparticles and has to be considered as a special case since primary aggregates were obtained.

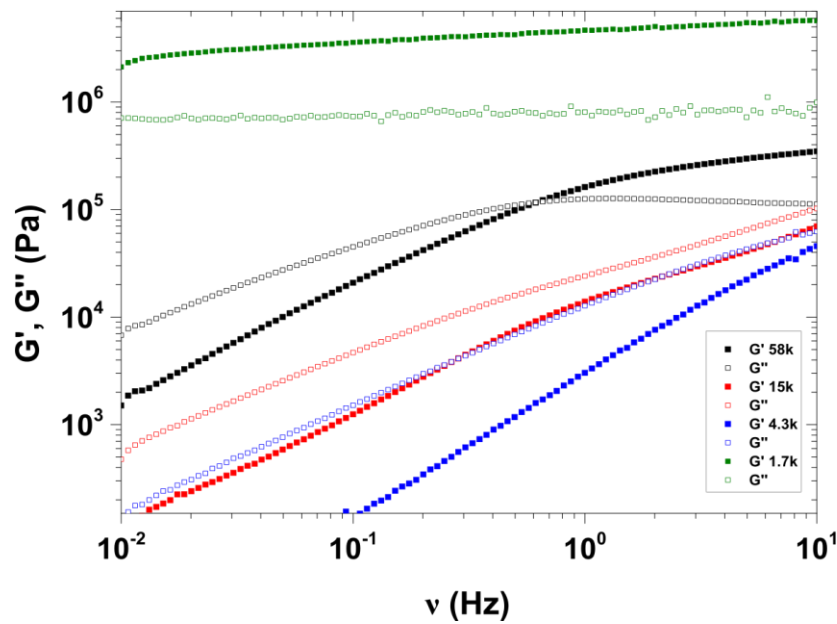


Figure 7.6: Storage modulus G' (closed squares) and loss modulus G'' (open squares) of PbS@PI-X nanoparticles as a function of frequency with varying molecular weights at 10 °C. X= 1.7 kg/mol, 4.3 kg/mol, 15 kg/mol, 58 kg/mol.

Figure 7.6 represents the results of the oscillatory shear experiments for the coated PbS nanoparticles with different molecular weights at 10 °C. For polymer-nanoparticle system with a molecular weight of 15 kg/mol, 4.3 kg/mol and 1.7 kg/mol the crossover between the storage G' and the loss G'' modulus could not be reached in the available frequency

and temperature range and therefore the relaxation times are not accessible. Nevertheless, it can be shown that shortening the grafted chain length of isolated particles (transition from 58 kg/mol to 16 kg/mol and 4.3 kg/mol) does not lead to a huge reinforcement effect by means of solid-like behavior. The situation is changed for the sample with the shortest chains, which consists of primary aggregates. A clear solid-like mechanical behavior is observed. The values of the storage and loss moduli are strongly increased, becoming almost independent of frequency over the whole available frequency range. This shows a direct correlation between the bulk mechanical behavior and the local nanoscale structure. Strong reinforcement effects are often explained by the formation of percolated networks and are well known and described for nanoparticles with high aspect ratios (nanofibers or nanotubes).^{20–23} Consequently, this observed reinforcement is mainly due to the spatial arrangement and interaction of the small anisotropic aggregates.

Conclusion

In our work we demonstrate the relationship between structure and mechanical properties of polymer-coated nanoparticles in a polymer matrix. With increasing nanoparticle loading the polymer chain dynamics are retarded, which is indicated by the increase of the moduli in the terminal flow regime. A significant reinforcement of the mechanical properties was not observed due to the good miscibility of the nanoparticles in the matrix indicating weak brush-brush interactions. Additionally, primary aggregated structures were investigated. These aggregates are well-defined and can be compared to anisotropic structures. In this case we observe a strong reinforcement of the material result in a solid-like behavior and “rubber-like” plateau in the rheological measurements. The investigations reveal a direct correlation between mechanical behavior and local structure of the materials.

Supporting Information

Characterization of polymeric ligands

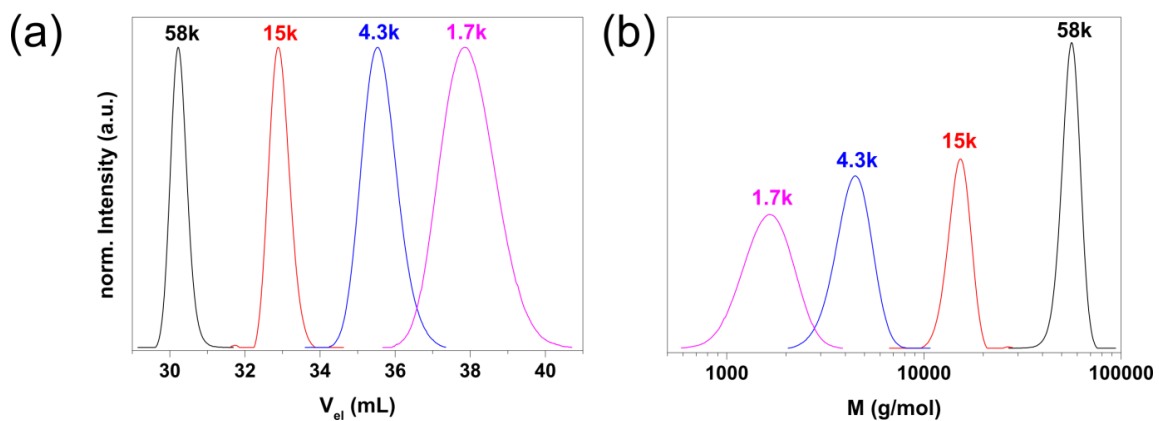


Figure 7.S1: Molecular weight distributions of the synthesized polyisoprenes (1.7, 4.3, 15, 58 kg/mol) determined from GPC measurements in THF at a flow of 1 mL/min by using 1,4-polyisoprene standard calibration. (a) RI-intensity as a function of the elution volume and (b) as a function of the molecular weight.

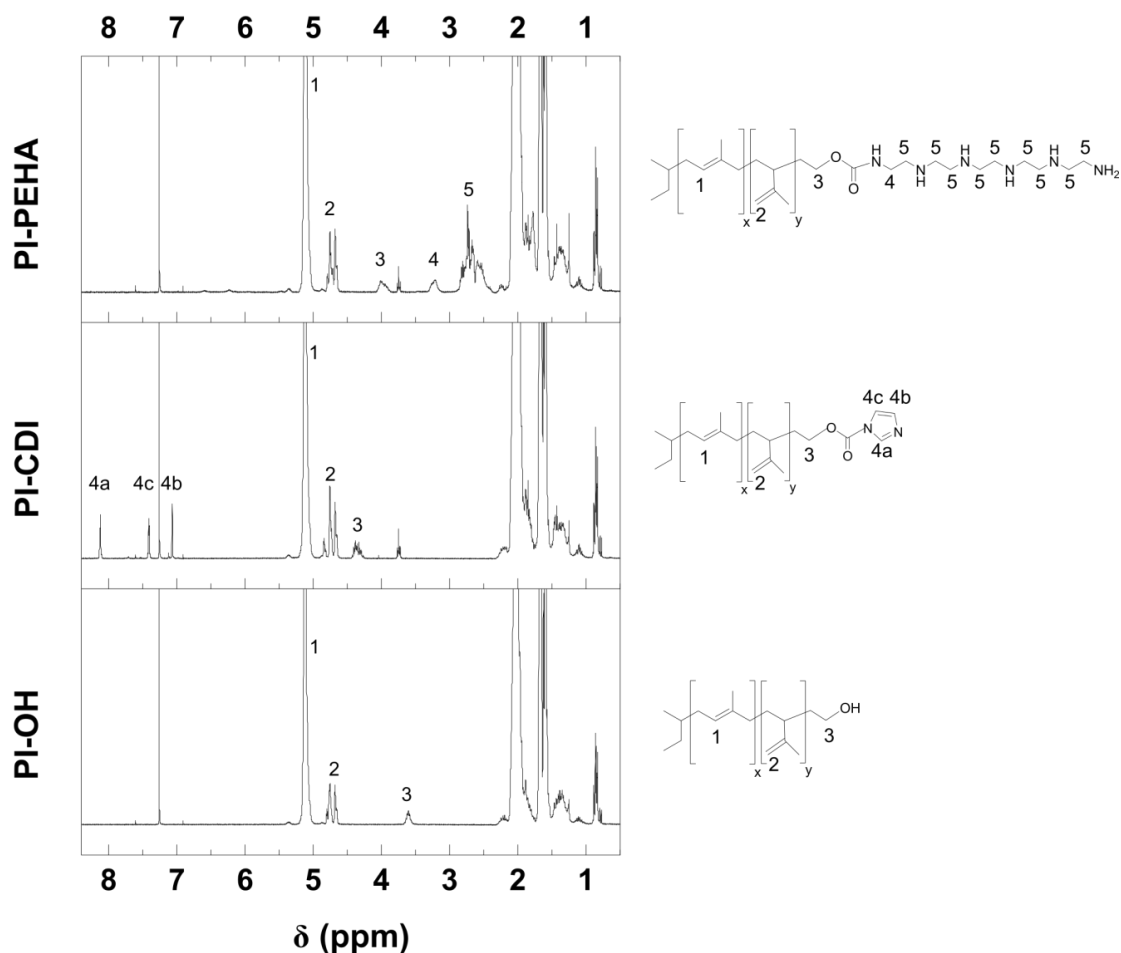


Figure 7.S2: $^1\text{H-NMR}$ (300 MHz, CDCl_3) spectra of the different functionalization steps illustrated for PI-4.3k starting with the initial hydroxyl end group to the CDI activated polymer to the PEHA functionalized polyisoprene.

PI-OH

$^1\text{H-NMR}$ (300 MHz, CDCl_3): δ (ppm) = 0.76-0.88 (m, 3H, *sec*-butyl, $\text{CH}_3\text{-CH}_2\text{-}$), 1.01-1.17 (m, 1H of *sec*-butyl, $\text{-CH(-CH}_3\text{-)}$), 1.18-1.50 (m, 3H, *sec*-butyl, $\text{-CH(-CH}_3\text{-)}$); 2H, *sec*-butyl, $\text{CH}_3\text{-CH}_2\text{-}$; 2H per unit 3,4-PI, $\text{CH-CH}_2\text{-}$), 1.51-1.73 (m, 3H per unit 3,4-PI, C-CH_3 ; 3H per unit 1,4-PI, $\text{-C(-CH}_3\text{)=}$), 1.74-2.31 (m, 1H per unit 3,4-PI, -CH- ; 2H per unit 1,4-PI, $\text{-HC=CH-CH}_2\text{-}$; 2H per unit 1,4-PI, $\text{-CH}_2\text{-C(-CH}_3\text{)=}$); 3.6 (t, 2H, $\text{-CH}_2\text{-OH}$); 4.62-4.81 (m, 2H per unit 3,4-PI, $\text{-C=CH}_2\text{)}$; 5.00-5.21 (m, 1H per unit 1,4-PI, C=CH-).

PI-CDI

$^1\text{H-NMR}$ (300 MHz, CDCl_3): δ (ppm) = 0.76-0.88 (m, 3H, *sec*-butyl, $\text{CH}_3\text{-CH}_2\text{-}$), 1.01-1.17 (m, 1H of *sec*-butyl, $\text{-CH(-CH}_3\text{-)}$), 1.18-1.50 (m, 3H, *sec*-butyl, $\text{-CH(-CH}_3\text{-)}$; 2H, *sec*-butyl, $\text{CH}_3\text{-CH}_2\text{-}$; 2H per unit 3,4-PI, $\text{CH-CH}_2\text{-}$), 1.51-1.73 (m, 3H per unit 3,4-PI, C-CH_3 ; 3H per unit 1,4-PI, $\text{-C(-CH}_3\text{)=}$), 1.74-2.31 (m, 1H per unit 3,4-PI, -CH- ; 2H per unit 1,4-PI, $\text{-HC=CH-CH}_2\text{-}$; 2H per unit 1,4-PI, $\text{-CH}_2\text{-C(-CH}_3\text{)=}$); 4.28-4.45 (m, 2H, $\text{-CH}_2\text{-O-}$); 4.62-4.81 (m, 2H per unit 3,4-PI, -C=CH_2); 5.00-5.21 (m, 1H per unit 1,4-PI, C=CH-); 7.01 (s, 1H, CDI); 7.44 (s, 1H, CDI); 8.14 (s, 1H, CDI).

PI-PEHA

$^1\text{H-NMR}$ (300 MHz, CDCl_3): δ (ppm) = 0.76-0.88 (m, 3H, *sec*-butyl, $\text{CH}_3\text{-CH}_2\text{-}$), 1.01-1.17 (m, 1H of *sec*-butyl, $\text{-CH(-CH}_3\text{-)}$), 1.18-1.50 (m, 3H, *sec*-butyl, $\text{-CH(-CH}_3\text{-)}$; 2H, *sec*-butyl, $\text{CH}_3\text{-CH}_2\text{-}$; 2H per unit 3,4-PI, $\text{CH-CH}_2\text{-}$), 1.51-1.73 (m, 3H per unit 3,4-PI, C-CH_3 ; 3H per unit 1,4-PI, $\text{-C(-CH}_3\text{)=}$), 1.74-2.31 (m, 1H per unit 3,4-PI, -CH- ; 2H per unit 1,4-PI, $\text{-HC=CH-CH}_2\text{-}$; 2H per unit 1,4-PI, $\text{-CH}_2\text{-C(-CH}_3\text{)=}$); 2.35-2.86 (m, 18H, $\text{-CH}_2\text{-}$ groups PEHA); 3.14-3.30 (m, 2H, $\text{-CH}_2\text{-O-C(=O)-NH-CH}_2$); 3.88-4.08 (m, 2H, $\text{-CH}_2\text{-O-C(=O)-NH}$); 4.62-4.81 (m, 2H per unit 3,4-PI, -C=CH_2); 5.00-5.21 (m, 1H per unit 1,4-PI, C=CH-).

Characterization of the nanocomposites

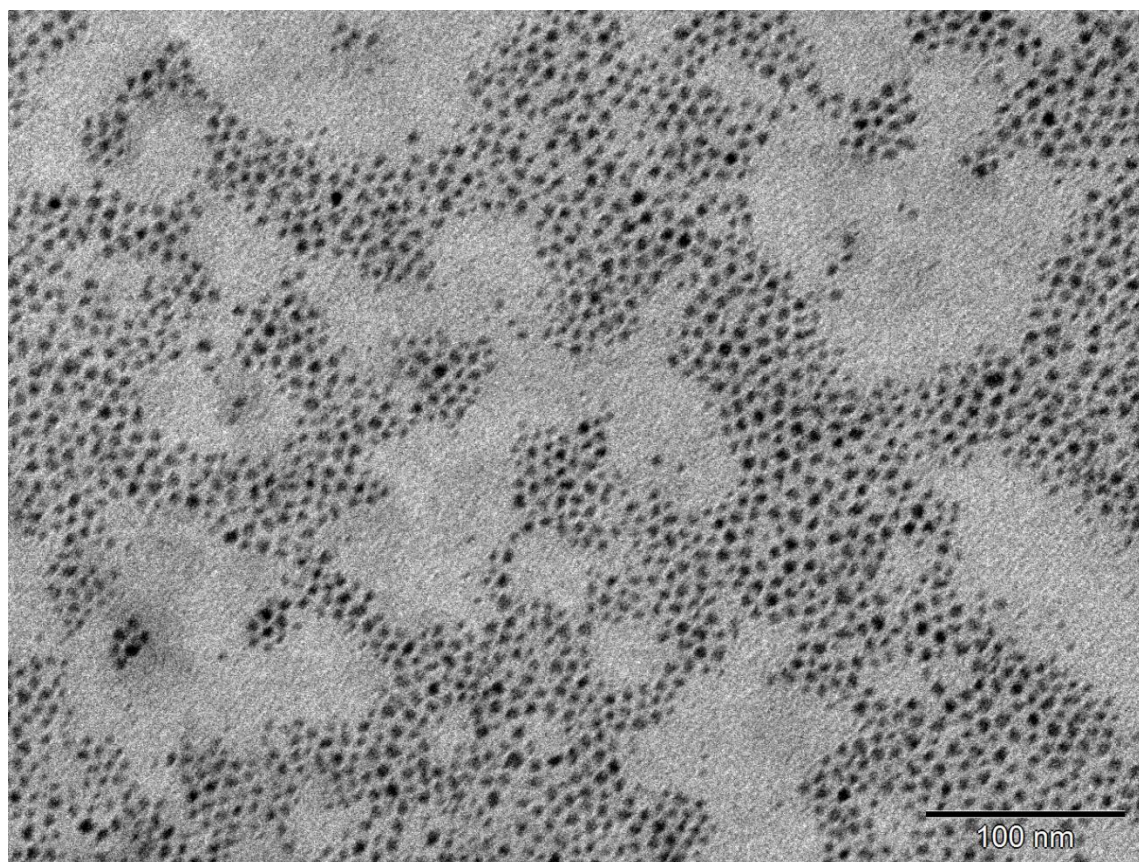


Figure 7.S1: TEM image of PbS-nanoparticles stabilized with oleic acid.

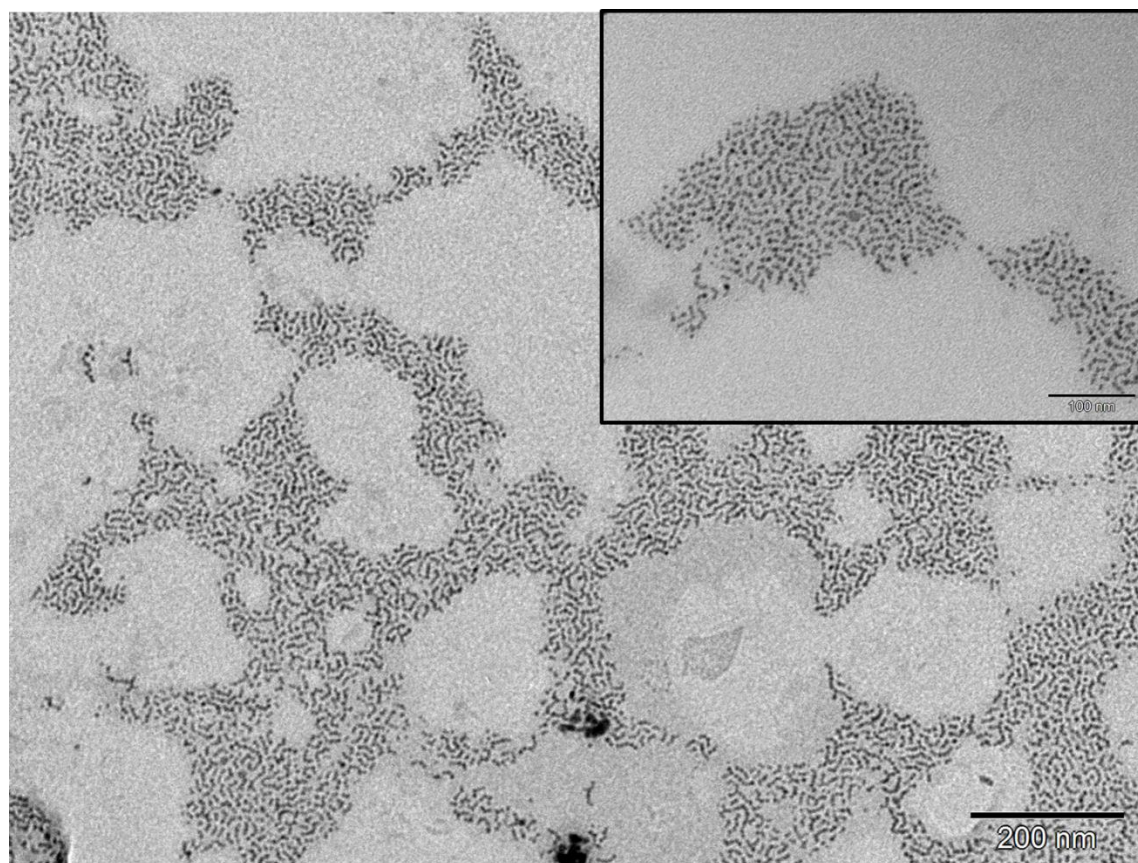


Figure 7.S2: TEM image of PbS@PI-1.7k-nanoparticles.

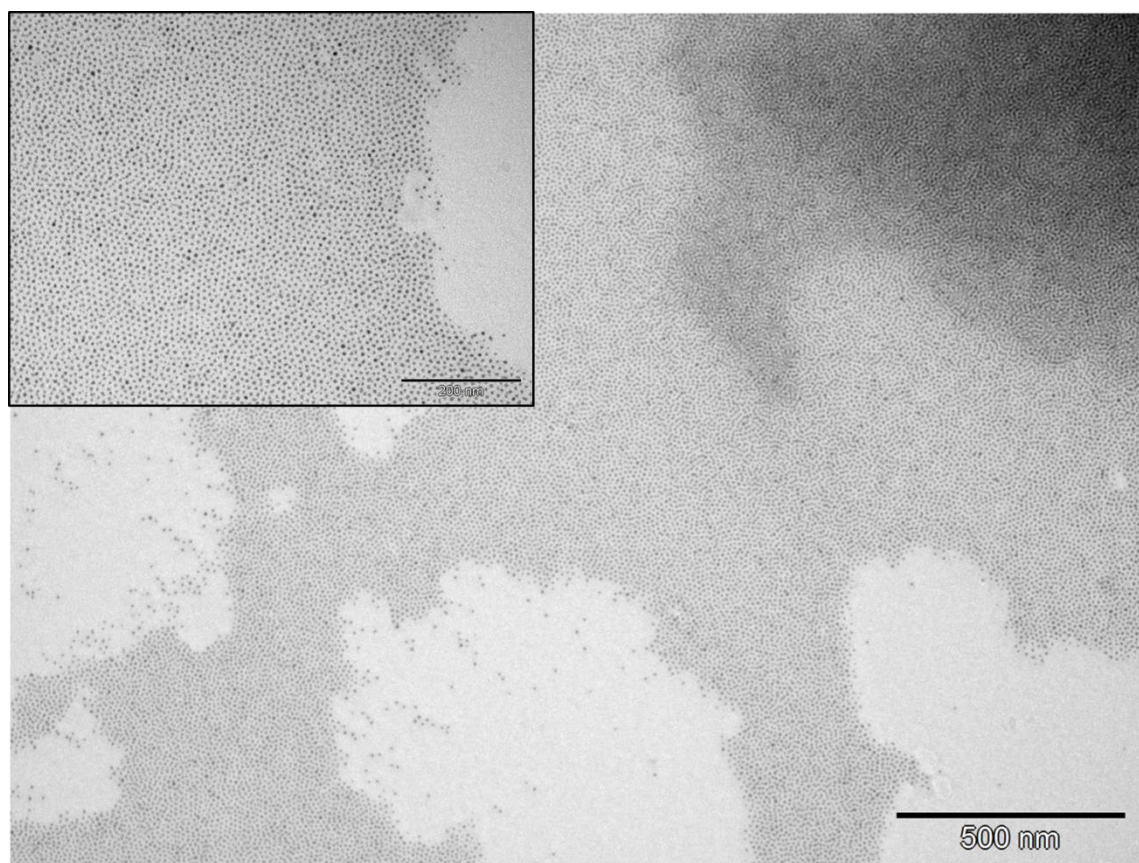


Figure 7.S3: TEM image of PbS@PI-4.5k-nanoparticles.

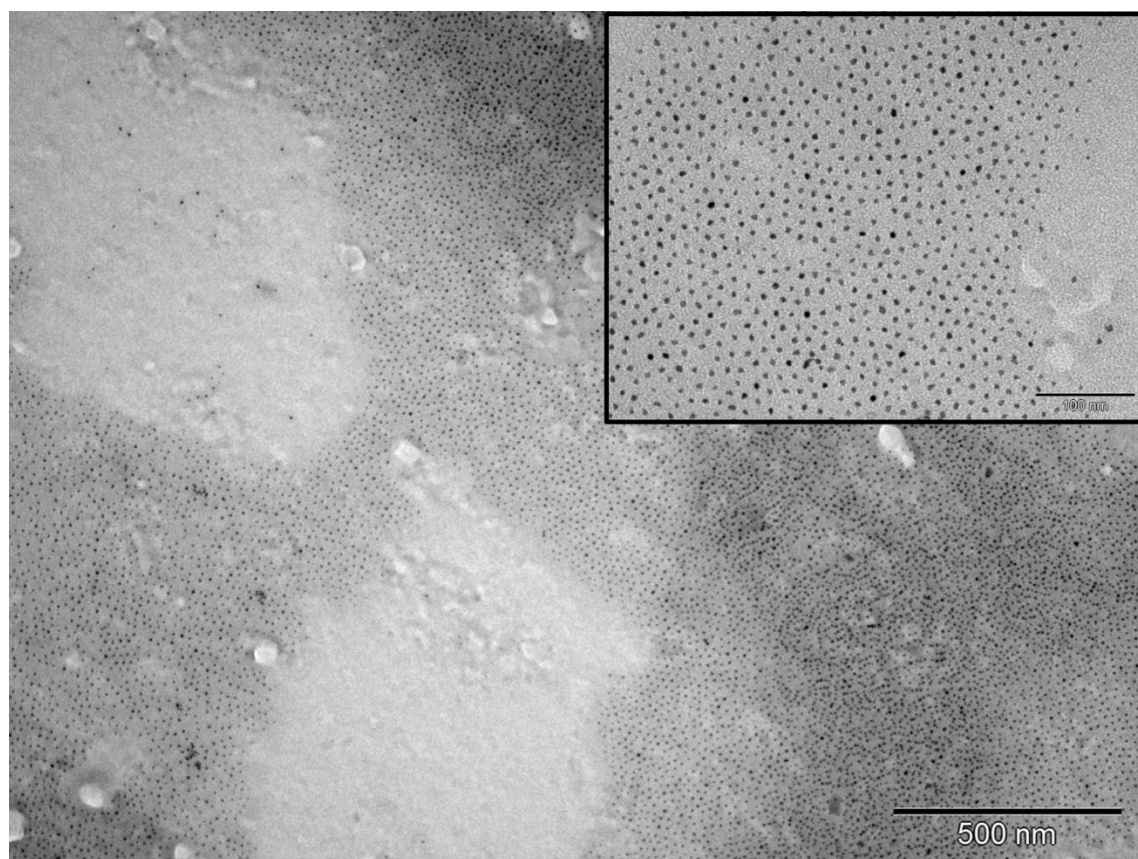


Figure 7.S4: TEM image of PbS@PI-16k-nanoparticles.

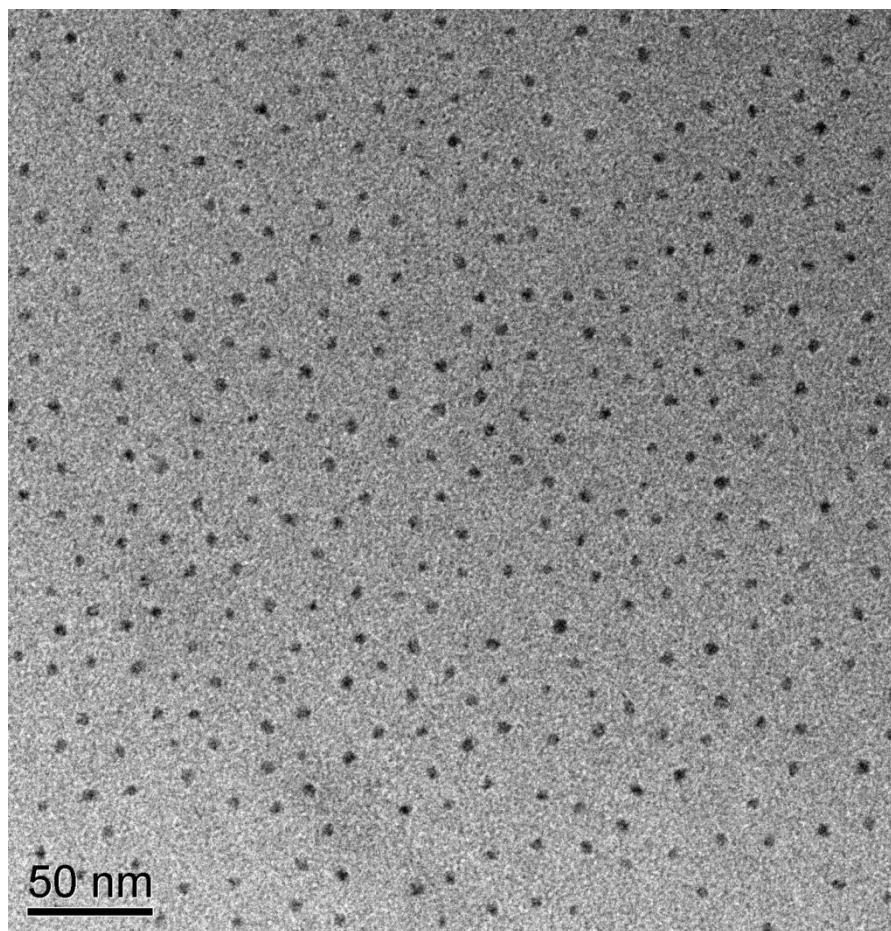


Figure 7.S5: TEM image of PbS@PI-58k-nanoparticles.

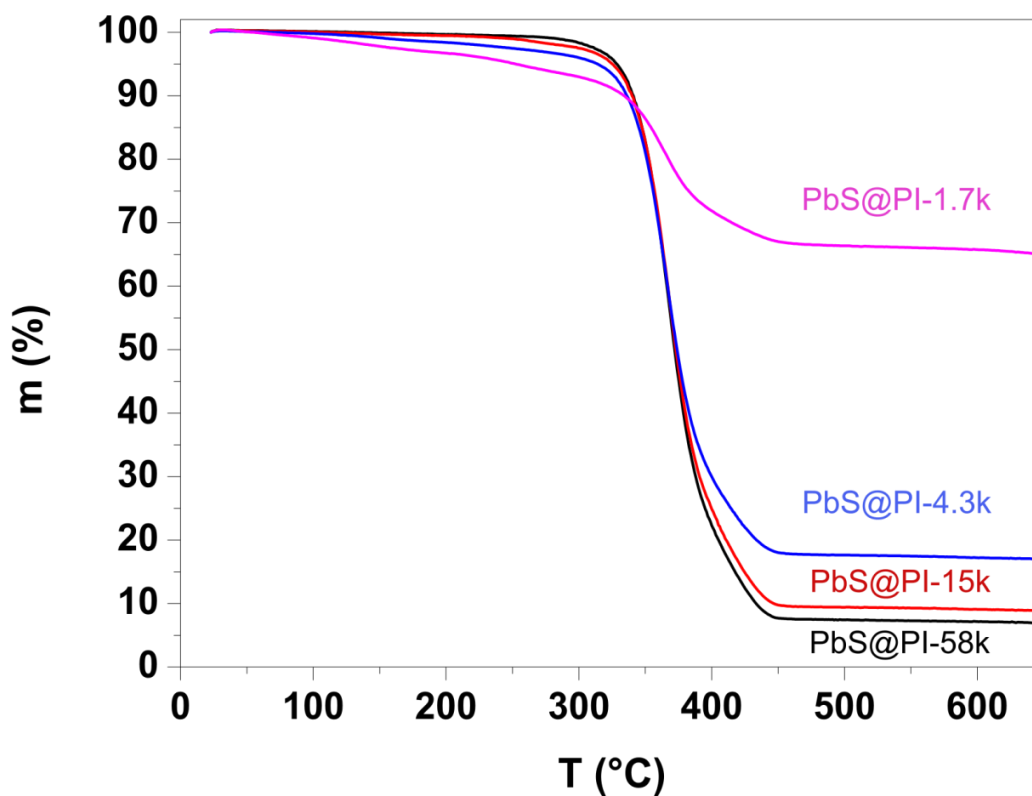


Figure 7.S8: TGA measurements of the polyisoprene stabilized nanocrystals.

Table 7.S1: Weight fractions of the polymer coated nanoparticles and their corresponding grafting densities obtained from TGA measurements.

Sample	PI/PbS (wt%)	Grafting density (nm ⁻²) ^a
PbS@PI-58k	92.8 / 7.2	0.98
PbS@PI-15k	90.9 / 9.1	2.86
PbS@PI-4.3k	82.8 / 17.2	4.90
PbS@PI-1.7k	34.2 / 65.8	1.49

^aCalculated from the determined weight fractions under the assumption of spherical particles using the density of the bulk material and that no free polymer is present.

Additional rheological measurements

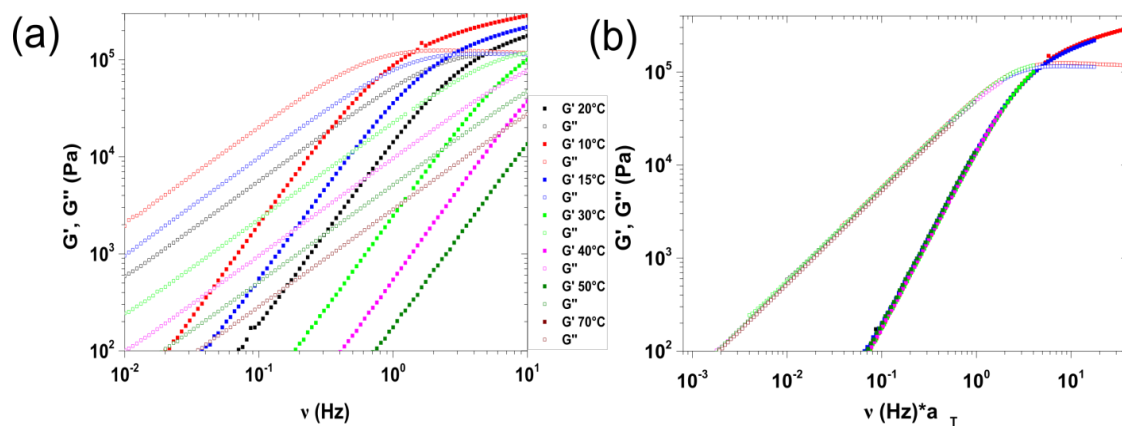


Figure 7.S9: (a) Storage modulus G' (closed squares) and loss modulus G'' (open squares) of PI58k at different temperatures and (b) the constructed master curve of PI58k using the time-temperature superposition method with reference temperature $T_0 = 20$ °C.

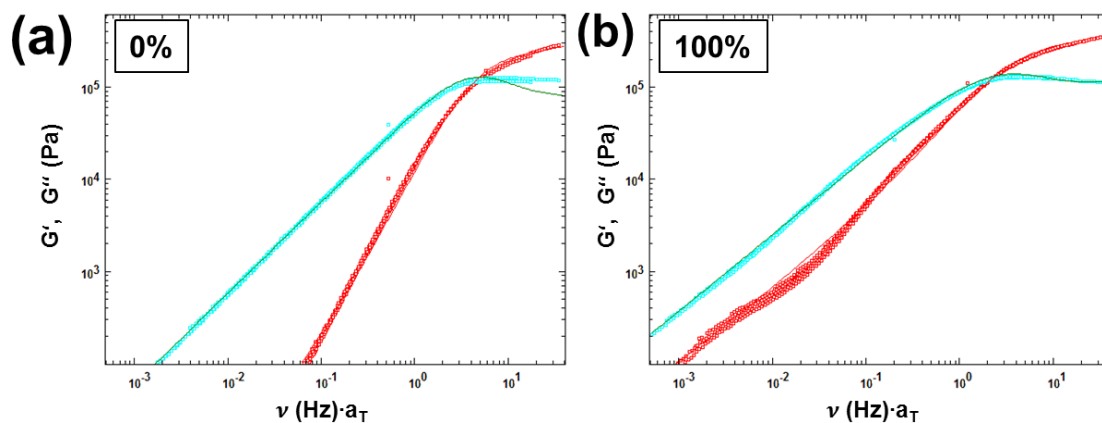


Figure 7.S10: Master curves and corresponding Havriliak-Negami fit curves of (a) PI-58k+PbS@PI-58k-0% and (b) PI-58k+PbS@PI-58k-100%.

References

1. Q. Zhang and L. A. Archer, “Poly(ethylene oxide)/Silica Nanocomposites: Structure and Rheology,” *Langmuir* **18** (26), 10435–10442 (2002).
2. C. Chevigny, F. Dalmas, E. Di Cola, D. Gigmes, D. Bertin, F. Boué, and J. Jestin, “Polymer-Grafted-Nanoparticles Nanocomposites: Dispersion, Grafted Chain Conformation, and Rheological Behavior,” *Macromolecules* **44** (1), 122–133 (2011).
3. D. Kim, S. Srivastava, S. Narayanan, and L. A. Archer, “Polymer Nanocomposites: Polymer and Particle Dynamics,” *Soft Matter* **8** (42), 10813–10818 (2012).
4. S. Fischer, A. Salcher, A. Kornowski, H. Weller, and S. Förster, “Completely Miscible Nanocomposites,” *Angew. Chem. Int. Ed.* **50** (34), 7811–7814 (2011).
5. A. P. Holt, J. R. Sangoro, Y. Wang, A. L. Agapov, and A. P. Sokolov, “Chain and Segmental Dynamics of Poly(2-vinylpyridine) Nanocomposites,” *Macromolecules* **46** (10), 4168–4173 (2013).
6. P. C. LeBaron, Z. Wang, and T. J. Pinnavaia, “Polymer-Layered Silicate Nanocomposites: An Overview,” *Appl. Clay Sci.* **15** (1-2), 11–29 (1999).
7. H. S. Woo, R. Czerw, S. Webster, D. L. Carroll, J. Ballato, A. E. Strevens, D. O’Brien, and W. J. Blau, “Hole Blocking in Carbon Nanotube–Polymer Composite Organic Light-Emitting Diodes based on Poly(m-phenylene vinylene-co-2, 5-dioctoxy-p-phenylene vinylene),” *Appl. Phys. Lett.* **77** (9), 1393–1395 (2000).
8. F. Dietsche, Y. Thomann, R. Thomann, and R. Mülhaupt, “Translucent Acrylic Nanocomposites Containing Anisotropic Laminated Nanoparticles Derived from Intercalated Layered Silicates,” *J. Appl. Polym. Sci.* **75** (3), 396–405 (2000).
9. P. B. Messersmith and E. P. Giannelis, “Synthesis and Barrier Properties of Poly(ϵ -caprolactone)-Layered Silicate Nanocomposites,” *J. Polym. Sci. A Polym. Chem.* **33** (7), 1047–1057 (1995).

10. R. A. Vaia and H. D. Wagner, “Framework for Nanocomposites,” *Mater. Today* **7** (11), 32–37 (2004).
11. A. C. Balazs, T. Emrick, and T. P. Russell, “Nanoparticle Polymer Composites: Where Two Small Worlds Meet,” *Science* **314** (5802), 1107–1110 (2006).
12. S. K. Kumar, N. Jouault, B. Benicewicz, and T. Neely, “Nanocomposites with Polymer Grafted Nanoparticles,” *Macromolecules* **46** (9), 3199–3214 (2013).
13. S. Ehlert, S. M. Taheri, D. Pirner, M. Drechsler, H.-W. Schmidt, and S. Förster, “Polymer Ligand Exchange to Control Stabilization and Compatibilization of Nanocrystals,” *ACS Nano* **8** (6), 6114–6122 (2014).
14. S. Srivastava, J. L. Schaefer, Z. Yang, Z. Tu, and L. A. Archer, “25th Anniversary Article: Polymer-Particle Composites: Phase Stability and Applications in Electrochemical Energy Storage,” *Adv. Mater.* **26** (2), 201–234 (2014).
15. N. Jouault, P. Vallat, F. Dalmas, S. Said, J. Jestin, and F. Boué, “Well-Dispersed Fractal Aggregates as Filler in Polymer–Silica Nanocomposites: Long-Range Effects in Rheology,” *Macromolecules* **42** (6), 2031–2040 (2009).
16. P. Akcora, H. Liu, S. K. Kumar, J. Moll, Y. Li, B. C. Benicewicz, L. S. Schadler, D. Acehan, A. Z. Panagiotopoulos, V. Pryamitsyn, V. Ganesan, J. Ilavsky, P. Thiyagarajan, R. H. Colby, and J. F. Douglas, “Anisotropic Self-Assembly of Spherical Polymer-Grafted Nanoparticles,” *Nat. Mater.* **8** (4), 354–359 (2009).
17. J. D. Ferry, *Viscoelastic Properties of Polymers*, 3d ed. (Wiley, New York, 1980).
18. M. Abdel-Goad, W. Pyckhout-Hintzen, S. Kahle, J. Allgaier, D. Richter, and L. J. Fetters, “Rheological Properties of 1,4-Polyisoprene over a Large Molecular Weight Range,” *Macromolecules* **37** (21), 8135–8144 (2004).
19. S. Havriliak and S. Negami, “A Complex Plane Representation of Dielectric and Mechanical Relaxation Processes in some Polymers,” *Polymer* **8**, 161–210 (1967).
20. Karen I. Winey and Richard A. Vaia, “Polymer Nanocomposites,” *MRS Bulletin* **32**, 314–322 (2007).

21. R. Krishnamoorti and E. P. Giannelis, “Rheology of End-Tethered Polymer Layered Silicate Nanocomposites,” *Macromolecules* **30** (14), 4097–4102 (1997).
22. R. Krishnamoorti, “Strategies for Dispersing Nanoparticles in Polymers,” *MRS Bull.* **32** (04), 341–347 (2007).
23. D. Paul and L. Robeson, “Polymer nanotechnology: Nanocomposites,” *Polymer* **49** (15), 3187–3204 (2008).

Summary

In this thesis the controlled preparation of well-defined nanoparticles and polymer core-shell structures was performed in order to investigate the structure-property relationship of the polymer based nanostructured materials.

On the one hand self-assembled block copolymer micelles were used as subunits to create thermoreversible organogels with tunable macroscopic properties and a high nanoscale order. A specific fraction of the diblock copolymer was covalently linked with a hydrogen bonding group (ureidopyrimidinone (UPy)) at the periphery resulting in self-assembled micelles with a tunable number of active units on the surface. The UPy groups are able to form self-complementary 4-fold hydrogen bonds and to mediate attractive, reversible junctions between adjacent micelles resulting in transient network structures. Furthermore, the attached hydrogen bonding units are able to associate and dissociate reversibly depending on temperature. Changing the number of active units allowed one to tune the viscoelastic properties of the organogels. With increasing UPy content the storage modulus of the gels increased and the melting temperatures of the networks were shifted to elevated temperatures. At temperatures ranging from 55 °C to 65 °C the organogels melt into low-viscous solutions allowing mold casting as an applicable feature. The highly ordered micelle assemblies were used to form micron sized channels by imprinting the organogels at elevated temperatures into a fluoropolymer master. Subsequent cooling and removal of the master result in well-defined nanostructured channels. Additionally, two mechanical models were developed and a direct correlation between the UPy-dimer lifetime, the nanoscale structure, and their macroscopic viscoelastic properties could be elaborated.

On the other hand polymer nanocomposites were designed and systematically studied regarding their viscoelastic properties. The incorporated nanoparticles were densely coated with a polymer shell in order to make them completely miscible in polymer matrices. Therefore, an efficient ligand exchange approach was developed based on thermodynamic considerations which allowed grafting of nearly all types of polymers onto a variety of nanocrystals. Grafting densities above 1 nm⁻² were achieved due to a deliberate end-functionalization of the polymer ligands allowing a reversible surface coordination. Additionally, controlled nanoparticle aggregation (nanochains, nanoparticle networks) could be induced by a systematic variation of the ligand exchange procedure.

The prepared hybrid core-shell structures have an excellent stability in bulk and solution. Consequently, they are excellent candidates for the use as nanofillers in polymer nanocomposites. Thin transparent nanocomposite films were generated with high weight fractions (up to 45 wt%) of non-aggregated, well-dispersed nanofillers in polymer matrices. The nanocomposites can be tailored depending on the material requirements and exhibit improved optical, mechanical, and magnetic properties. For example, the prepared ZnO/poly(methyl methacrylate) (PMMA) nanocomposites form high modulus films with improved scratch resistance compared to neat PMMA films, which is useful for applications in industry. Additionally, the fundamental polymer dynamics in such nanocomposites were studied systematically on the basis of a model system. The hybrid core-shell bulk materials are well-stabilized and the interparticle distance could be controlled precisely by reducing the brush layer thickness/ molecular weight of the polymer ligand. The viscoelastic properties were correlated to the nanoscale structures. As a result, the prepared spherical hybrid core-shell structures showed a high miscibility in compatible polymer melts without aggregation effects. Increasing nanoparticle loading leads to a systematic retardation of the polymer chain relaxation. In addition, anisotropic core-shell structures (nanochains) were prepared *via* controlled aggregation of nanoparticles. The investigation of these nanofillers reveals a solid-like behavior and a strong reinforcement effect of the materials due to network formation.

Zusammenfassung

Die vorliegende Arbeit befasst sich mit der Untersuchung von nanostrukturierten Materialien und deren Struktur-Eigenschaftsbeziehungen. Die Herstellung dieser nanostrukturierten Materialien wurde durch kontrollierte Anordnung von wohldefinierten, kolloidalen Bausteinen erzielt. Dabei wurden zwei unterschiedliche Arten von Systemen verwendet.

Einerseits wurden thermoreversible Organogele aus Blockcopolymer Mizellen konstruiert. Diese Organogele verfügen über eine hohe Ordnung auf der Nanoebene und wurden gezielt modifiziert um die makroskopischen Eigenschaften der Gele zu verändern. Dazu wurde ein bestimmter Anteil der Blockcopolymer mit einer funktionellen Gruppe (Ureidopyrimidinon (UPy)) verknüpft, welche Wasserstoffbrückenbindungen zueinander ausbilden kann. In selektivem Lösungsmittel bilden diese Blockcopolymer monodisperse Mizellen durch Selbstorganisation, deren Oberfläche durch die Anzahl an aktiven Gruppen (UPy) variiert werden kann. Die UPy-Gruppen ermöglichen es selbstkomplementäre vierfach Wasserstoffbrückenbindungen zwischen benachbarten Mizellen auszubilden, was zur Entstehung von Netzwerkstrukturen führt. Diese Wasserstoffbrückenbindung hat einen dynamischen Charakter und kann durch Temperaturveränderungen gesteuert werden. In diesem Zusammenhang wurden die viskoelastischen Eigenschaften der Organogele untersucht. Mit steigendem UPy-Anteil erhöhte sich nicht nur das Speichermodul der Gele, sondern auch die Schmelztemperatur der Netzwerke. In einem Temperaturbereich von 55 °C bis 65 °C begannen die Netzwerkstrukturen aufzubrechen und die Gele verwandelten sich zu niedrig viskosen Flüssigkeiten. Diese reversible Umwandlung wurde ausgenutzt um parallele Linien aus den hochgeordneten Organogelen zu prägen. Dabei wurden die Gele bei erhöhten Temperaturen verflüssigt und in einen Fluorpolymer-Master gegossen. Nach dem Abkühlen wurde der Master abgezogen und wohldefinierte, nanostrukturierte Linien aus Organogelen erhalten. Des Weiteren wurden zwei mechanische Modelle entwickelt, welche eine direkte Verbindung zwischen der UPy-Dimer Lebensdauer, der Nanostruktur und den makroskopischen, viskoelastischen Materialeigenschaften herstellten.

Andererseits wurden polymere Nanokomposite hergestellt und systematisch, in Bezug auf ihre viskoelastischen Eigenschaften, untersucht. Die eingebetteten Nanokristalle wurden mit einer dichten Polymerhülle beschichtet um eine komplette Mischbarkeit mit der

Polymermatrix zu gewährleisten. Dazu wurde eine effiziente Ligandenaustausch-Methode entwickelt, welche es erlaubt fast alle Arten von Polymerketten auf unterschiedlichste Nanokristalle zu pflöpfen. Basierend auf thermodynamischen Betrachtungen wurden die Polymerketten gezielt endfunktionalisiert, was eine reversible Oberflächenkoordinierung der Polymerliganden auf der Nanopartikeloberfläche ermöglichte und somit Pflöpfdichten von über 1 nm^{-2} . Darüber hinaus konnten durch die systematische Variierung der Ligandenaustausch-Methode, kontrollierte Nanopartikelaggregate (Nanoketten, Nanonetzwerke) synthetisiert werden. Alle hergestellten Kern-Schale Strukturen zeigten eine exzellente Stabilität in Masse und in Lösung, wodurch sich diese Materialien besonders als Füllmaterial für polymere Nanokomposite eignen. Es wurden dünne transparente Nanokomposit-Filme mit hohem Füllanteil (bis zu 45 Gew%) hergestellt, wobei die beschichteten Nanopartikel gut vermischt und nicht aggregiert in der Polymermatrix vorlagen. Die Materialfähigkeiten der Nanokomposite können dabei gezielt eingestellt werden um verbesserte optische, mechanische und magnetische Eigenschaften zu erlangen. Beispielsweise führten die hergestellten ZnO/Polymethylmethacrylat (PMMA) Nanokomposite zu hoch-Modul Filmen mit verbesserter Kratzresistenz im Vergleich zu reinen PMMA-Filmen. Zusätzlich wurden die Polymerkettendynamiken in den Nanokompositen an einem Modellsystem untersucht. Die Kern-Schale Strukturen der Materialien führten zu einer guten Stabilisierung. Durch die Reduzierung der Polymerhüllendicke/ Molekulargewicht der Polymerketten konnte der Interpartikelabstand der Nanopartikel kontrolliert eingestellt werden. Darüber hinaus wurde eine Beziehung zwischen den viskoelastischen Eigenschaften und den Nanostrukturen hergestellt. Die sphärischen Kern-Schale Partikel zeigten eine hohe Mischbarkeit in kompatiblen Polymerschmelzen ohne Aggregation der Nanopartikel. Der steigende Füllanteil der Nanopartikel in der Matrix führte zu einer systematischen Verlangsamung der Polymerkettenrelaxation. Zusätzlich wurden anisotrope Kern-Schale Strukturen (Nanoketten) über kontrollierte Aggregation hergestellt. Die Nanoketten bildeten netzwerkartige Gebilde in Masse aus, was zu einem feststoffartigen Verhalten und einer erheblichen Materialverstärkung führte.

List of Publications

- [1] **Pirner, D.**; Dulle, M.; Förster, S.
Rheological Study of Polymer Nanocomposites: Influence of Nanoparticles on Polymer Chain Dynamics
To be submitted
- [2] Schröder, J. H.; Doroshenko, M.; **Pirner, D.**; Mauer, M. E. J.; Förster, B.; Volodymyr, B.; Reck, B.; Roschmann, K. J.; Müller, A. H. E.; Förster, S.
Interfacial Stabilization by Soft Janus Nanoparticles
To be submitted to Polymer
- [3] **Pirner, D.**; Dulle, M.; Mauer, M. E. J.; Förster, S.
Reinforcement of nanostructured organogels by hydrogen bonds
RSC Adv. **6** (48), 42730 (2016)
- [4] Ehlert, S.; Stegelmeier, C.; **Pirner, D.**; Förster, S.
A General Route to Optically Transparent Highly Filled Polymer Nanocomposites
Macromolecules **48**(15), 5323 (2015)
- [5] Ehlert, S.; Mehdizadeh Taheri, S.; **Pirner, D.**; Drechsler, M.; Schmidt, H.-W.; Förster, S.
Polymer ligand exchange to control stabilization and compatibilization of nanocrystals
ACS Nano **8**(6), 6114 (2014)
- [6] Schmelz, J.; **Pirner, D.**; Krekhova, M.; Ruhland, T. M.; Schmalz, H.
Interfacial activity of patchy worm-like micelles
Soft Matter **9**(47), 11173 (2013)
- [7] Goldmann, A.S.; **Pirner, D.**; Xu, Y.; Barner, L.; Barner-Kowollik, C.; Müller, A.H.E.
Thiol-ene and thiol-oxirane chemistries for the synthesis and modification of cylindrical polymer brushes and surface modification of microspheres
Prepr. (Am. Chem. Soc., Div. Polym. Chem.) **51**(2), 742 (2010)

Danksagung

Zu guter Letzt möchte ich hier die Gelegenheit nutzen um mich bei einigen Personen zu bedanken, ohne die es mir nicht möglich gewesen wäre diese Arbeit anzufertigen.

Mein allergrößter Dank gilt Prof. Dr. Stephan Förster, der mir die Möglichkeit gegeben hat die Arbeit an seinem Lehrstuhl durchzuführen und mich in die interessanten Themenstellungen eingeführt hat.

Herzlichen Dank an meine Mentoren Prof. Dr. Ernst Rößler und Prof. Dr. Carlo Unverzagt für die zahlreichen wissenschaftlichen Diskussionen.

Als nächstes möchte ich mich recht herzlich bei den Sekretärinnen Jenny und Elisabeth bedanken, die mir oft geholfen haben bürokratische Hürden zu meistern. Ohne euch wäre viel weniger Zeit zum Forschen geblieben.

Ich bedanke mich auch bei Stephan Hauschild, der immer da war wenn ich ein Computer- oder Druckerproblem hatte und er es immer so schnell wie möglich gelöst hat.

Ein großer Dank geht auch an Karlheinz und Julia, die den Laborbetrieb am Laufen gehalten haben.

Auch bei meinen Praktikanten, die ich im Laufe der Jahre betreut habe, bedanke ich mich recht herzlich.

Natürlich danke ich auch dem gesamten Lehrstuhl der PCI: Martin D., Sascha, Caro, Eddie, Miriam, Maria M., Matze, Jan, Susi, Denise, Misha, Alex, Sara, Corinna, Martin T., Katja, Kilian, Sebastian, Nonio. Und auch den Mitarbeitern der Arbeitsgruppe Karg und Retsch: Tobi H., Astrid, Kirsten, Kristina, Arne, Patrick, Fabi, Alex, Pia, Christian, Bernd, Anna.

Einen besonderen Dank gebührt auch meinen Büro- und Laborkollegen Tobi G. und Maria Ritter. Ohne euch wäre die Zeit auf jeden Fall nicht so lustig geworden. Besonders die Abende in Freiburg waren legendär. Ihr wart immer für mich da und hattet immer ein offenes Ohr. Ich hoffe wir bleiben weiterhin in Kontakt.

Weiterhin möchte ich mich auch noch bei sehr wichtigen Personen in meinem Leben bedanken: Danke an Moritz für die zahlreichen Diskussionen und den Rückhalt. Danke an Tina für die schöne Zeit auch abseits der Uni.

Zu guter Letzt bedanke ich mich bei meinen Eltern. Danke für eure Unterstützung nicht nur während der Promotion, auch während meines Studiums. Ohne euch hätte ich es nicht geschafft. Auch bei meinen Schwestern, Sabrina und Katrin, sowie bei Manuel, Hannah, Stefan, Lea und Julian möchte ich mich bedanken. Schön, dass es euch gibt.

(Eidesstattliche) Versicherungen und Erklärungen

(§ 8 Nr. 6 PromO BayNAT)

Hiermit erkläre ich mich einverstanden, dass die elektronische Fassung der Dissertation unter Wahrung meiner Urheberrechte und des Datenschutzes einer gesonderten Überprüfung hinsichtlich der eigenständigen Anfertigung meiner Dissertation unterzogen werden kann.

(§ 8 Nr. 8 PromO BayNAT)

Hiermit erkläre ich an Eides statt, dass ich diese Arbeit selbständig verfasst und keine anderen als die von mir angegebenen Quellen und Hilfsmittel benutzt habe.

(§ 8 Nr. 9 PromO BayNAT)

Hiermit erkläre ich, dass ich nicht bereits anderweitig ohne Erfolg versucht habe, eine Dissertation einzureichen oder mich der Doktorprüfung zu unterziehen.

(§ 8 Nr. 10 PromO BayNAT)

Hiermit erkläre ich, dass ich keine Hilfe von gewerblichen Promotionsberatern bzw. -vermittlern in Anspruch genommen habe und diese auch künftig nicht in Anspruch nehmen werde.

.....
(Ort, Datum, Unterschrift)